INTEGRATED NANOREACTOR SYSTEM: TRIGGERING (BIO-) CHEMICAL REACTIONS IN SINGLE VESICLES

THÈSE N^{O} 3605 (2006)

PRÉSENTÉE LE 26 OCTOBRE 2006

À LA FACULTÉ DES SCIENCES DE BASE

Institut de sciences biomoléculaires

SECTION CHIMIE ET GÉNIE CHIMIQUE

ÉCOLE POLYTECHNIQUE FÉDÉRALE DE LAUSANNE

POUR L'OBTENTION DU GRADE DE DOCTEUR ÈS SCIENCES

PAR

Pierre-Yves BOLINGER

ingénieur chimiste diplômé EPF

de nationalité suisse et originaire de Kaiseraugst (AG)

acceptée sur proposition du jury:

Prof. M. Mutter, président du jury

Prof. H. Vogel, directeur de thèse

Prof. M. Textor, rapporteur

Prof. W. P. Meier, rapporteur

Prof. M. Winterhalter, rapporteur

ÉCOLE POLYTECHNIQUE
FÉDÉRALE DE LAUSANNE

Lausanne, EPFL

2006

Je dédie cette thèse à ma famille;

Sandra, Noé et Nathan.
Anne-Marie, Jean, Marianne et Jean-Marc.

"La théorie, c'est quand on sait tout et que rien ne fonctionne.
La pratique, c'est quand tout fonctionne et que personne ne sait pourquoi.
Si la pratique et la théorie sont réunies,
rien ne fonctionne et on ne sait pas pourquoi."

A. Einstein

The present thesis has been conducted between November 2001 and June 2006 in the laboratory of physical chemistry of polymers and membranes (LCPPM) at the Swiss Federal Institute of Technology in Lausanne (EPFL) under the supervision of Professor Horst Vogel. The work has been financially supported by TopNano21 program.

Parts of the thesis have been published in:

Pierre-Yves Bolinger, Dimitrios Stamou, and Horst Vogel. Integrated Nanoreactor Systems: Triggering the Release and Mixing of Compounds Inside Single Vesicles. JACS, 28 (2004).

Publications in preparation:

Pierre-Yves Bolinger, Dimitrios Stamou, and Horst Vogel. Review on Single Nanocontainers Manipulation.

Pierre-Yves Bolinger, and Horst Vogel. Integrated Nanoreactor Systems: Triggering Enzymatic Reactions Inside Single Vesicles.

Contents

Abstract

This thesis describes a method that allows the production in parallel of nano-reactor systems whose function is controlled by a remote stimulus. The reactors comprise a nested system of lipid vesicles part of which release their content during a thermotropic phase transition.

The integration of all components (substrate and enzyme for instance) in a single element eliminates the need for external manipulation/intervention and therefore renders this nanoscopic system entirely autonomous. The smallest attainable size for vesicles (diameter 20 nm, volume 10^{-21} L) puts a lower limit to the total volume of the device of about 10^{-18} L making it ideally suited for manipulating interacting partners at the single molecule level.

The proof of principle of individual reactors immobilized on glass is first characterized using confocal microscopy and a fluorescent dye that reports dilution during the release. In a further step, enzymatic reactions were performed and recorded by fluorescence microscopy down to single vesicle level. Initial reaction rates were evaluated and compared between several containers showing a dependency with encapsulated substrate concentration. Using vesicles of several different lipid phase transition temperatures, the process was extended to perform 2 consecutive enzymatic reactions.

In addition to confined enzymatic reactions, the system was characterized by fluorescence correlation spectroscopy providing the determination of the concentration of fluorophores and small vesicles incorporated inside individual larger containers.

Combination of this method with vesicle microarray technology will permit the simultaneous observation and quantitative analysis of confined (bio)chemical reactions in millions of separated reactors and may find applications as high-throughput screening of single enzyme reaction system. The possibility to perform multiple consecutive biochemical reactions may permit to use this system as artificial cells.

Keywords: Nanoreactor, Single Vesicle, Confined Reaction, Controlled Release, Immobilization, Self-assembly, High-throughput Screening, FCS.

Résumé

Cette thèse décrit une méthode qui permet la production en parallèle d'un système de nano-réacteurs dont la fonction est commandée par un stimulus extérieur. Les réacteurs comportent un système des vésicules lipidique dont une partie libère leur contenu pendant une transition de phase thermodynamique.

L'intégration de tous les composants (substrat et enzyme par exemple) dans une vésicule élimine le besoin de manipulation ou d'intervention externes et rend donc ce système nanométrique entièrement autonome. La plus petite taille possible pour des vésicules (diamètre 20 nanomètres, volume 10^{-21} L) donne une limite inférieure à tout le volume du réacteur à environ de 10^{-18} L le rendant idéalement adapté pour manipuler les réactifs partenaires jusqu'au niveau de la molécule unique.

La preuve du principe des réacteurs immobilisés sur le verre est d'abord caractérisée en utilisant la microscopie confocale et un colorant fluorescent qui permet le rapport d'une dilution pendant le relâchement au sein de chaque réacteur. Dans une autre étape, des réactions enzymatiques ont été exécutées et mesurées par microscopie de fluorescence dans plusieurs vésicules individuellement. Des vitesses initiales de réaction ont été évaluées et comparées entre plusieurs réacteurs montrant une dépendance avec la concentration de substrat encapsulé. Utilisant des vésicules ayant différentes températures de transition de phase lipidique, le processus a été étendu pour exécuter 2 réactions enzymatiques consécutives.

En plus des réactions enzymatiques confinées, le système a été caractérisé par la spectroscopie de corrélation de fluorescence (FCS) fournissant la détermination de la concentration des fluorophores et des petites vésicules au sein de plusieurs grandes vésicules individuellement.

La combinaison de cette méthode avec des micro-technologies alignant les vésicules permettra l'observation simultanée et l'analyse quantitative (de bio) réactions chimiques confinées dans les millions de réacteurs séparés et peut trouver des applications comme un système de criblage de réaction d'enzyme unique. La possibilité d'exécuter de multiples réactions biochimiques consécutives peut permettre d'employer ce système comme cellules artificielles.

Mots-clés: nanoréacteur, vésicule unique, réaction confinées, relâchement contrôlé, immobilisation, auto-assemblage, criblage, FCS.

Chapter 1

General introduction

This introduction presents the techniques and approaches developed up to now from many different research groups to precisely manipulate very small volume containers. Different types of containers already existed since many years, the most common of them are:

1. Lipid vesicles.
2. Emulsions.
3. Micro-fabricated structures.

These containers were mostly used in bulk dispersion or as an ensemble, however benefiting from recent microscopy technique developments; they become more and more attractive as individual entities for (bio-) chemical manipulations. This introduction emphasis selected articles which provide major contribution for manipulating containers in an individual manner.

1.1 (Nano-) containers:

Containers offer the possibility to encapsulate several kinds of (bio-)chemical molecules from small ions to complex proteins, enzymes or DNA. One common application of these containers is to isolate the incorporated molecules from their environment thus reduce their degradation depending on the permeability and physical properties of the container membrane. Another recent application is the development of innovative containers to confined (bio-) chemical reactions. This possibility is of wide chemical and biological interest. In particular, the possibility to confine and control biological processes such as enzymatic reactions at the single molecule level

will provide novel information on structural fluctuations which cannot be obtained from ensemble measurements. Reducing the volume of a biochemical reaction makes it also more physiologically relevant. Cellular chemistry takes place in ultra-small dimensions, within compartments that are defined by a phospholipid bilayer boundary. With such small dimensions (10^{-21} to 10^{-12} liter), the surface-area-to-volume ratio is extremely high and the contained molecules can experience collisions with the phospholipid surface at frequencies much greater than their reaction collisional frequencies.

A few published reviews are already devoted to the field of confined reactions. Some of them report on self-assembled nanoreactors [1], lipid vesicles used for enzymatic reactions [2] and biomimetic nanoscale reactors [3]. Other reviews concern theoretical aspects of confined reactions kinetics [4, 5].

The rapid development and progress of single-molecule detection techniques has opened up a new era of biological research. Single molecule data enhance qualitatively and quantitatively biological studies. Effectively, the data obtained by these sensitive techniques are not averaged over an ensemble as probed by classical techniques, therefore the dynamics and mechanics of biological molecules are better evaluated and understood. The review published by Ishijima and Yanagida [6] summarizes single-molecule experiments that have been designed to investigate molecular motors, enzyme reactions, protein dynamics, DNA transcription and cell signaling. Other interesting reviews which focused either on single-protein folding studies [7] or single molecule enzymology [8] demonstrate the progress performed in the field of single-molecule detection.

The combination of single-molecule detection techniques and nano-container systems will highly improve the data obtained from confined (bio-) chemical reactions and may open new systems for nanotechnology applications. This gave us the motivation to present selected articles which report innovative and powerful approaches to manipulate and analyze individual micro- or nano- sized containers. The choice to select these articles is based on the improvement brought towards single-enzyme reactions studies but also other useful technological applications like high-throughput screening systems.

Lipid vesicles can be regarded as artificial cell membranes. They are stabilized by hydrophobic interactions between natural or artificial amphiphilic lipids mainly phospholipids. The cylindrical shaped lipids self-assemble into bilayers with their hydrophobic chains packed together in the middle of the membrane and presenting on both sides their polar head groups to the aqueous solution. They form spontaneously spherical hollow structures with one (unilamellar) or more (multilamellar)

bilayers. These so-called lipid vesicles are particularly suitable containers for biological molecules due to their similarity with native biological membranes. Vesicles can in addition be produced directly from cells, in this case we refere to them as "native vesicles". From living cells, small native vesicles can be produced [9] having the same membrane composition as their mother cell. That opens the possibility to investigate cellular signaling reactions within attoliter volumes useful for new miniaturized bioanalytics systems

1.1.1 Lipid vesicles on surfaces.

In order to distinguish single containers in an ensemble, several prerequisites have to be fulfilled. One appropriate way is to immobilize chemically functionalized nanocontainers on a glass substrate. This offers the possibility to apply useful microscopy techniques mainly based on fluorescence (e.g. confocal, wide-filed, near-filed or TIRF microscopy) and follow single containers over time in a parallel manner.

The work of Rhoades [10] demonstrates the advantages offered by immobilizing small lipid vesicles via avidin-biotinylated lipids interactions. In these vesicles, a protein, adenylate kinase, was encapsulated and labeled with two fluorophores. The FRET efficiency between these two fluorophores was monitored and enabled to study the conformational fluctuation of single protein molecules between a folded and unfolded state. The lipid vesicles were used to spatially trap individual protein near the glass surface but without direct surface interactions. This approach demonstrates an interesting single molecule analysis that can be effectively scaled up and parallelized. A similarly strategy was developed to tether small lipid vesicles functionalized with cholesterol-tagged DNA to a supported lipid bilayer on glass. This technique [11] allowed the vesicles lateral mobility in the x, y plane due to the fluidity of the supported bilayer and could be applied to study vesicle-vesicle (i.e. membrane-membrane) interactions as they occur in endocytosis or t-cell recognition.

Another complex protein-vesicle construction was applied to investigate the ATP synthases molecular motor down to single molecule level [12]. To achieve this performance, functional His-tagged ATP synthase was reconstituted on small lipid vesicles. The proteoliposome was than immobilized on a Ni_2^+ coated glass surface. As one part of the enzyme was immobilized, the rotation of the liposome was monitored by polarization-resolved confocal microscopy. This work demonstrates the importance of immobilization for single molecular motor analysis.

Patterned immobilization: — The aforementioned techniques enable the random immobilization of small lipid vesicles on the surface. In combination with

micro-fabricated surfaces, immobilization of tagged vesicles can produce two dimensional arrays of encoded vesicles, [13], [14]. In these cases the containers were used to detect biomolecular recognition reactions. An improved system to create vesicles or protein arrays [15] was based on the combination of surface modification and crossing microfluidic channels. That has the advantage to easily keep the modified surface hydrated but also increase surface functionalization possibilities. An alternative approach [16] used an atomic force microscope (AFM) to direct the immobilization of small vesicles. The idea is to damage a region of a supported bilayer with the AFM tip where the vesicles will spontaneously adsorb and stay immobilized. AFM has also been used [17] to characterize single vesicle adsorbed on SiO_2 surfaces.

The application of colloidal lithography [18] reduced the pattern sizes down to 50 nm. The reduction of the pattern size extends the applications to powerful high-throughput screening systems for proteins or DNA. The ultimate step in size reduction is to immobilize one single vesicle per pattern spot. This was possible [19] by precisely controlling the specific and non-specific patterned regions with the micro-contact printing technique. This approach produced a high-density array of single attoliter containers over large areas by self-assembly processes. Recently similar results have been obtained by combining the micro-contact printing and photolithography techniques [20]. That approach resulted in the immobilization of single 1 μm vesicles inside functionalized microwells. In addition to immobilization, microfabricated devices were also used to electrophoretically deform and manipulate soft lipid vesicle membrane [21]. This work demonstrated an alternative way to immobilize single lipid vesicles suspended in solution.

1.1.2 Single vesicle (micro-)manipulation.

Confined reactions: — This section focuses on the processes developed to control confined reactions within lipid vesicular reactors. One example of optical manipulation of lipid vesicles is shown by the work of Sun et al. [23]. Individual vesicles encapsulating a certain reactant were optically trapped in the focus of a fluorescent microscope. A surrounding reactant met the other one because of an UV laser-induced fast breakdown of the sensitized-lipid bilayer allowed the rapid mixing of the encapsulated molecules with the surrounding and was monitored by the concomitant production of a fluorescent signal. The induced reaction was not spatially confined however. Due to the fast (0.3 s) barrier breakdown the two reactants remained geometrically localized only during a certain small time interval. This approach was also useful [24] to determine the encapsulation efficiency of individual

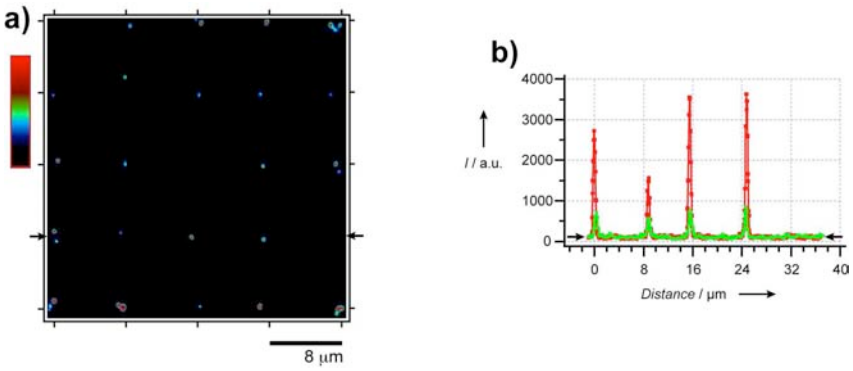

Figure 1.1: Confocal fluorescence microscopy characterization of groups of vesicles arrayed on a glass surface. *(a) Fluorescence from the lipid bilayer indicates the position of the vesicles. (b) Line trace from the image in (a) showing the rhodamine signal (red) and the simultaneously acquired fluorescence signal of CF (green). The vesicles are positioned site-specifically on the surface and remain intact, as indicated by their retention of CF. Taken from Stamou et al. [22].*

vesicles.

In some cases, giant vesicles (20 μm) remained sufficiently immobilized by sedimentation between two glass coverslips for analysis at single container level. They were used as bioreactors [25] for cell-free expression. The encapsulated protein expression was prolonged during few days by inserting a pore forming protein which induces a selective permeability through the lipid membrane. Preparation of large vesicles in high salt concentration [26] permitted the growth of protein crystals in confined volumes of micrometer dimensions. Reconstruction of fluorescent actin networks in large vesicles [27] was performed to elucidate the effect of spatial constraints and the chemical and structural properties of the cross-linker. The network was generated inside the vesicles by polymerization through influx of Mg_2^+. Actin networks inside vesicles were also analyzed at high resolution [28] with energy filtered electron tomography. This microscopy technique was also applied to study phage genome transfer into liposomes [29]. The presented methods demonstrate how single lipid vesicles can be used for biologically relevant studies. These methods take advantage of the selective permeability of the thin lipid membrane. Dynamic control of protein distribution within vesicles was performed by temperature changes [30]. By temperature or osmolarity, the miscibility of the encapsulated polymer solution could be reversible converted from two phase to one phase, manipulating like this the local protein concentration. This system represents an experimental model for cytoplasmic organization inside a model synthetic cell.

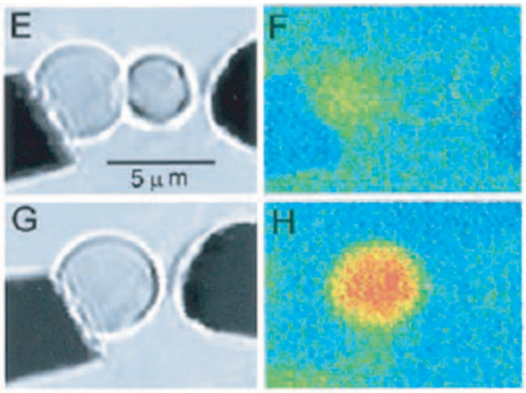

Figure 1.2: Electrofusion between two individual large vesicles. *Bright-field images before (E) and after (G) electrofusion of a 10 μM fluo-3 containing vesicle (left) and a 10 μM Ca^{2+} containing vesicle (right). Corresponding fluorescence images are shown in (F) and (H). Taken from Chiu et al. [31].*

Vesicle fusion: — Optical and micromanipulation setups were applied to trigger chemical reactions confined within single vesicles. Chiu et al. [31] reports the possibility to trap with optical tweezers a single 3 μm vesicle containing few molecules of the enzyme alkaline phosphatase. The vesicle was positioned in the focus of a fluorescence microscope and electroporated by a short electric pulse delivered by a microelectrode close to the vesicle. This electric pulse created transient pores in the lipid membrane which permitted the substrate present in the surrounding solution to penetrate inside the vesicle and react with the encapsulated enzyme. These microelectrodes were also used to mix and initiate the reaction by fusion between two vesicles containing different fluorescent reactants. The combination of optical and micrelectrodes enabled to monitor the kinetics of an enzymatic reaction inside a single vesicle. This work demonstrates good quality of results at very small volume but requires a complex experimental setup.

As shown above, the fusion between two lipid vesicles is an interesting approach to mix different reactants and thus initiate chemical reactions. This was also exploited by Kulin et al. [32] with an all-optical method. Two vesicles containing two sorts of reactants were brought into contact with two optical tweezers. The fusion was then triggered by a single UV laser pulse. The development of high-speed microfluorescence spectroscopy [33] enabled studying the fusion process of two fluorescent vesicles. An electrophoretic chamber allowed selection of pairs of vesicles having a high density of opposite charges which fuse spontaneously when brought into contact. The high time resolution obtained by this technique allowed studying fast fusion intermediates like hemifusion. Another interesting approach has been

reported to handle large vesicles [34]. Within a microfluidic chip composed of tiny asymmetric electrodes, an electoosmotic flow enabled control of the displacement of loaded vesicles but also induce electrofusion. This integrated micro-chip opens the possibilities to handle several individual vesicles which may increase the statistical quality of the results.

Micropipet applications: — Micropipets were intensely applied to manipulate large lipid vesicles. They offer the possibility to select single vesicles of interest from an ensemble and manipulate them by controlling the pressure induce inside the micropipet. This technique is thus useful to characterize the mechanical properties of biologically relevant membrane as demonstrated very early by Needham and Evans [35]. The rigidity and viscoelasticity of protein coated lipid vesicle were characterized more recently [36] by this technique. In addition to those analyzing techniques, micropipets were used to create impressive ultasmall networks of lipid vesicles interconnected with lipid nanotubes. This original manipulation was first demonstrated by Evans et al. [37] and optimized further by the group of Orwar [38] who were able to build complex 3D lipid networks. More interestingly, enzymatic reactions were initiated by injection of enzyme inside these lipid networks [39]. The confined enzymatic reaction was dynamically controlled by the network geometry that generated wave like patterns in the formation of product. This demonstrates the possibility to initiate confined bio-chemical reaction inside volumes at conditions similar to physiological ones.

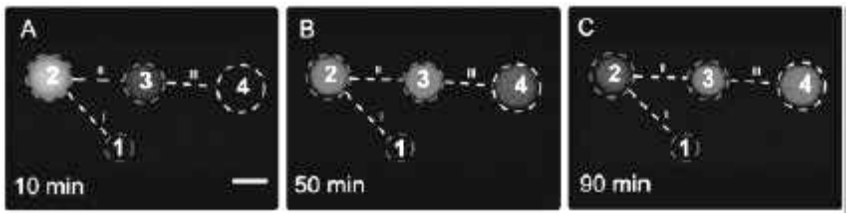

Figure 1.3: Fluorescence microscopy images showing product (fluorescein) formation in networks. *Taken from Sott et al. [39].*

1.1.3 Types of containers:

The articles reported in the previous sections deal with techniques to manipulate lipid vesicles, which represent ideal containers for biochemical applications due to their similarity with natural biological cell membranes. In addition to lipid vesicles a few other materials and structures represent promising candidates for assembling nanocontainers. The following sections will review the most interesting possibilities

which demonstrate improvements on the field of "single ultra-small volume manipulation". Like in the case of lipid vesicles, most of the containers were fabricated by self-assembly processes. Effectively, in order to produce in sufficient amounts defined structures with dimensions down to nanometer scale, control of the supramolecular assembly appears to be a really powerful and efficient approach.

Emulsions: — Emulsions of water droplets in oil phase provide confined volumes which can be quickly prepared. For example, one article reports single enzyme activity within small water droplets [40]. The enzymatic reaction was initiated by simply mixing the aqueous and oil phase before introducing it in a microchamber above a fluorescence microscope. Even if the size of the droplets can not be controlled, this system allowed probing simultaneously single enzyme reactions within a significant number of droplets. Several other biochemical reaction systems were developed based on emulsion technology. For example, cell-free protein synthesis [41] was performed within water in oil emulsion compartments. The results show however exchange of content among the differently loaded water droplets in a noncontroled unspecific manner. One more complex double emulsion system was also used as cell-like compartments [42]. Gene expression was performed inside these containers which produced enzymes and thus transformed the co-encapsulated substrate in a fluorescent product. A fluorescence-activated cell sorting (FACS) system could be applied to sort these microcompartments. This technology demonstrates a potential application for high-throughput screening of gene and enzyme activity. In order to produce emulsions of better defined size and polydispersity a few groups have employed microfluidic systems. They produced other single water in oil emulsions [43], [44] or more complex double emulsion [45] structures.

With a similar idea, small arrayed water droplets were deposited on a solid support using a bouble-barrel pipet [46]. For the objective to perform single biomolecular reactions, these techniques are attractive since they allow to control the encapsulated concentration solution thus the number of incorporated molecule in each droplet. In addition they also provide precursors for lipid or polymer vesicles with defined encapsulated solution. Other possibilities to manipulate within emulsion single water droplets are microburet injection [47] or optical tweezers [48].

Capsules: — In addition to lipid vesicles and emulsions, polyelectrolyte capsules provide mechanically resistant containers. Caruso et al. [49] developed an interesting strategy to produce hollow sphere polyeletrolyte capsules from colloidal templates. Starting from a latex bead, several layers of polyelectrolyte were deposited on the

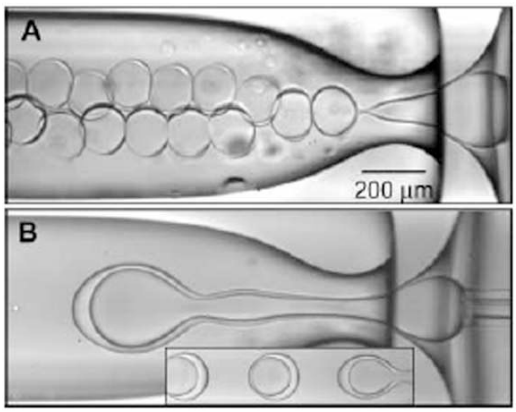

Figure 1.4: Steady-state drop formation mechanisms that result in monodisperse double emulsions with a single internal droplet. *Figure taken from Utada et al. [45].*

bead which was removed by dissolution, yielding in a hollow polyelectrolyte capsule. These capsules were functionalized by insertion of gold nanoparticles [50] and permitted fast controlled release of their contents by short IR laser pulse. They were also metallized [51] by reduction of encapsulated silver through photoirradiation. These polelectrolyte capsules have the advantage to exhibit a narrow size distribution and thus a controlled number of loaded molecules. An alternative way to produce capsules was presented by Dinsmore et al. [52]. They created a novel type of capsules so-called colloidosomes formed by the self-assembly of colloids in spherical structures, the diameter of the assembled colloids defined the gaps left in between them and hence the permeability of the colloidosomes.

Polymer vesicles represent another important kind of container. They were produced by amphiphilic block-copolymers whose hydrophobic parts aggregates spontaneously in water to generate soft hollow vesicles. Graff et al. [53] demonstrated the incorporation of lamB transmembrane protein which provided a binding region for virus-assisted DNA loading. These kinds of polymeric structures could also be stabilized by polymerization [54] once the membrane is formed.

Micro-fabrication: — Microfabrication provides interesting devices for (bio)-chemical reaction confinement and sensitive high-throughput systems. The most relevant example was demonstrated by Rondolez et al. [55] where arrays of femtoliter chambers were produced in soft PDMS layers. Under pressure these layers attached tightly on glass surfaces and enclosed an enzyme-substrate solution. By adjusting the enzyme concentration in solution, the immobilized PDMS layer provided arrays of femtoliter chambers where single enzyme reactions took place. Once

the PDMS layers are fabricated, this system allows fast, simple and applicable for parallel analysis. Similarly, single enzyme assays were performed on sealed femtoliter chambers of an etched optical fiber surface [56]. Also working with small chambers arrays, Rindzevicius et al. [57] demonstrated that a single 60 nm hole can be used to detect successive molecular adsorption process near the metal surface. For genome sequencing, a highly parallel system was presented [58] using microfabricated picoliter reactors. Single strand of DNA bound to beads were amplified within emulsion droplets and then sequenced within the small wells of a fibre-optic slide.

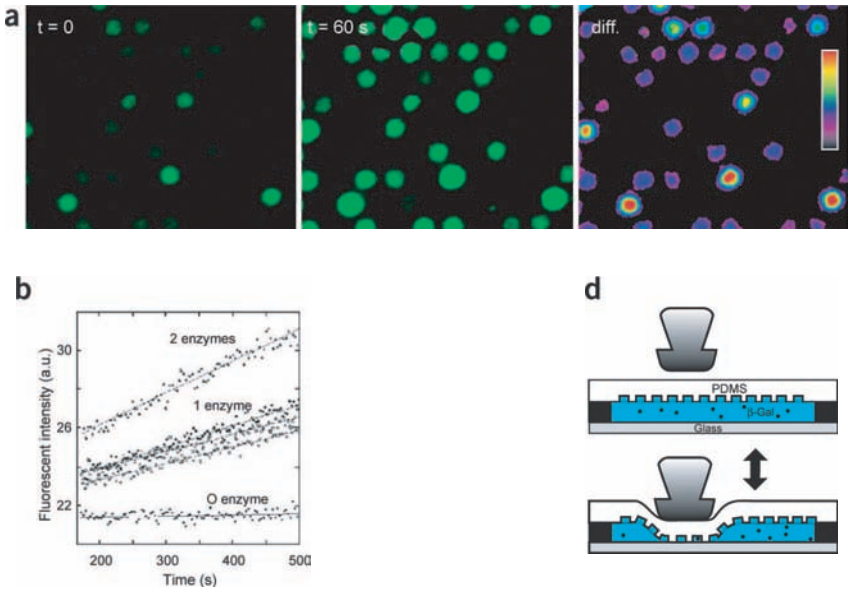

Figure 1.5: Detection of the activity of single β-galactosidase molecules. *(a) Fluorescent images of the activity in the chambers. (b) Continuous recording of β-Gal activity. (d) By pressing the PDMS sheet with glass needle, successive opening/closing rounds could be performed, allowing the exchange of the content of each chamber. Taken from Rondelez et al. [55].*

1.2 Scope of the thesis

The aim of the research project presented here is to create an innovative system of ultrasmall containers to analyze synchronically (bio-) chemical reactions. With this system, individual reactors should be identifiable in order to monitor the confined reaction and compare it to the other reactors. This objective needs to develop a strategy to trigger the reaction at the same time for each reactor. The reactors are reduced to the micrometer range to provide a spatial environment as found in biological cells.

The goal is thus to join several possibilities and functionalities in order to create an unprecedented system with could study single (bio-)chemical confined reactions in a parallel manner.

To reach the mentioned objectives, we chose lipid vesicles as containers for several reasons:

1. They mimic cell membranes, thus they are biologically relevant.
2. The self-assembly production processes allow to control their size to a certain extent.
3. They are composed of commercially available lipids with many different properties including fluorescence labels and tags for immobilization on glass surfaces.
4. The permeability of their membrane can be controlled by temperature, which represents a major advantage to trigger the reaction in a parallel manner.

The following chapter will describe in details the strategy developed to exploit the properties of lipid vesicles to use them as ultrasmall controllable reactors.

Chapter 2

Concept

2.1 Introduction

Over 30 years ago, Papahadjopoulos [59] observed that ion permeability through a lipid bilayer membrane showed an peak as the lipid membrane went through its gel-to-liquid phase transition. This phase transition is specific to the lipid identity, which mainly on acyl chain length and the degree of unsaturation of the lipid hydrocarbon chains, as well as on the type of the lipid headgroup. At this transition, gel and liquid phases coexist, creating interfacial tension between lipids with large incompatibilities in molecular packing and hydrophobic matching [60]. To explain this increased permeability, a number of groups have developed models and theories based on two principal hypotheses.

The first hypothesis relates the increase in permeability to the increased in lateral compressibility of the membrane at the phase transition [61, 62]. Measurements with the micropipet technique of the elastic area compressibility of DMPC giant vesicles at the lipid phase transition region [63] indicates that the membrane is highly compressible during the transition. Density fluctuations in the bilayer open up cavities in the hydrophilic headgroup region that allow ions to enter and then permeate through the bilayer [61].

The second hypothesis is based on the microstructural level and relates the permeability increase to the formation of leaky interfacial regions appearing at micrograin boundaries between gel and liquid domains at the transition [60, 64–66].

As recently noted by Needham [67], the two views can combined: compressibility could indeed be extremely high at melting grain boundaries, allowing for high density fluctuations particularly in these regions.

2.2 Concept of the nanoreactor system

2.2.1 General idea

The general strategy developed in this thesis to mix reactants inside a single large unilamellar vesicle (LUV) employs thermotropic permeability changes of lipid bilayers to polar solutes. As illustrated conceptually in figure 2.1, we create a nested system of different lipid vesicles with different lipid phase transition temperatures (Tt). This enables us to define conditions under which small unilamellar vesicles (SUVs), trapped in the interior of a LUV, release their cargo that is subsequently confined and mixed in the interior of the LUV. To monitor the function of the reactor systems on an individual basis but in a parallel manner, the LUVs are immobilized on a solid support via biotin-neutravidin interaction.

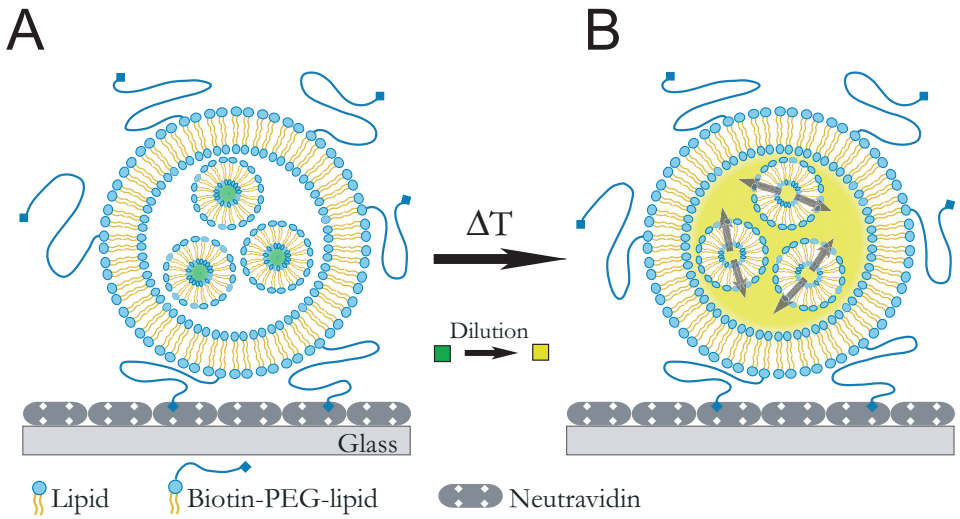

Figure 2.1: Principle of temperature-induced release and mixing of water soluble molecules in the interior of an immobilized vesicular reactor. *(A) A large unilamellar vesicle (LUV) contains small unilamellar vesicles (SUVs) that are loaded with water soluble reactants (high concentration of CF, quenched fluorescence (dark green)). The LUV is immobilized via a biotin-PEG-lipid to a neutravidin covered glass surface. (B) Increasing the temperature (ΔT) through the ordered-fluid lipid phase transition of the SUVs results in the release (arrows) of their cargo, which is subsequently confined and mixed inside the LUV (dilution of CF, fluorescence increase (intense green)).*

2.2.2 Choice of lipids

The SUVs are typically composed of negatively charged lipids, for example a 9:1 mixture of DPPC and DPPG. They show low permeability for polar molecules below

and above 41 °C (the Tt of both lipids [68, 69]) allowing their convenient manipulation and storage at room temperature. Reactors stored for up to one week showed content-release properties identical to those of freshly made reactors. The presence of negatively charged lipids in the bilayer of the SUVs and the LUVs is a precaution against leakage. The resulting electrostatic repulsion keeps the SUVs suspended in the LUV suppressing interactions between themselves or the walls of the reactor that could cause uncontrolled aggregation. The lipids of the LUVs have a Tt of -18 °C ensuring efficient confinement of the released polar solutes throughout the investigated temperature range. Fluorescent lipids such as TRITC-DHPE (figure 2.2 can be incorporated into the lipid bilayers of LUVs in order to monitor of the vesicles by fluorescence microscopy. Figure 2.2 illustrates the chemical structures of the current used for the nested vesicle systems.

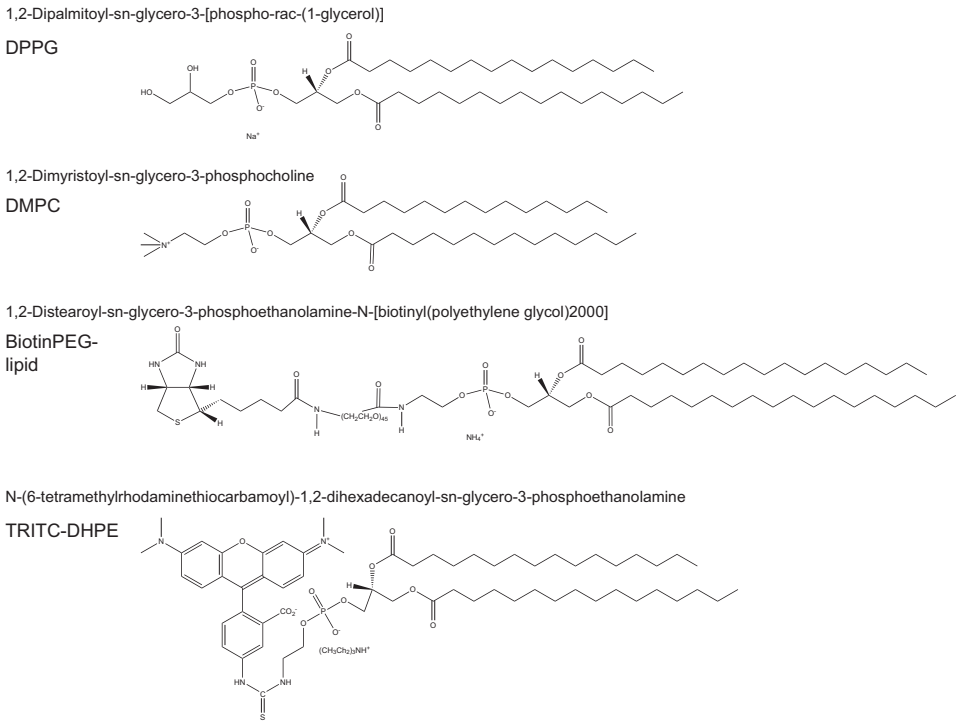

Figure 2.2: Lipids used for production of the different vesicles. *DPPG is a saturated, negatively charged lipid for SUVs. DMPC is a saturated, neutral lipid for SUVs. Biotin-PEG-lipid is the functionalized PEG lipid for immobilization of LUVs. TRITC-DHPE is a fluorescent lipid for monitoring LUVs.*

Immobilization of the LUVs is of major importance for long-lasting data acquisition. Biotin-PEG-lipids inserted in the membrane of the LUVs ensure their immobilization [22, 70] on microscope glass slides covered with streptavidin, neutravidin or avidin (figure 2.3). The long PEG spacers [71] between the lipid and the

biotin serve as elastic buffer of the LUVs to avoid destabilization or destruction on the solid support.

2.3 Production of the nanoreactors

2.3.1 Production of small vesicles

There are different possibilities to produce vesicles with different lamellar and size properties. In order to reach a controlled and efficient release of cargo, the vesicles should be unilamellar and not too small in order to contain a sufficient amount of reactants. Thus, the extrusion technique [72–74] is used to produce SUVs.

The lipids, typically, DPPC and DPPG (9:1), are dissolved and mixed in chloroform. The solvent is then evaporated under vacuum yielding a dry lipid film on the wall of the glass vessel. The lipid film is then hydrated with the desired aqueous solution: high or low concentration of fluorescent dyes, enzymatic substrate or ions. This solution is buffered with Tris-HCl 10 mM at a pH 7.0 to control the fluorescent properties of the encapsulated reactants. When heated above the Tt, the solution becomes turbid which reveals the presence of multilamellar, large vesicles. Freeze-thaw cycles [75] are applied to the turbid solution to enhance the entrapment efficiency. The vesicle dispersion is then extruded with nitrogen pressure more than five times through polycarbonate filters with 400 nm sized pores. Proved by NMR, light-scattering and electron microscopy [73, 74], the extrusion produces mainly unilamellar vesicles with a diameter of around 210 nm.

2.3.2 Purification of the SUVs

After extrusion, the dispersion of SUVs is cooled below the lipid pase transition temperature Tt, and non-encapsulated reactants are then removed by size-exclusion chromatography [68]. The purified vesicle solution should not pass through any phase transitions. For example, DPPC or DPPG vesicles, can be purified and stored at room temperature because their Tt is at 41 °C, but SUVs of DMPC or DMPG are purified and stored at 5 °C because their Tt of 23°C is close to room temperature. The vesicles are sensible to osmotic pressure [76], but also to mechanical stress. The eluant solution is then prepared carefully, using sorbitol, sucrose or potassium chloride to compensate the osmotic pressure due to the encapsulated solution. For example, when the SUVs are loaded with 50 mM carboxyfluorescein (CF), the osmotic pressure is measured to be ∼0.128 osmol/kg and therefore the eluant solution will contain 100 mM of sorbitol and 10 mM of KCl (osmotic pressure measured

~0.13 osmol/kg). The difference in size between the SUVs and the reactants is so large that a column of around ten centimeters is suitable to purify the SUVs.

2.3.3 Production of large unilamellar vesicles

The purified SUVs are incorporated into LUVs at a temperature below their Tt using either of two techniques described in the mentioned articles: the hydration method [77,78] or electro-swelling [79,80]. In each case, DOPG, 0.3 - 1% (weight %) biotin-PEG-lipid and if needed 0.2 - 1% of fluorescent lipid are mixed in chloroform solution.

For the hydration method, a lipid film is formed on a teflon vessel by solvent evaporation. This film is then hydrated with 2 ml of a solution of SUVs and incubated for 2 days. The SUVs will spontaneously incorporate inside the LUVs. The incorporation efficiency is good as demonstrated in chapter 6. The mechanism of incorporation of such large objects is not known, but on the basis of observations made during LUV formation one can provide the following hypothesis. The lipid film is quickly hydrated, resulting in stacks of planar lipid bilayers, separated by nanometer-sized water films. By incubating these multilamellar lipid systems with a dispersion of SUVs, the vesicles may sediment on top of the multilayers. Finally the SUVs are enclosed in the LUVs when the solution is aspirated by the pipette.

For the electro-swelling method, the lipid film is created on two electrically conductive Indium-Tin Oxide (ITO) glass surfaces. Then the film is hydrated with 1 ml solution of SUVs between the two ITO glass slide separated with a PDMS spacer. To swell the film, a alternating electrical potential (1.2V, 10Hz) between the two surfaces is applied during 4 to 5 hours. In order to detach the created LUVs from the glass surface, additional electrical potential is applied (2.0V, 4Hz) during 1 hour.

We observed during several experiments, that it is necessary to first remove the non -incorporated SUVs by micro-filtration using polycarbonate filters (pores diameters from 0.8 to 3μm), in order to be able to immobilize the LUVs on the microscope glass slide. After this purification step, the two different methods used to produce LUVs give very similar results in term of size distribution and fraction of unilamellar large vesicles. The electro-swelling method is faster, but the hydration method gives a larger volume of vesicles formed which is practically easier to handle during the filtration process.

2.4 Immobilization strategies

The major challenge for an efficient reactor immobilization is to find a balance between too strong adhesion which may disrupt the LUVs on the surface and too weak interaction which could be insufficient for long-time monitoring. As already described, biotin-PEG-lipids give a certain restricted mobility and elasticity and the strength of the interaction can be modulated by the electrostatic interaction between the charge of LUVs bilayer and the protein adsorbed on the glass surface. Three different proteins having almost the same binding properties and specificity to biotin can be chosen; avidin, neutravidin or streptavidin which have different isoelectric points: (10.5, 7.0, 5 respectively). Those proteins are adsorbed on the microscope glass slide by chemisorption which requires very clean glass surfaces for reproducibility and preservation of the protein activity. It is particularly important to remove the hydrophobic molecules with several cycles (around three to five) of sonication with strong detergent (Helmanex) solution, rinsing and sonication with ethanol. The cleaned slides can be stored in methanol which is removed with nitrogen flux just before the adsorption of the proteins. In addition, it is also possible to activate the glass surface with oxygen plasma just before use which increases the hydrophillicity and could improve the adsorption (improvement not analyzed).

The most important practical problem which can prevent immobilization of the reactors, is the presence of none incorporated SUVs which can rapidly diffuse to the surface and shield the binding sites of streptavidin on the adsorbed proteins. The non-incorporated SUVs can be removed to a certain extent by micro-filtration, but this purification process destabilizes mechanically the LUVs probably by interaction with the filters used. Thus, if the initial concentration of SUVs needs to be high, another strategy is required. Here, the idea is to reduce the non-specific interaction between the SUVs and the proteins by using BSA, BSA-biotin [70] or a mixture of BSA and BSA-biotin. Then, as illustrated in figure 2.3, the adsorbed BSA-biotin need to be covered by avidin, neutravidin or streptavidin. In addition, charged SUVs can be slightly repulsed electrostatically by adsorbing a protein with the same charge and/or using neutral lipids for the LUVs.

In order to accelerate the sedimentation of the LUVs to the glass surface, a density gradient can be created using different sugars. Here, the idea is to produce the LUVs in a high density solution (sucrose 100 mM) and just before immobilization add them in an equimolar concentration of a lower density carbohydrate (glucose 100 mM). This difference in density between the LUVs and their external solution reduces the time needed to get the LUVs in close proximity of the binding proteins

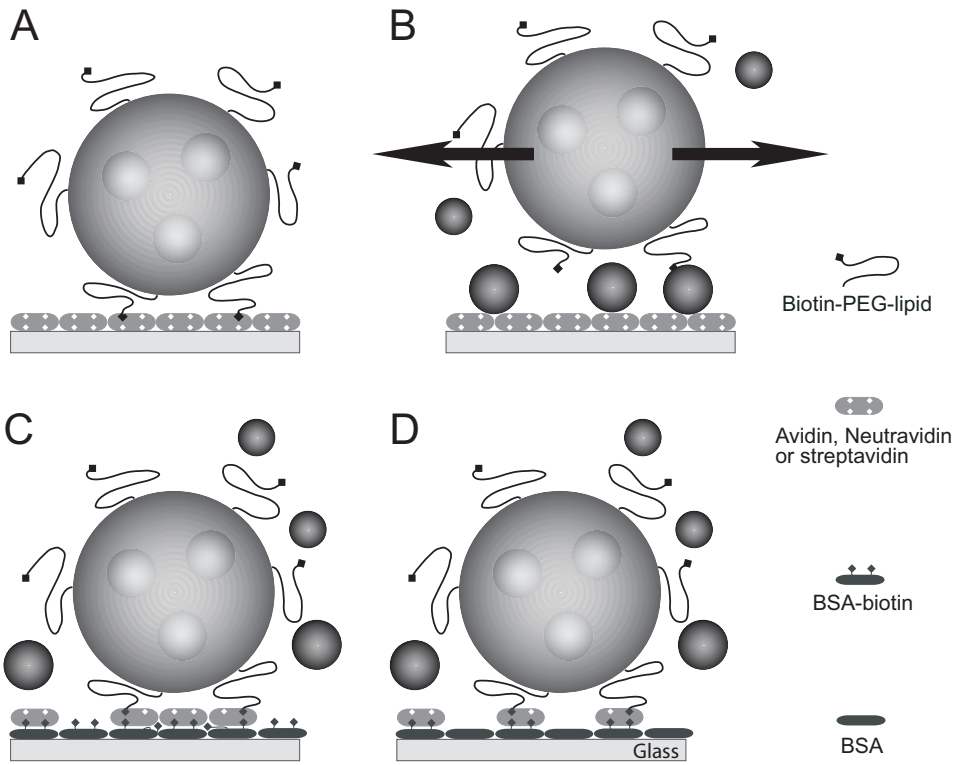

Figure 2.3: Illustration of different immobilization strategies. *(A) streptavidin adsorbed on the glass binds the biotin-PEG-lipids incorporated in the LUVs' bilayer. (B) Too many non-incorporated SUVs free in solution shield the bind to streptavidin and thereby prevent immobilization of LUVs. (C) BSA-biotin or (D) a mixture of BSA / BSA-biotin reduces the non-specific interaction of the free SUVs with the surface which increases the accessibility to the protein; the immobilization is more efficient.*

but can not replace the strong interactions needed to immobilize the LUVs on the surface.

2.5 Temperature control

2.5.1 Design and performance

The thermotropic release of reactants in integrated nanoreactor requires precise measurement and control of the temperature of the sample. A conventional water-circulating thermostat has high inertia for fast temperature change. That is the reason why a computer controlled device has been developed and adapted to a microscope table. As shown in figure 2.4, the temperature is directly measured in the solution with a small thermocouple. This temperature is communicated to the computer which regulates two Peltier elements to reach the desired temperature. Two Peltier elements (in gold on the picture, on both sides of the microscope slide) transfer the heat with an immersed silver ring (on the picture: in the center of the slide). One face of the two peltier elements is maintained at a fixed temperature with a copper ring in which water is connected to a thermostatic bath. The thermocouple placed directly inside the solution and close to the surface where the LUVs are immobilized is small (few millimeters) to increase its response time. The temperature accuracy depends on the thermometer used (DES 1303 thermometer, precision 0.1°C) and its reading value is, in addition, averaged ten times within one second by the computer.

The temperature controller is optimized to small (1ml) aqueous volumes. The Peltier elements permit to heat and cool this volume and thus rapidly control its temperature. As demonstrated in the figure 2.5A, the device responds just within 10 seconds and reaches the desired temperature after only 1 minute. As illustrated in figure 2.5B, a defined ramp of $\Delta T/\Delta t$ can be applied.

Figure 2.6 shows details of the developed interface (labview) which permits to choose between three different main modes to control the temperature. One mode offers the possibility for a certain value of temperature (Tc) to be reached as fast as possible and maintain it during the time needed. To do that, the setup was first calibrated to give the polynomial relation between the potential applied to the peltier elements and the temperature measured after the system has reached its steady state. The calibration curve is a function of the temperature chosen at the connected thermostat bath. The steady state is reached only after several tenths of minutes. To accelerate this process a so-called proportional term is added which

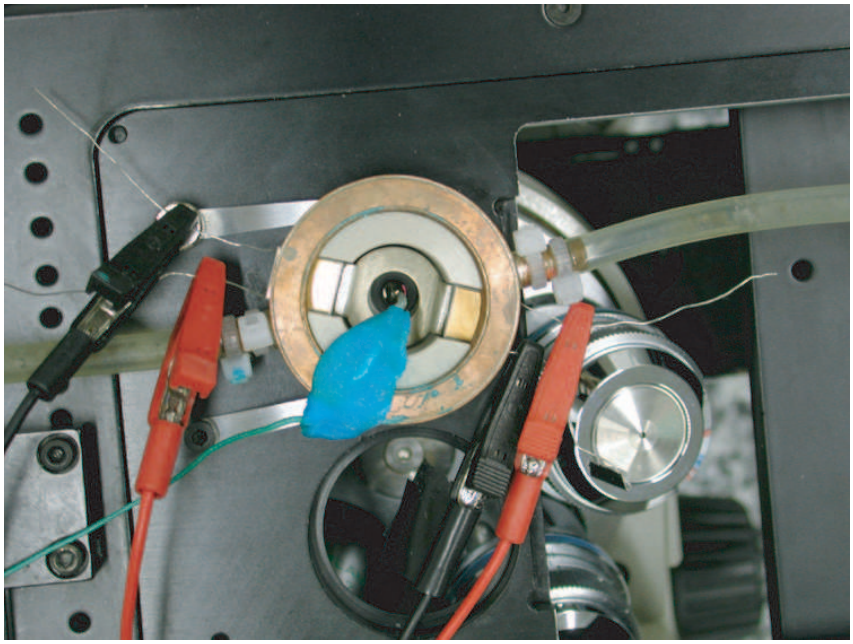

Figure 2.4: Picture of the home-made temperature controller. *The temperature is adjusted by two computer controlled Peltier elements which transfers heat into the solution via a silver ring. One side of these Peltier elements is held at arbitrary temperature by a copper ring connected to a water bath. The local temperature in the sample compartment is measured with a small thermocouple placed on the glass surface.*

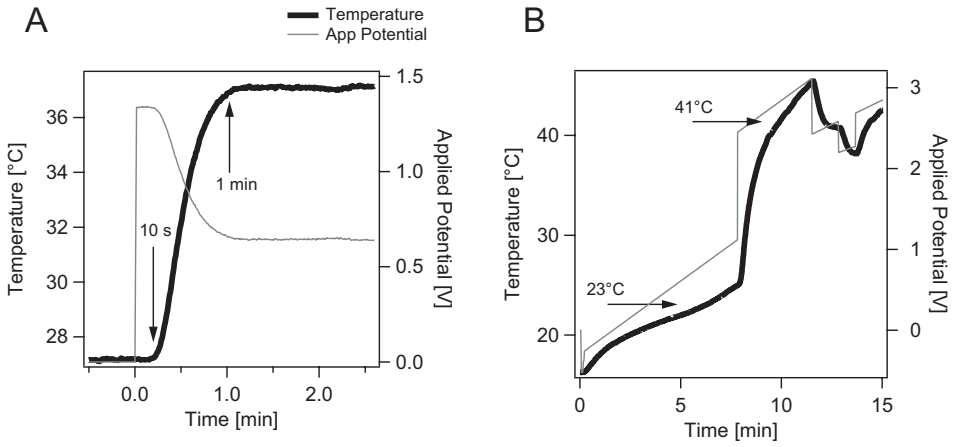

Figure 2.5: Performance of the temperature controller installed on the microscope table. *(A) Rapid (10 seconds) temperature response of sample solution. (B) demonstration of cooling, heating or following a ramp* $\Delta T/\Delta t$.

generates a tension proportional to the error (ek) between the desired temperature and the actual measured temperature according to a constant (KR) chosen in the stability limit. This proportional term not only accelerates the process but also increases the stability in correcting each time the measured temperature deviates from the desired one.

A second mode gives the possibility to follow a ramp p = $\Delta T/\Delta t$ starting at a certain temperature (Tc). This mode also needs a calibration curve to convert the temperature needed in a applied tension as mentioned above. The ramp mode offers the possibility to first jump to a certain temperature Tc and than apply a ramp which can be useful to accelerate the acquisition time.

Another simpler and fast mode is not based on the calibration curve but controls the Peltier elements only with the desired tension. That can be useful to cool down rapidly after a ramp, or variate around a certain temperature like oscillating around the temperature of phase transition for example.

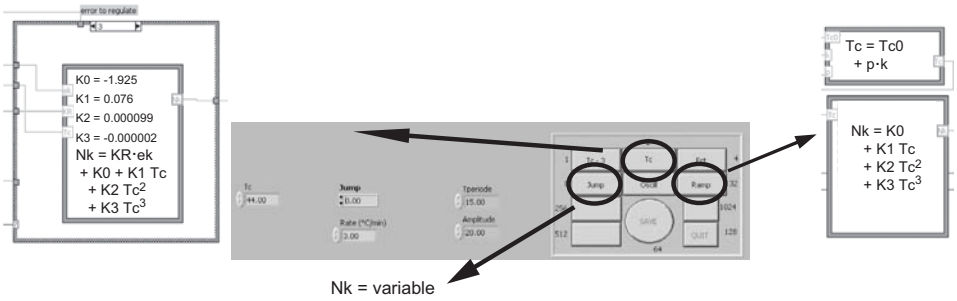

Figure 2.6: Details of the interface developed to control the temperature. *Different possibilities to control the Peltier elements which transfer the heat produced or absorbed. Three main different ways to interact, either by presetting a certain temperature to regulate and maintain, or by giving an order to follow a ramp of temperature with a certain slope or just by applying a certain tension to the Peltier elements which will generate a temperature jump (up or down).*

The device is efficient, precise and well adapted to control the temperature of the sample volume, but a practical problem is related to the difference in temperature between this special slide holder and the optical parts of the microscope. The temperature difference will cause a permanent de-focalization during heating or cooling. For the moment, the focalization is adapted manually and is the major origin of imprecisions during data acquisition with the confocal microscope but also with wide-field microscope. By using an non-immersed objective, this problem is reduced but the images obtained have less resolution.

2.6 Conclusion

This chapter gave an overview of the concept and described the methodology to produce the different nanoreactor systems. The SUVs are produced by extrusion through membrane with pores of 100 or 400 nm. The LUVs are produced more often by the hydration method yielding 2 ml of vesicle solution which is more easy to handle than the electro-swelling method. The immobilization of the reactors is obtained by interaction with biotin-PEG-lipids incorporated in the vesicle bilayer and adsorbed streptavidin or neutravidin. The SUVs non-incorporated need to be removed by micro-filtration for an efficient immobilization.

The temperature of the vesicle solution is controlled during microscopy measurements with a home-build controller composed of two Peltier elements. This temperature controller is optimized for small (1ml) sample solution and permits fast temperature changes.

Chapter 3

Release of One Dye

This chapter provides the proof of principle of the concept described in chapter 2. Before triggering confined enzymatic reactions, we first demonstrate the feasibility of mixing reactants inside LUVs. For that purpose, a specific so-called fluorescence de-quenching method is applied to the nested vesicle system.

3.1 Material and methods

The fluorescence of carboxyfluorescein (CF) is strongly quenched at high concentration. As reported in figure 3.1A fluorescence intensity decreases almost linearly when the concentration increases above 4 mM. This property is used to demonstrate the dilution of highly concentrated CF from SUVs into the lumen of LUVs. Remaining disadvantages are that CF is rapidly destructed by photo-bleaching and that fluorescence quenching increases with temperature. For example heating (27°C to 59°C) or cooling CF solutions decreases the fluorescence intensity around 10% (Figure 3.1B. The concentration induced quenching stems from the formation of non-fluorescent dimers due to homo-FRET as studied in detail in [81]. Because the fluorescence properties of CF strongly depend on the pH [82] of the solution, the aqueous solution in the present work is always buffered at to pH 7.0 generally with Tris-HCl. The well-known photo-bleaching effect [83] was not characterized in detail here.

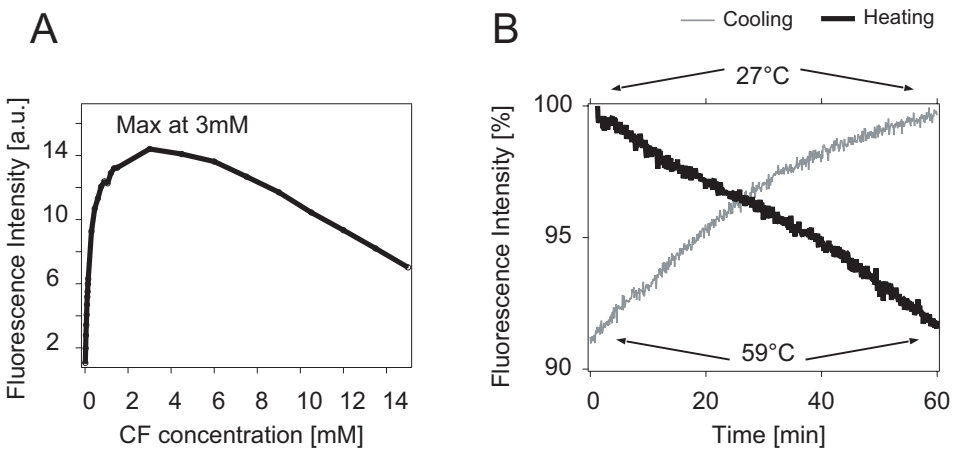

Figure 3.1: Fluorescence intensity of carboxyfluorescein as function of concentration (A) and temperature (B) (25mM CF in Tris-HCl 10 mM pH 7.0).

3.2 Release of CF from SUVs in solution

3.2.1 Temperature dependence of permeability of SUVs

The permeability properties of SUVs were analyzed in solution since this property will be of major importance to realize the proposed concept. The permeability should be high at a certain temperature in order to release enough reactants at a predefined temperature. As illustrated in figure 3.2A the fluorescence intensity of DPPC-DPPG (9:1) SUVs loaded with 25 mM of CF are measured in a fluorimeter over time as the solution is heated. The temperature scan demonstrates a maximal increase of fluorescence intensity at 41°C, which corresponds to the main phase transition temperature Tt of DPPC-DPPG. At Tt, 50% of the lipid molecules are in so called gel phase and 50% of them are the in so-called liquid-crystalline phase. The increase in permeability is well known and due to the mismatching between the lipids in different phases ([84] and chapter2).

The calorimetric properties of the same (DPPC-DPPG 9:1, loaded with 25 mM of CF in 10 mM Tris-HCl) SUVs preparation is reported in figure 3.2B. The data are obtained by differential scanning calorimetry (DSC) which gives informations about the thermodynamics of lipid membranes. In a DSC, a sample (SUVs dispersion) and inert reference (buffer) are heated independently to maintain an identical temperature in each. This technique measures the heat needed for the endothermic gel-to-liquid crystalline bilayer transition, for example, required in excess over the heat required to maintain the same temperature in the reference.

A heat capacity peak is observed at 41.8°C which is close to 41°C for pure

DPPC, begins at 38°C and is quite broad (2°C at half peak height). This breadth is caused from the lipid mixture (DPPC and DPPG) ([84]; The same acyl chains are mixed ideally together but the difference in polar head groups could induce thermodynamic perturbations due to (electrostatic-) interactions between different lipids. A closer analysis of the SUVs permeability 3.2A exhibits a maximum intensity increase before this phase transition temperature Tt. The reason could come from the broadness of the transition caused which implies a large proportion of lipids in the liquid-crystalline phase even before Tt.

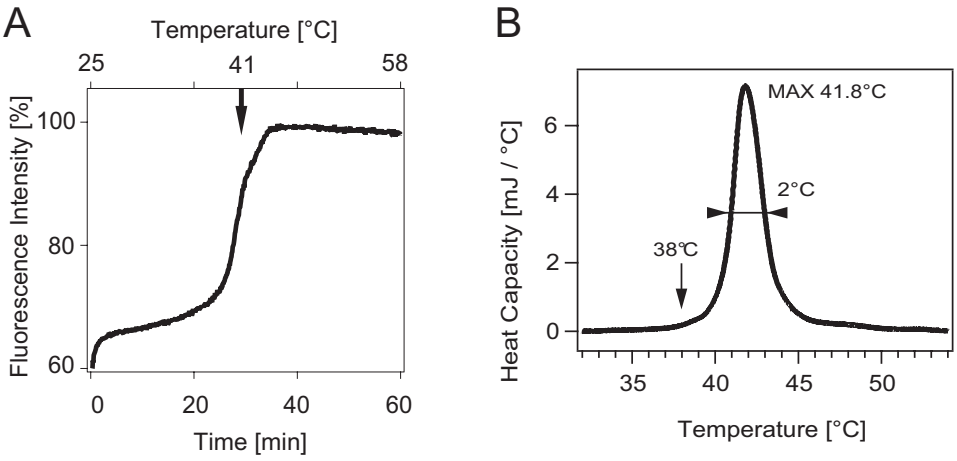

Figure 3.2: Behavior of SUVs loaded with high concentration (25mM) of CF exposed to temperature change of 35 °C/60min. *(A) Time course of fluorescence intensity of CF entrapped in DPPC-DPPG (9:1)(5 mg lipids/ml) 210 nm sized SUVs in buffered (Tris-HCl 10 mM pH 7.0) solution. The fluorescence intensity increase is maximal at Tt = 41 °C. This fluorescence increase is due to the de-quenching of the CF released into the bulk. (B) Differential scanning calorimetry (DSC) of the same sample in the same buffer solution yielded a lipid phase transition at 41.8 °C and a width of 2 °C at half peak height.*

3.2.2 Analysis of different SUVs

Different SUVs were tested composed of different lipids, buffer, extrusion pore sizes. The table 3.1 summarizes the relative fluorescence intensity changes $\Delta I/I$ induced by the lipid phase transition of different vesicle preparations. From this table, two main conclusions can be drawn for the rest of this work. (i) Larger SUVs (extruded) give a higher response, probably due to the higher amount of molecules entrapped. (ii) Thinner bilayers like DMPC compared to DPPC have larger permeability as observed also by others [68]. But DMPC is practically more difficult to handle due to its Tt really close to room temperature. This lipid will be used later but only in

one specific case.

Table 3.1: Release of CF from SUVs in solution. *5 mg lipids/ml, 25 mM CF, ex. 480 nm, em 520 nm, slits 1.0 nm with gray filter, 1 × 1 cm^2 quartz cuvette. Data obtained with a SPEX fluorimeter*

Type of vesicle	**Lipid used**	**Buffer**	**Intensity increase $\Delta I/I_{max}$**
Sonicated ∼50nm	DPPC	PBS	**13**
Sonicated ∼50nm	DMPC	PBS	**26**
Extruded ∼250nm	DPPC	PBS	**35**
Extruded ∼250nm	DPPC	Tris-HCl	**62**
Extruded ∼250nm	DPPC	Tris-HCl, sorbitol 100 mM	**63**

3.3 Data treatment of time series of images of LUVs

To measure the release of FC from SUVs encapsulated in LUVs, it is necessary to monitor and localize the fluorescent intensity with microscopic techniques. The confocal microscope is chosen because it enables to visualize a planar cross-section of controlled optical thickness. This offers the advantage to analyze only those vesicles which are immobilized on the glass slide surface. This excludes any fluorescence which arises from moving vesicles in the bulk solution.

To analyze the time series of the microscopic images, two major procedures are used here. (i) The first one determines, with the software provided with the Zeiss Confocor microscope, the average intensity inside a specific area of interest. As shown in figure 3.3A on the right-hand-side, in the case of a spherical vesicle, a circular area is drawn defining the region of interest; the software then calculates the average fluorescence intensity in this area. For time series, these average intensities are reported in table 3.3A. (ii) The second procedure, determines automatically regions with intensity above a chosen threshold (figure3.3B). In that way, each area (representing LUVs) is highlighted from the background and the tracking software (Imaris from Bitplane AG) calculates automatically the fluorescent characteristics for all those surfaces at same time and for each time point.

The major advantages of the second automated procedure is the ability to quickly analyze a high number of LUVs present in the focus and an additional possibility enables to track the area in the X and Y directions, which is important when the variation of temperature creates a displacement of the surface supporting

the LUVs. In the case of time series showing a fluorescence intensity increase, the threshold (constant for each time points) should be carefully chosen. A too high threshold will eliminate weak intense LUVs at early time points, and too low threshold will generate overlapping of LUVs close to each other. The first procedure is not dependent on any threshold and gives the intensity in the chosen area; but when the LUVs are moving, this area needs to be manually repositioned during time. This disadvantage makes the first procedure very laborious for analyzing large numbers of LUVs.

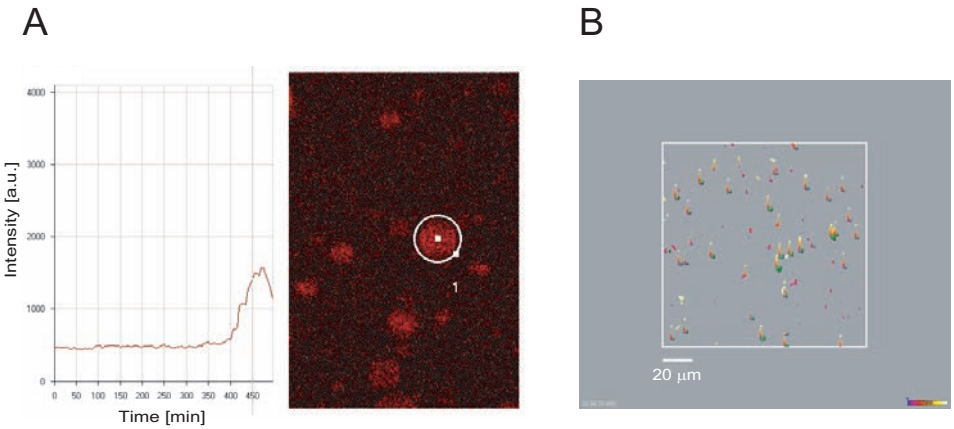

Figure 3.3: Two different possibilities to analyze the time series of images of LUVs taken with the confocal microscope. *(A) Average fluorescence intensity calculated over a defined area (white circle manually positioned and adjusted) using the Zeiss Confocor image treatment software. (B) Tracking analysis with the Imaris software. Each region with an intensity higher than a chosen threshold is tracked during all time points. This figure shows the automatically selected regions on the image at the beginning (t0) and the tracked displacement with time (blue color at t0 to yellow color at last time point).*

3.4 Results and discussion

To evaluate the feasibility of the concept (release cargo from SUVs into LUV), SUVs loaded with high concentration of CF and already characterized in solution are incorporated inside LUVs. The results are presented in the following figures. First fluorescence confocal microscopy in figure reveal a low average fluorescence intensity per immobilized LUV originating from diffusing CF-loaded SUVs (figure 3.4A). Thermotropic release and subsequent dilution of CF into the LUVs reduces self-quenching and increases fluorescence, (Figure 3.4B). This figure demonstrates that the quality of confocal microscopy images is well adapted to analyze and monitor

the release processes occurring in the lumen of LUVs.

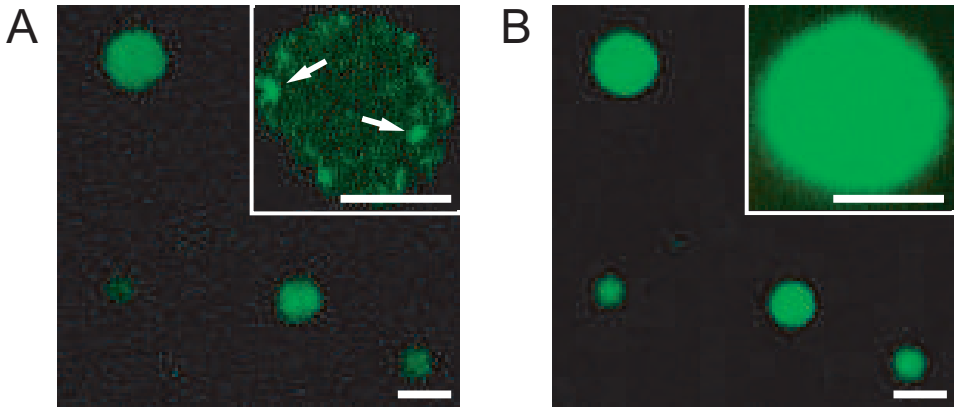

Figure 3.4: Principle of temperature-induced release and mixing of watersoluble molecules in the interior of immobilized LUV reactors. *(A) Confocal fluorescence microscopy (LSM 510, Zeiss) of LUVs immobilized on glass. At a concentration of 50 mM, the fluorescence intensity of carboxyfluorescein (CF) inside the SUVs is low due to self-quenching. Here, intensity was digitally enhanced to enable vesicle visualization. Inset: higher magnification of a LUV allows identification of SUVs (white arrows). (B) Increase of the temperature from 25 to 45 °C causes release of the dye, which is then diluted. This is monitored as a sharp increase in the fluorescence intensity of all LUVs under observation. Inset: increase of fluorescence is uniform over the whole vesicle. All scale bars are 5 μm.*

From a time series of these images at different temperatures a detailed analysis was extracted and is presented in figure 3.5. Figure 3.5 A depicts a typical fluorescence intensity scan across a single 2 μm diameter vesicle (total volume 4 fL). Figure 3.5 B shows the time course of fluorescence intensity for two different reactors (2 and 10 μm diameters) whose intensity increases 2.5 fold during a temperature scan through the ordered-fluid phase transition of the SUVs. The increase of the mean fluorescence is maximal at 41 °C, the Tt of the SUVs. The temperature dependance of the fluorescence intensity revealed a transition width of 3 °C and a half time of release of $\sim$1 min. Despite the tendency of CF to decrease its fluorescence with temperature by dynamic quenching and with time by photo-bleaching (explained in the previous section), these results prove that the self-quenched dye is released from the loaded SUVs at Tt but remains confined in the interior of the larger vesicle. As shown by the stable baseline in figure 3.5 A, and a constant intensity after release for a least 4 minutes in figure 3.5 B, all the released compounds are retained in the reactor.

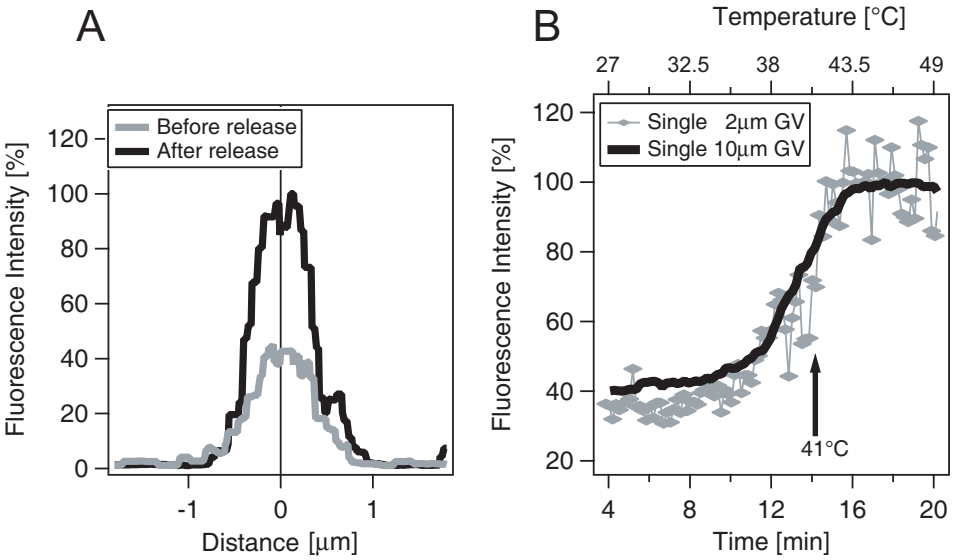

Figure 3.5: Thermotropic phase transition-induced release of CF inside LUVs. *The values of both graphs were extracted from fluorescence confocal microscopy images. (A) Fluorescence intensity profile across a 2 µm diameter LUV at 25 °C (grey) and after an increase of the temperature to 45 °C (black), 4 °C above the phase transition temperature of the lipid bilayer. (B) Time course of the increase of the mean fluorescence intensities of two single LUVs during a continuous temperature scan (1.5 °C/min). The point of inflection is very close to the Tt = 41 °C of the SUVs. During the temperature scan, the confocal plane had to be manually adjusted to compensate for the thermal expansion of the sample holder. Proper alignment is more critical for the 2 µm vesicle than for the 10 µm vesicle, resulting in an increase of experimental noise.*

3.5 Statistical results

For a specific application of the system developed here, for example statistical characterization of the activity if a small number of confined enzymes in compartments similar to biological cells, one would like to obtain small variation in the final concentration of released reactants. This variation in concentration of the released compound can be related to the variation of fluorescence intensity per individual LUV. This was analyzed for about 300 LUVs by calculating histograms of mean intensity per LUV before and after release as depicted in figure 3.6.

The histogram depicted in figure 3.6 is obtained as follow. From images with a good resolution (1024×1024 pixels) the mean fluorescence intensity of every LUV is reported before and after CF release within different images. The identity of the LUVs is not taken into account. The number of LUVs analyzed before release is less than the number of LUVs after release. This difference results from LUVs originally diffusing in the bulk solution becoming immobilized on the surface after the heating process. Priority is given to evaluate a maximal number of LUVs in order to have sufficient data for each histogram.

For comparison, the variation of the fluorescence increase between identical vesicles is shown in the insert of figure 3.6 for 61 identified LUVs. The major result of this statistical analysis is that the intensity has a standard variation between each individual LUVs of 62% before heating and 66% after heating with a fluorescence increase factor per reactor of f = 2.3. This factor f and its variation is a direct measure of the dilution ratio and depends mainly on (i) the number of encapsulated SUVs and (ii) the reproducibility of the release process efficiency. The standard variation of 62% before release comes certainly from a difference in the number of loaded SUVs per large vesicle, which, at the moment, is limiting the performance of the device.

From a calibration curve (fluorescence intensity of CF versus concentration), a 10fold dilution leads to a 2.3 fold fluorescence increase. These results enable to evaluate the average number of SUVs per LUV. In order to reach a tenfold dilution, the number of SUVs per LUV must be $V_{LUV2\mu m}$ $/(10 \cdot V_{SUV210nm}) = 70$, which corresponds to a concentration of 18 SUVs/fL.

3.6 Analysis at low SUVs concentration

At certain condition, when the number of SUVs incorporated in LUVs is low, the dilution of CF is too high which results in a constant average intensity over the

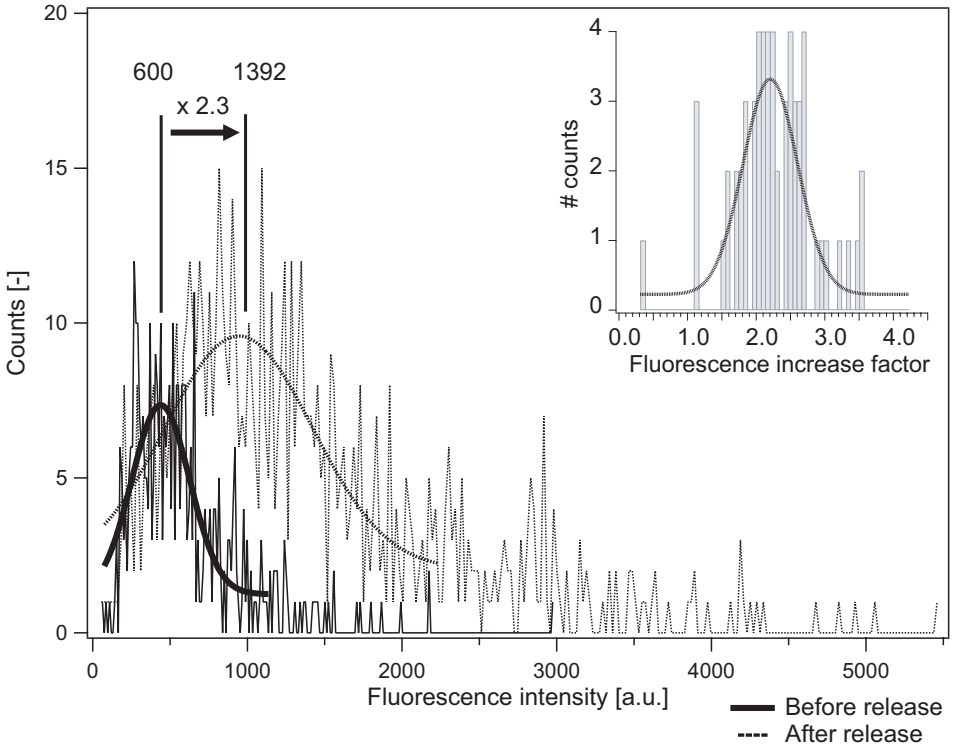

Figure 3.6: Histogram of mean fluorescence intensity per LUV before and after heating. *The histogram in black represents the mean intensity for about three hundred LUVs before heating. The histogram in gray reports the mean intensity which increases after heating by release and dilution. The average intensity is calculated; 600 [a.u.] with 62% of standard deviation before and 1392 [a.u.] 66% of standard deviation after release, which corresponds to a fluorescence intensity increase by a factor of f=2.3. The inset reports a histogram of the gain factor (mean intensity after divided by mean intensity before) of 61 LUVs analyzed individually by the tracking method. This analysis gives an average gain of 2.25 [a.u] with 57% of standard deviation which is close two the none-tracking method presented above.*

entire LUV. In that specific case, the release of reactants can not be measured in the same way as presented previously by reporting the mean intensity. As shown in figure 3.7 (A) and (B), before release (at time 9.2 min) the confocal images reveal the presence of bright SUVs which give an heterogenous intensity inside the LUVs. After release (at time 16.6 min) the fluorescent molecules are no longer retained in the SUVs but diffuse in the lumen of the LUVs and give a more homogenous distribution of intensity. Under this specific condition, the release can be demonstrated quantitatively by building histograms of fluorescence intensity at different times as shown in figure 3.7 (C) and (D). Before the release, the heterogeneity give two populations; one sharp corresponding to the background between intensity 0 and 10 [a.u.] with around 145 counts and another wide distribution of counts corresponding to the SUVs which cover all the possible intensities up to the maximum at 4096 [a.u.]. After release the histogram is more homogenous, the intensity between 0 and 10 [a.u.] reports only 8 counts and the second distribution of counts less extended without any counts above 3000 [a.u.]

3.7 Optimization test

The group of Prof. D. Needham [67] has published a procedure to enhance the permeability at the lipid phase transition of vesicles by incorporating in the bilayer monoacyl chain lipids (MPPC: stucture depicted in figure 3.8B). They interpreted this finding by the formation of pores stabilized by lysophospholipid molecules at grain boundary regions within the lipid bilayer at the phase transition temperature. This enhancement procedure was adapted and tested for SUVs in solution but also inside LUVs; the results are illustrated in figure 3.8.

Figure 3.8 A shows that no substantial enhancement for SUVs (containing MPPC; $\Delta I/I_{MAX} = 70\%$) in solution was observed compared to previous results (3.1 $\Delta I/I_{MAX} = 63\%$). It also demonstrates that a release starts already at 35°C which could prevent an efficient trigger at Tt. The test with SUVs inside LUVs shows that there is release without perceptible improvement compared to previous results 3.8 (C). The confocal microscopies of figure 3.8 (C) and (D) exhibit a certain shape deformation of the LUVs during heating. The deformation stems from the presence of the monoacyl-chain lipid in the bilayer and in the surrounding solution. According to the outcome of these experiments the we decided not to use MPPC for the rest of the work.

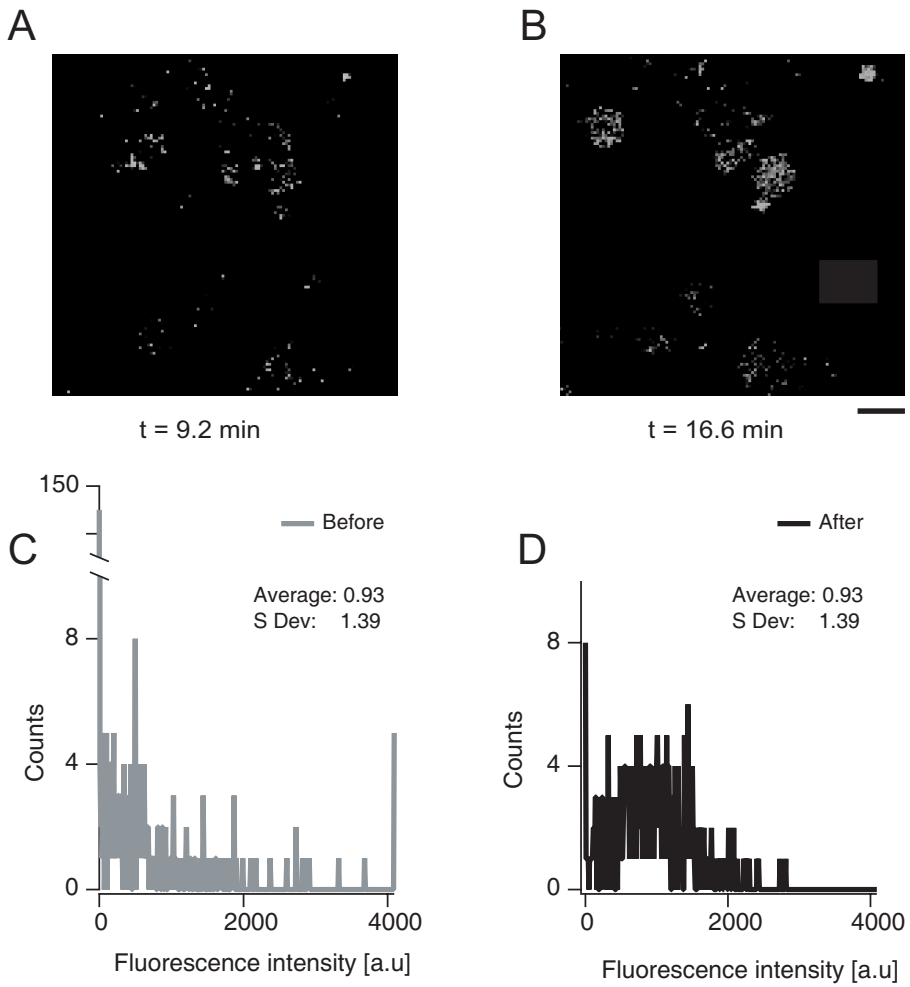

Figure 3.7: Temperature-induced release and mixing of CF in LUVs. *(A)+(B) Confocal fluorescence microscopy of LUVs immobilized on a glass slide. Compared to figure 3.4, the concentration of SUVs is here lower which yields heterogenous spotlike intensity distribution inside the LUVs at time 9.2 min also reflected by the intensity histogram in (C). After heating to 41°C at time 16.6 min, the mean fluorescence intensity remains almost constant but the interior of the LUVs becomes more homogenous as demonstrated with the histogram (D). Scale bar is 5 μm.*

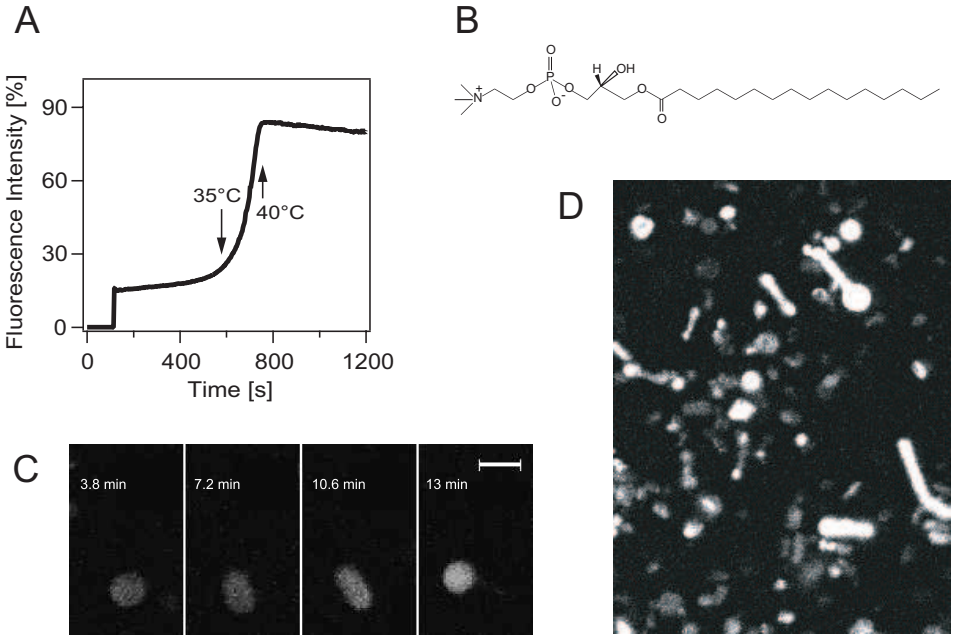

Figure 3.8: Release enhancement by incorporating a monoacyl lipid MPPC in the bilayer of SUVs. *(A) Fluorescence time course of SUVs loaded with 25 nM CF in buffered solution. DPPC:DPPG:MPPC:PEG-PE (9:1:1:0.4, buffer solution: Tris-HCl 10mM + MPPC 2 μM, pH 7,0.) (B) Chemical structure of MPPC (1-Palmitoyl-2-Hydroxy-sn-Glycero-3-Phosphocholine). (C) Confocal microscopy images of SUVs incorporated in a single LUV (DOPG:Biotin-PEG-lipid:TRITC-DHPE 100:3:1) at different times during temperature increase and (D) for many different LUVs, illustrating the deformation of vesicle shape due to MPPC.*

3.8 Conclusion

The results shown and discussed in this chapter demonstrate that it is possible to release on-demand reactants in single ultra-small containers which could be exploited in a parallel format without micro-manipulations. By applying the fluorescence dequenching procedure combined with confocal microscopy, the release of reactants was proved by an increase in fluorescence intensity localized inside the immobilized LUVs as the CF was diluted from SUVs. The impermeability of the container was also observed as the intensity remains constant for several minutes. These proofs are valuable as long as they are opposite to photo-bleaching and dynamic-quenching. From results of hundreds of LUVs, the system demonstrates an ideal release process but also a relatively high standard variation 62% between each LUV, in the concentration of encapsulated SUVs which could limit its performance.

Chapter 4

Confined Enzymatic Reactions

4.1 Introduction

As presented in the introduction chapter, several articles have reported different systems to perform enzymatic reactions in confined volumes either in micro-fabricated devices [56, 86], multiple emulsion droplets [40], in lipid networks [39, 87] or within single vesicular reactors [88, 89] using micromanipulation systems.

This chapter concentrates on the possibility to trigger enzymatic reactions in multiple individual vesicular reactors of ultra-small volumes, down to femtoliters (10^{-15} L). Using the nested vesicular system presented in the previous chapter, enzymatic reaction kinetics were studied simultaneously in many different LUVs. Up to now, the effect of confinement on the enzyme activity compared to bulk activity could not be quantified in detail due to technical limitations.

4.2 Materials and methods

4.2.1 Concept

The general concept is the same as outlined in chapter 2, with small variations. Figure 4.1 illustrates the strategy and explains how a large lipid vesicle can act an "integrated" reactor with all the reactants present in its interior. The SUVs loaded with substrates are encapsulated together with the enzyme (black star) inside the immobilized LUVs. Initially, the substrate (blue color) is isolated from the enzyme inside the SUVs. The enzymatic reaction is initiated when the substrate is released (gray arrow) from the SUVs into the LUV by shifting temperature, which finally yields a fluorescent product (green color).

Confocal microscopy is used to localize the reactors immobilized on the glass slide and to monitor the reaction. In order to monitor the enzymatic reaction by fluorescence, substrates are required that change their fluorescent properties during their enzymatic transformation.

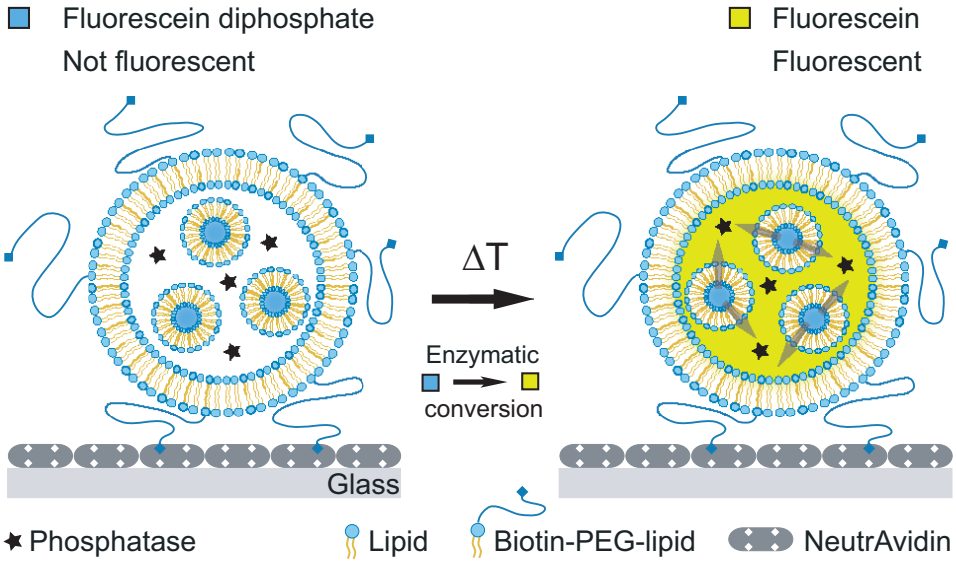

Figure 4.1: Principle of temperature-induced substrate release and subsequent enzymatic reaction in the lumen of an immobilized vesicular reactor. *SUVs loaded with a substrate are incorporated together with an enzyme (black star) in LUVs. The enzymatic reaction is triggered inside the LUVs when the substrate is released from the SUVs by a shift of temperature.*

4.2.2 Enzyme substrates

Commercially available substrates and enzyme (alkaline phosphatase (PP2A) from Amersham Bioscience) were chosen with particular attention for the excitation and emission properties that need to match the characteristics of excitation laser lines and emission filters of the microscope. The phosphatase substrates used are shown in figures 4.2 and 4.3.

Fluorescein diphosphate (FDP, from Molecular Probes) is a derivative of fluorescein containing two phosphate groups eliminating electronic resonance, and thus it is non-fluorescent. FDP carries four negative charges at pH 7.0. As shown in figure 4.2 The enzyme alkaline phosphatase interacts with this substrate and cleaves its phosphate groups in two steps yielding the highly fluorescent product fluorescein (excitation maximum at 480 nm, emission maximum at 520 nm).

The second phosphatase substrate used is 9H-(1,3-dichloro-9,9-dimethylacridin-

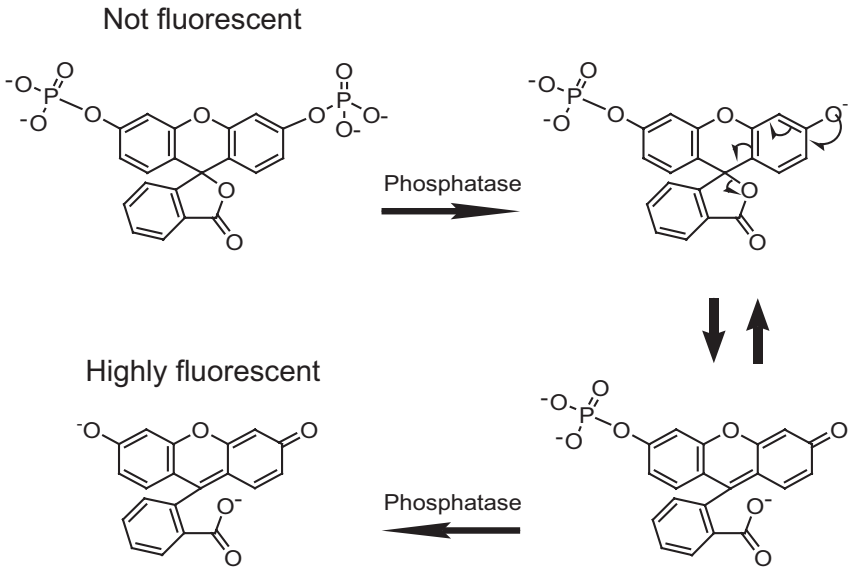

Figure 4.2: Transformation of non fluorescent substrate fluorescein diphosphate (FDP) into the highly fluorescent product fluorescein by the enzyme phosphatase (excitation 480 nm, emission 520 nm).

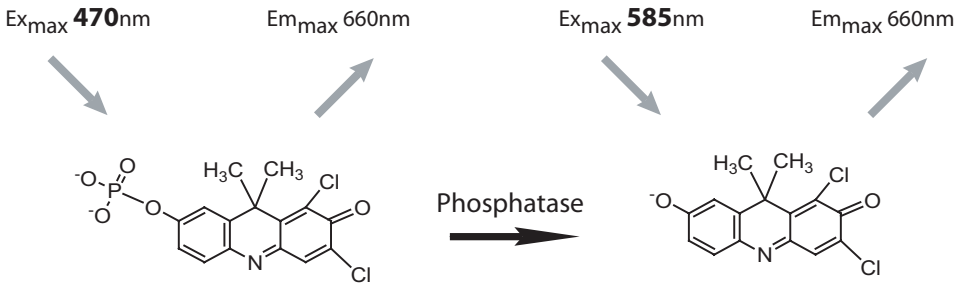

Figure 4.3: Transformation of substrate 9H-(1,3-dichloro-9,9-dimethylacridin-2-one-7-yl) phosphate (DDAO phosphate). *Before reaction with the enzyme, DDAO phosphate has an excitation maximum at 470 nm and emission maximum at 660 nm. After enzymatic cleavage of the phosphate ester bond the product DDAO has an excitation maximum at 585 nm and an emission maximum at 660 nm.*

2-one-7-yl) phosphate (DDAO phosphate) shown in figure 4.3, from Molecular Probes. This molecule carries one phosphate group and two negative charges at neutral pH, is fluorescent before and after its transformation by the enzyme with a change of the excitation spectra (excitation at 470 nm before and 585 nm after enzymatic reaction, with an emission maximum at 660 nm in both cases). This facilitates the localization of loaded LUVs before reaction and gives the opportunity to better select the observation area.

4.2.3 Enzymatic reaction kinetics

Michaelis and Menten [90] proposed a simple model to describe the enzymatic reaction kinetics with the following reaction scheme:

$$E + S \rightleftharpoons ES \rightarrow E + P \tag{4.1}$$

E represents the enzyme, S the substrate and P the product and ES an intermediate enzyme-substrate complex.

Related to this scheme, figure 4.4A describes theoretically the evolution with time of the concentration of different components during an enzymatic reaction. When the reaction is initiated and as the product concentration [P] is very low, the concentration of enzyme-substrate complex [ES] and product [P] increases with time during the pre-steady state and the substrate concentration [S] decreases. After a certain period of time, a steady-state is reached during which [ES] remains constant, [P] increases and [S] decreases. Finally, the equilibrium might be reached where no further concentration changes occur.

Assuming that free enzyme and substrate are in equilibrium with their ES complex, the following is valid when all active sites of the enzyme are identical and independent, and the substrate or product act not as inhibitors or activators [92]:

$$E + S \rightleftharpoons ES \tag{4.2}$$

and the kinetics of enzymatic reaction can be characterized by the Michaelis-Menten equation:

$$V_0 = V_{max} \frac{[S]}{[S] + K_M} \tag{4.3}$$

With this equation the initial reaction rate V_0 (figure 4.4B), can be estimated in a first approximation by the maximal velocity V_{max}, the substrate concentration [S] and the Michaelis-Menten constant K_M. This constant is a property of a particular enzyme-substrate couple and is independent on their concentrations. With

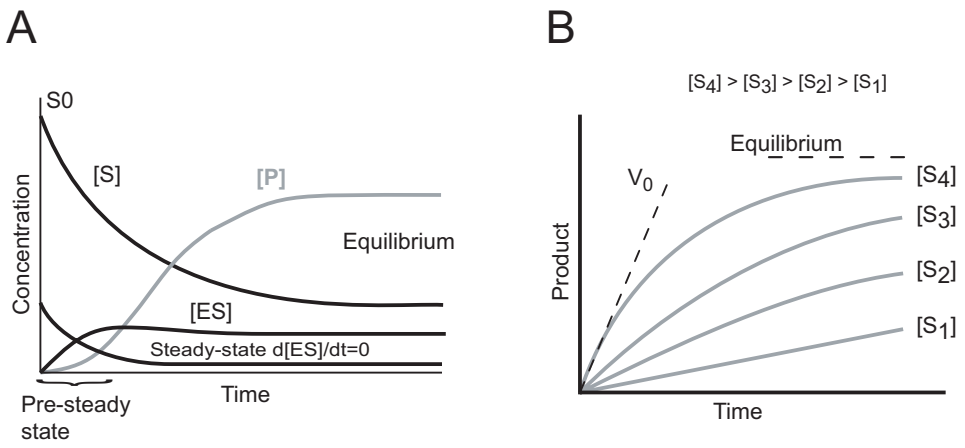

Figure 4.4: Changes of the concentration of reactants during an enzymatic reaction (from [91]). *(A) Concentration of substrate [S], enzyme-substrate complex [ES] and product [P] at pre-steady-state period and steady state. (B) Changes of product concentration with time at different initial substrate concentrations. This figure shows also how to determine the initial reaction rate V_0.*

PP2A, the K_M of DDAO phosphate and FDP is around 0.2 [μM]. The equation describes the initial reaction rate only when the product concentration is low and thus the back reaction can be ignored. From this equation one can easily distinguish two theoretical extreme conditions: (i) at very low substrate concentration, [S] $\ll$ K_M the reaction rate is directly proportional to [S]/K_M as in the case of [S1] in figure 4.4B; (ii) at high substrate concentration, as in the case of [S4] in figure 4.4B, [S] $\gg$ K_M, the rate is equal to V_{max} and independent of [S].

In addition to concentration dependence, the activity of an enzyme depends also on the pH and temperature. The activity of PP2A was checked from 20 up to 60°C and the pH was maintained constant with buffer for each experiments.

4.3 Test with small vesicles in solution

Triggering an enzymatic reaction by the release of substrate from SUVs has, in my knowledge, never been published before. In order to investigate the different experimental conditions (permeability of substrate, concentrations, lipid composition, etc.), the concept is first tested in bulk solution. Thus, the substrate is encapsulated in SUVs and the enzyme is added to the surrounding buffer before heating the whole solution. This is also useful to verify the fluorescent properties of the substrate and its corresponding product.

4.3.1 Reaction with the substrate DDAO phosphate

For DDAO phosphate, the chosen conditions are the following:

1. The initial encapsulated concentration of the substrate used during the SUVs preparation is 0.5 mM.

2. The surrounding concentration of enzyme is 0.47 [units/mL] (1 Unit corresponds to 1 μmole of substrate transformed in 1 min). Both concentrations are relatively high to reach a fast response after release, facilitating microscopic monitoring.

3. The lipid is DMPC because it exhibits a better response than DMPG or DPPC. This certainly results from a better loading efficiency of DDAO phosphate in DMPC than in DMPG vesicles as observed during production of vesicles but it is not quantified further. In addition, DMPC shows a better release of substrates than DPPC probably due to its shorter acyl chain length [68].

4. The buffer is Tris-HCl 10 mM, pH 7.0.

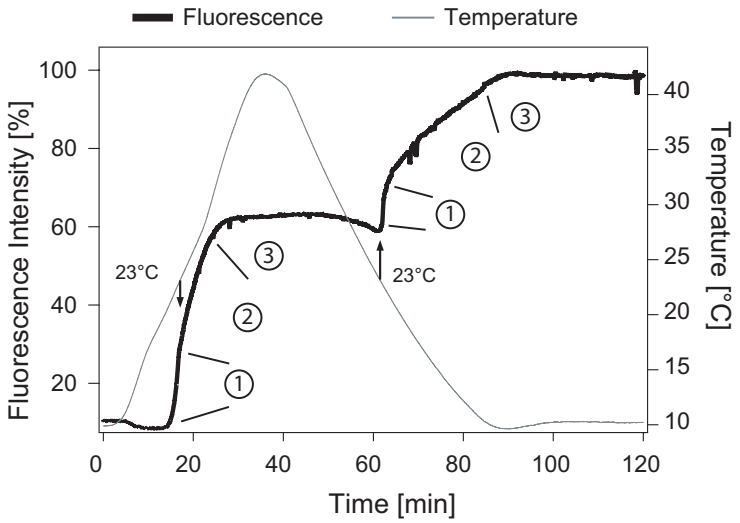

Figure 4.5: Phosphatase enzymatic reaction triggered by release of DDAO phosphate from DMPC (5mg/ml) SUVs in bulk solution observed by the appearance of a fluorescent product. *Time course of fluorescence intensity (thick black curve) of DDAO (Ex 585 nm, Em 660 nm). Fluorescence increases due to the transformation of the released DDAO phosphate (initial concentration is 0.5mM) into DDAO by PP2A (0.47 [Units/mL]) present in the buffer solution. The numbers correspond to the different stages of reaction rate. The corresponding solution temperature in the 1 × 1 cm^2 cuvette is reported by the thin gray curve (right hand side).*

Figure 4.5A reveal several important points. The first one is the two step fluorescence increase near 23 °C (by DSC, Tt varies between 23 °C [72] (heating) and 24 °C [84]) (cooling). This demonstrates that the bilayer permeability increases substantially at the phase transition temperature of the lipid. It demonstrates also the fact that the vesicles remain intact during the temperature scan. It is important to analyze in detail this curve since it reflects the product concentration variation with time and thus the reaction kinetics. This curve exhibits a particular time course, compared to enzymatic reactions in solutions figure 4.4B, both during heating and cooling. Three main "stages" can be distinguished. The main reason of this particular time course comes from the variation of substrate concentration with time. Effectively, in parallel to its enzymatic transformation, a quantity of fresh substrate is added during its release from the SUVs. Some explanations of this complex reaction kinetics can be given by the experimental release time course which follows a sigmoidal shape as shown in figure 3.2A and with the concept explained above in figure 4.4B.

1. The first step is characterized by a fast increase in product concentration which remains constantly fast for a few minutes. That could be explained by a fast release of high amount of substrate into the bulk which reacts rapidly with the enzyme as expected from figure 4.4B for [S4].

2. The second step shows a slower reaction rate, as the substrate release is slower , nearly linear with time. The time at which the reaction rate starts to decrease corresponds to the inflection point in the sigmoidal release curve in figure 3.2A. The reaction may reach another regime dependent on [S] similar as between [S3] and [S1] in figure 4.4B, where the rate decreases but still maintained constant with continuous release of substrate.

3. In the final stage, the release of substrate stops, the product formation decreases slowly and finally reaches a maximal, constant product concentration.

Interestingly a similar reaction rate is observed during heating as during cooling with small differences arising from the different amounts of initially encapsulated substrate. The amount of substrate release after the first phase transition is 1.5 times higher than that after the second release transition due to different concentration gradients between inside the SUVs and the bulk.

4.3.2 Reaction with the substrate FDP

For the second phosphatase substrate FDP, the conditions are slightly different as for DDAO phosphate:

1. The initial encapsulated concentration of the substrate used during the SUVs preparation is also 0.5 mM.

2. The surrounding concentration of enzyme is 0.4 [units/mL] (1 Unit corresponds to 1 μmole of substrate transformed in 1 min). Both concentrations are relatively high to reach a fast response after release facilitating the microscopic monitoring.

3. The lipid is DPPG whose negatively charges headgroups prevent aggregation.

4. The buffer is 10 mM Tris-HCl, pH 7.0.

In a first step, the release and reactivity conditions are tested with the enzyme in the vesicle-surrounding bulk solution. The obtained results are presented in figure 4.6.

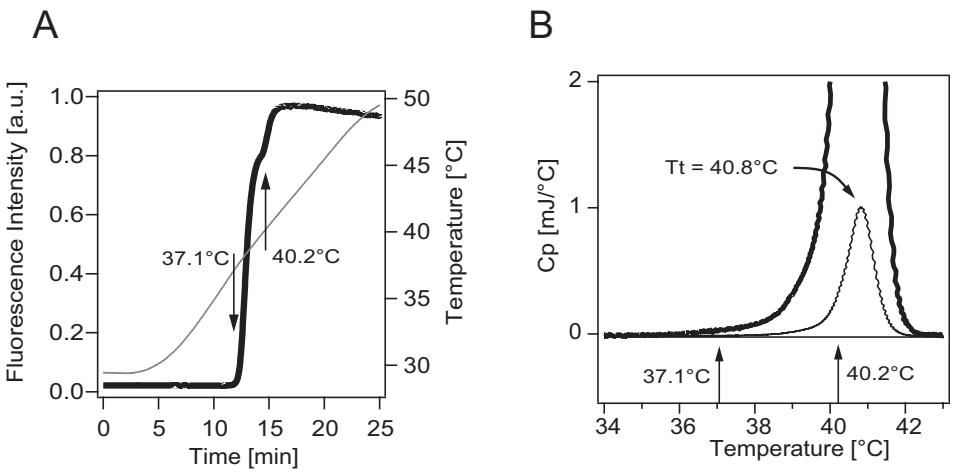

Figure 4.6: FDP released from lipid vesicles reacts with phosphatase in bulk solution. *(A) A suspension of DPPG SUVs (5 mg/ml DPPG containing 0.5 mM FDP in 10 mM Tris-HCl buffer at pH 7.0.) and PP2A enzyme in bulk solution concentration is 0.4 [units/mL]), is heated in a 1 × 1 cm^2 cuvette, from 29 to 50 °C (around 2 °C/min; gray line). The sample is continuously excited at 480 nm and the emission measured at 520 nm (black solid line) inside a fluorimeter. At 37 °C and at 40 °C the emitted light intensity increases stepwise due to the release of FDP from the DPPC vesicles and the subsequent enzymatic production of fluorescein from FDP outside the vesicles. (B) Differential scanning calorimetry (DSC) of DPPG SUVs containing FDP under the same conditions as in (A).*

The reaction rate is different to the one observed with DDAO phosphate which arises from the difference in chemical structure of FDP. The curve obtained in figure 4.6A exhibits also a particular shape reproduced several times with different samples. It reflects a two step release, one at 37.1°C and another one at 40.2°C. It is important to note that reactions performed in solution without vesicles give normal reaction rates without steps. Differential scanning calorimetry (DSC) showed that the main lipid phase transition occurs at 40.8°C starting gently at 36°C (figure 4.6 B).

Obviously, the first substrate release coincides with the calorimetrically detected onset of the phase transition, which is actually very close to the so-called pretransition detected at 35°C in non-sonified DPPG lipid multilamellar membranes [84]. The second substrate release is very close to the center of the calorimetrically determined phase transition.

4.4 Enzymatic reactions inside of LUVs

4.4.1 Using FDP as substrate

Here results are reported on triggering enzymatic reactions in the lumen of micrometer-sized LUVs applying the strategy presented in figure 4.1 at the beginning of the chapter. The two enzyme-substrate reactions investigated are those described previously. The lipid mixture of the LUVs is the same as that used for the CF dilution experiments presented in chapter 3. Figure 4.7 shows the proof of principle for the FDP substrate.

Figure 4.7A shows confocal microscopy images of LUVs immobilized on a glass plate before (left hand side; 0.5 min, ∼30 °C) and after (right hand side; 8.5 min, ∼45 °C) the reaction of phosphatase enzyme with FDP, released from the SUVs inside of the LUVs. The fluorescence intensities are given on the vertical axis in color code.

Figure 4.7B shows the confocal fluorescence microscopy cross-section of two immobilized LUVs before (left hand side) and after (right hand side) enzymatic reaction. The scale bar represents 10 μm. The lipid mixture of the SUVs is DPPC:DPPG (9:1) which apparently enhances enclosure of the SUVs into the lumen of the LUVs.

Figure 4.7C depicts the time course (= temperature dependence) of the fluorescence intensity (i) of a single LUV (black line), and (ii) averaged over 31 LUVs (gray line). As expected from previous results (figure 4.6), the substrate release starts a few degrees below the lipid phase transition temperature Tt. However, intensity increase in individual vesicles is much smaller (background intensity is 40%

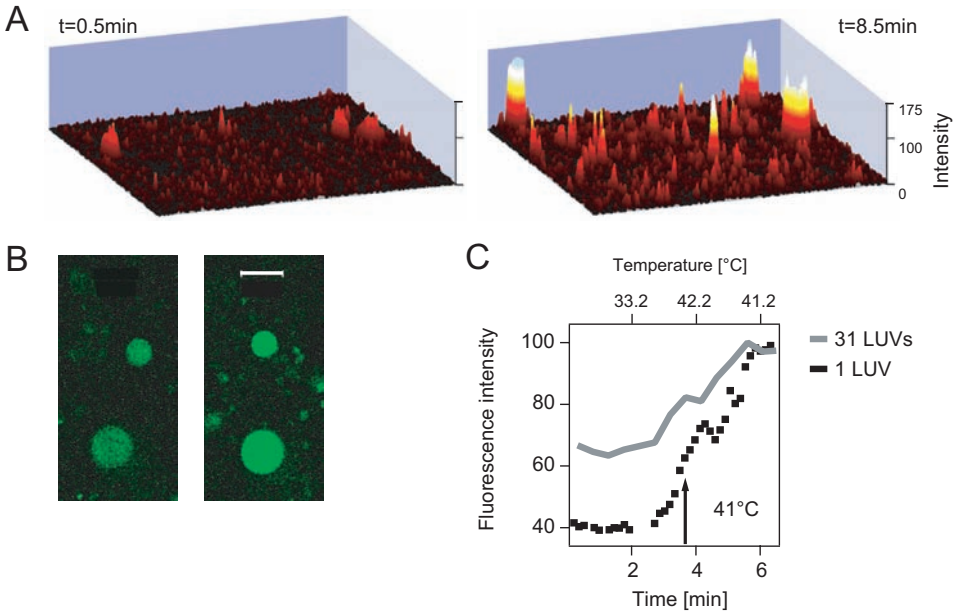

Figure 4.7: Fluorescence images of enzymatic reactions triggered by release of FDP from DPPC:DPPG (9:1) small vesicles inside of DOPG LUVs. *(A) Fluorescence images of LUVs before (left hand side; 0.5 min, ∼30 °C) and after (right hand side; 8.5 min, ∼45 °C) the release of FDP inside the LUVs (initial concentration of FDP is 0.5 mM and phosphatase 0.1 [Units/mL]). For a better representation intensity, it is given in color code perpendicular to the plane of glass support with immobilized vesicles. (B) Confocal fluorescence microscopy cross-section of two immobilized LUVs before (left hand side) and after (right hand side) enzymatic reaction. The scale bar represent 10 µm. (C) Time course of the fluorescence intensity of FDP (Ex 480 nm, Em 520 nm) reaction in one LUV (black line) compared to an average of 31 different LUVs (gray line).*

before the reaction) as compared to that in figure 4.6A (or with DPPC:DPPG (9:1) SUVs; not shown), probably due to passive diffusion of FDP substrates through the SUVs bilayer or due to a considerably lower concentration of SUVs encapsulated in the LUVs than in solution.

4.4.2 Using DDAO phosphate as substrate

In this section, the enzymatic reaction using DDAO phosphate as substrate is analyzed in greater detail. The test with SUVs in solution reveals a higher encapsulation of DDAO phosphate in DMPC SUVs than in DMPG. To prevent aggregation, 20 weight percent of the charged lipid DMPG is introduce in the SUV membranes (DMPC:DMPG 4:1). This allows longer storage of the SUVs.

Figures 4.8A and B depict confocal microscopy images. Figure 4.8C reports the time course of this reaction for two single LUVs (filled gray circle and open black square) compared to an average of 6 different LUVs (solid black curve). These data indicate that the reaction is triggered synchronously at the DMPC:DMPG phase transition temperature. This experiment worked particularly well and permited a deeper analysis especially of the kinetics as demonstrated in figure 4.9.

For this particular experiment, DDAO phosphate has been chosen for its possibility to be detected before and after the reaction. Unfortunately, the fluorescence efficiency of the substrate was too low to be detected reliably. A too high laser power was required which induced considerable photobleaching. Therefore, the decrease of substrate concentration was not quantified and only the formation of product was monitored and analyzed.

Figure 4.9A shows the time course of the enzymatic reaction inside of three selected LUVs. From the series of confocal microscope images, the average fluorescence intensities of product (DDAO) per LUV (from the images) were converted to product concentration during the monitored reaction. This was calculated by a calibration curve using different concentrations of product (DDAO) in bulk solution measured with the confocal microscope at the same detection settings.

The initial concentration of PP2A used during the formation of the LUVs was 0.5 [Units/mL] which represents $\sim$14 [μg/mL] (data provided by the supplier). From the molar mass of this enzyme of $\sim$80'000 [g/mol], the concentration is estimated as 175 [nM]. The ratio [S]/[E] ranges from 3-15, if the enzyme encapsulation efficiency in LUV is 100%.

The data are linearly fitted starting at the beginning of the reaction in order to compare the initial reaction rates between different LUVs. From these fits the slopes

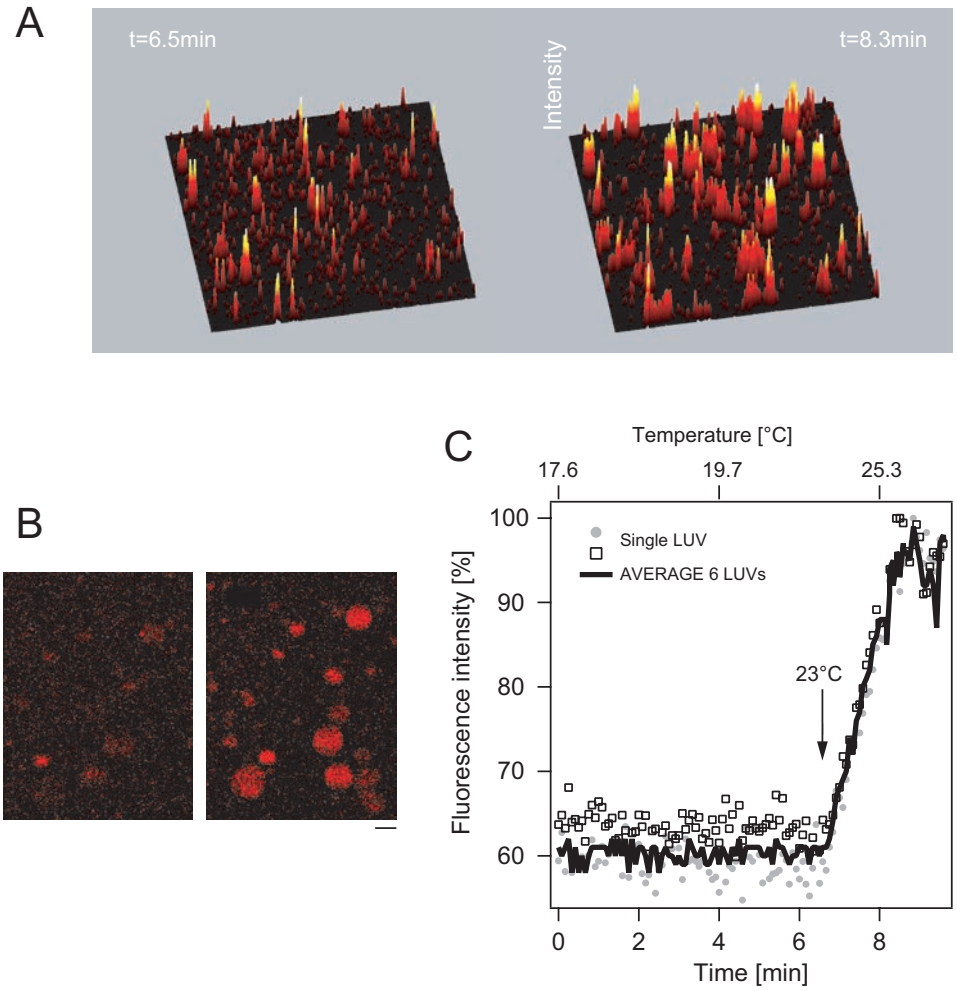

Figure 4.8: Enzymatic reaction of alkaline phosphatase in DOPG LUVs with DDAO phosphate released from DMPC:DMPG 4:1 SUVs inside these LUVs. *(A) Fluorescence intensity representation of LUVs at two different acquisition times before (6.5 min) and after (8.3 min) the release of DDAO phosphate (initial concentration of DDAO phosphate in SUVs is 0.5 mM and the concentration of phosphatase in hte LUVs is 0.47 [Units/mL]). (B) Confocal fluorescence microscopy of immobilized LUVs before (left) and after (right) enzymatic reaction. The scale bar represents 10 µm. (C) Time course of the fluorescence intensity of DDAO (Ex 543 nm, Em 650 nm) in two individual LUVs (gray circle and empty square) and averaged over six different LUVs (black line).*

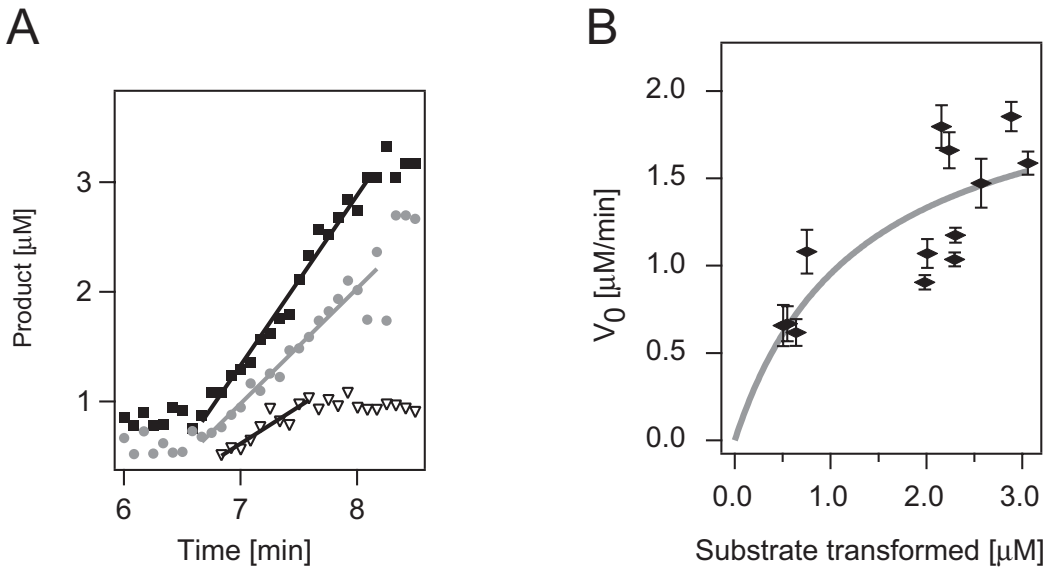

Figure 4.9: Reaction kinetics in single LUVs. Comparison between different individual vesicular reactors. *(A) Time course of three different LUVs with different product concentrations. Experimental data are fitted by a linear time dependence in order to determine the initial reaction rate V_0. (B) Dependence of the reaction rate V_0 on substrate concentration transformed, Each data point correspond to one individual LUV (total 13).*

are calculated and reported as reaction rates in figure 4.9B for different substrate concentration, assuming a complete transformation of substrates into products. The substrate concentration being higher than the K_M (0.2 μM measured in bulk), the initial reaction rate should not be linearly proportional to the substrate concentration. Therefore the initial reaction rate values were fitted using equation 4.3 (gray line) and shown a dependency on the substrate concentrations. The data obtained are too scattered to allow further quantitative analysis, but are in agreement with the Michaelis-Menten model.

In such small volume, a high concentration of enzyme should be slightly different in each LUVs but may effluence only slightly the reaction rate. The amount of enzyme should vary less than the number of SUVs per LUV since its size is much smaller and its encapsulation more homogeneous.

These results show the possibility to perform enzymatic reactions within individual ultra-small vesicular reactor. Even if the number of enzyme is not yet quantified, this system opens novel possibilities to investigate single enzyme reactions.

4.4.3 Control experiment

A control experiment has been performed in order to approve the experiments of the enzymatic reactions in the confined volume of the LUVs. Two different kinds of LUVs have been produced and analyzed. One kind was loaded with the enzyme together with SUVs containing substrate. The other sort was loaded with SUVs containing substrate but without enzyme. A fluorescent lipid was inserted in the membrane of the second sort of LUVs to distinguish the two different vesicle populations. The different LUVs were finally mixed, immobilized on the microscope slide and heated to release the substrate. The results are summarized in figure 4.10.

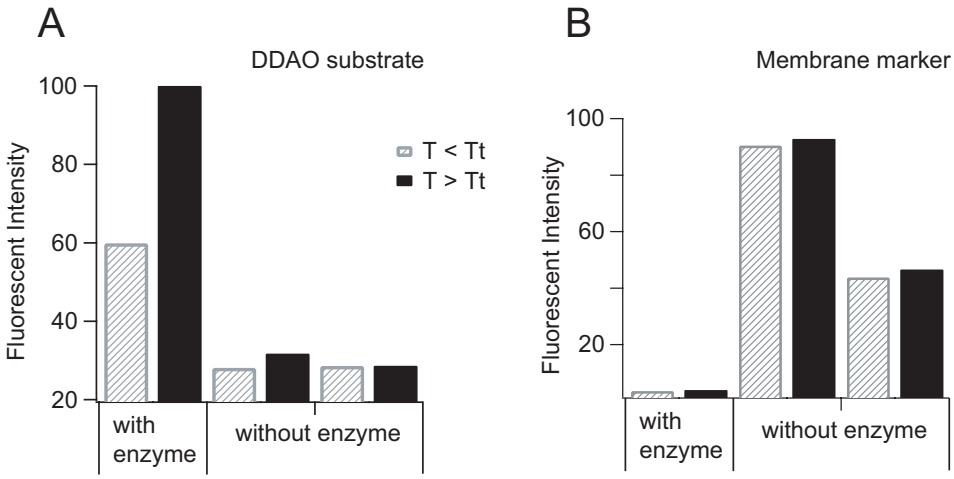

Figure 4.10: Control experiments. *(A) Comparison of two sorts of LUVs: One sort contains PP2A and SUVs' with DDAO phosphate. Another sort of LUVs contains only SUVs' with DDAO phosphate but no enzyme and is marked with fluorescent lipids in the membrane. As expected, in the presence of enzyme the fluorescence intensity increases from 60% (T < Tt gray bar) to 100% (T > Tt black bar) but in absence of enzyme no significant fluorescence variation is observed. (B) The fluorescence intensity of the fluorescent lipid marker remains constant at T <> Tt and can be used to properly focus to the vesicles.*

The plot in figure 4.10A reports the change of fluorescence intensity before and after temperature scan through lipid phase transition. The plot in figure 4.10B reports the fluorescence intensity of the membrane marker which depends on the proper focusing of the confocal microscope plane. Small observed variations are due to small differences in focusing. Once proper focusing was obtained, the plot in figure 4.10A proves that the fluorescence gain of the LUVs containing enzymes effectively comes from an enzymatic reaction as expected.

With the ability to fluorescently mark the membrane, different populations

of LUVs can be distinguished. This experiment supports the possibility to apply the system developed in this work for screening different sorts of reaction conditions with ultrasmall (down to few molecules) amounts of molecules.

4.5 Conclusion

Integrated vesicular reactors were produced and immobilized on a glass surface allowing to monitor enzymatic reactions by fluorescence confocal microscopy. By controlling the temperature the permeability of the SUVs containing substrates, enzymatic reactions in confined volumes were triggered synchronously in multiple LUVs. The proof of principle was demonstrated by enzymatic transformation of FDP into fluorescein using alkaline phosphatase. The expected increase of reaction rate with released substrate (concentration near the K_M value) was verified by comparing several individual LUVs with DDAO phosphate substrate.

Chapter 5

Consecutive Enzymatic Reactions in Single LUVs

5.1 Introduction

In chapter 4 we described key experiments how to trigger and observe enzymatic reactions in individual femtoliter sized vesicular containers by thermotropic release of substrates from attoliter sized SUVs. Two different substrates were released from two different sorts of SUVs showing different lipid phase transition temperatures. Combining these two systems gives the possibility to trigger inside the same LUV two consecutive enzymatic reactions as illustrated by figure 5.1.

First two different sorts of SUVs are prepared separately, each composed of different lipids displaying clearly distinguished lipid phase transitions. Each sort of SUVs contain a different substrate distinguished by the fluorescence of its final product. The two population of SUVs are then entrapped in the lumen of the LUVs together with the enzyme for the two different substrates. In the following we use (i) SUVs composed of DMPC:DMPG 4:1 containing DDAO phosphate and (ii) SUVs composed of DPPC:DPPG 1:1 containing FDP. The LUVs were then immobilized on a glass slide as described in figure 5.1.

By applying an increasing temperature ramp, first at Tt = 23 °C the DMPC:DMPG SUVs release DDAO phosphate which immediately reacts with the enzyme. Then after reaching Tt = 41 °C the DPPC:DPPG SUVs release FDP which reacts with the same enzyme. This chapter demonstrates the proof of principle that in ultra-small reactors consecutive enzymatic reactions can be initiated consecutively at distinct temperatures.

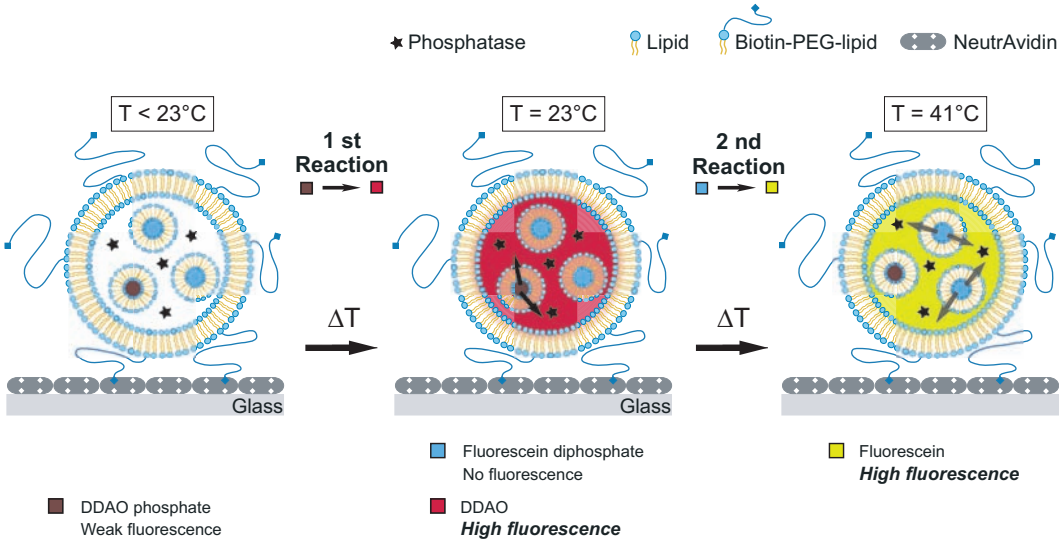

Figure 5.1: Concept of consecutive enzymatic reactions confined in a single LUV. *Phosphatase (black star) is incorporated in LUVs together with DDAO phosphate loaded in the first sort of SUVs (DMPC:DMPG 4:1, Tt around 23 °C) and FDP loaded in the second sort of SUVs (DPPC:DPPG 1:1, Tt around 41 °C). Each sort of substrates is released at the particular Tt of its container and reacts subsequently with the enzyme present in the LUV.*

5.2 Materials and methods

The experimental methods required in the present context have already been presented in detail in the different previous chapters. The conditions are only slightly modified after several experimental trials. For this particular application a good co-incorporation of DDAO phosphate containing SUVs as well as FDP containing SUVs inside the same LUV is required. In order to enhance this co-incorporation, the electrostatic interaction between the SUVs and LUVs must be balanced. The following lipid mixtures were chosen; DDAO-phosphate-SUVs are prepared from a mixture of DMPG:DMPC 4:1 (starting organic solution 5 mg/mL). FDP-SUVs are composed of DPPG:DPPC 1:1 (starting organic solution 5 mg/mL), and the LUVs are DOPC:DOPG:biotinPEGlipid 100:400:4 (starting organic solution of 2 mg/mL).

These compositions gave the best results, but still not all LUVs featured a good co-incorporation of the two sorts of SUVs. The amount of enzyme should also play an important role, but due to its small size compared to the SUVs, its loading efficiency is expected to be more homogenous between the different LUVs.

5.3 Results and discussion.

A proof of principle is shown in figure 5.2. It shows the confocal images (on the top) with their intensity profiles (measured at the position represented by the white line) at three different times (t = 0, 4.8, 12.4 min) after the temperature ramp started. At t = 0 min, the green color representing the fluorescence of fluorescein and the red color representing the fluorescence of DDAO, were of similar intensity with a maximum value measured around 2000 [a.u.] in the center of the 10 μm sized LUV. At t = 4.8 min, the red color was predominant with a maximum intensity value increased to 4000 [a.u.] due to the release DDAO phosphate from DMPC:DMPG SUVs and its enzymatic transformation to highly fluorescent DDAO. At t = 12.4 min, the green color was predominant with an intensity value increase to near 400 [a.u.] which resulted from the release of FDP from DPPC:DPPG SUVs and its transformation to fluorescein. These images also showed that the fluorescent substrates are homogenously distributed inside the LUV.

These qualitative results show unambiguously that two enzymatic reactions occurred consecutively within the same LUV.

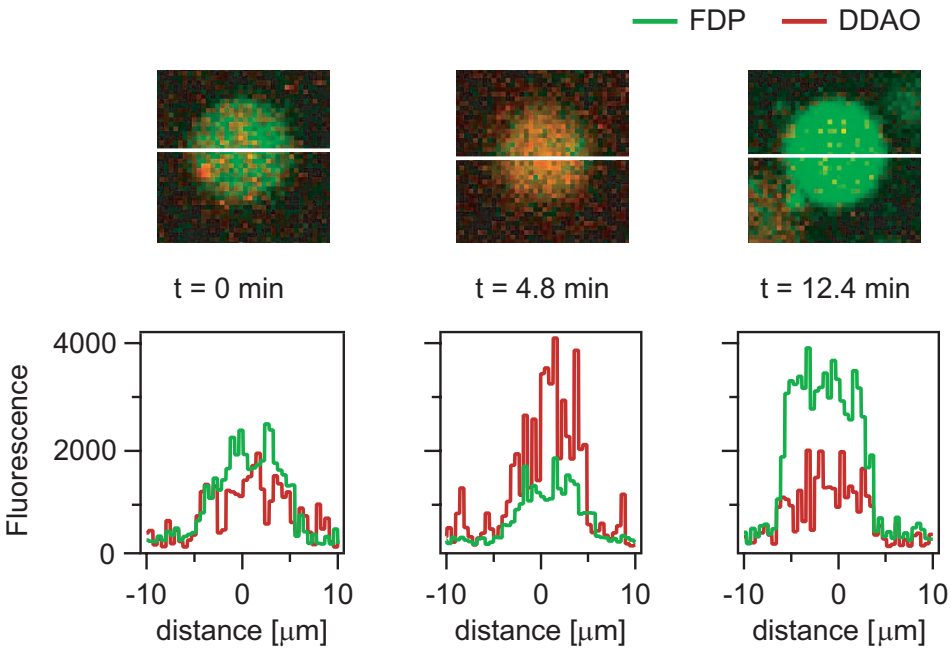

Figure 5.2: Confocal fluorescence micrographs of the same LUV at three different times (top). *Bottom: The intensity profile across the LUV (indicated by the white line) is measured for the two different products simultaneously by two separated channels (fluorescein in green and DDAO in red).*

For additional details, the fluorescence intensity time course of two different

LUVs from two different samples of same preparation, measured at two different days, are presented in figure 5.3A and B. The fluorescence intensity versus time traces show a relatively high noise due to the fact that in the absence of a membrane marker, it was quite difficult to precisely focus to the individual LUVs. The gray curves corresponding to the fluorescence of DDAO exhibits a clear increase in both samples near 23°C upon heating and cooling as indicated by the arrows at the button of figure (A) and (B). Similarly, the black curves corresponding to the fluorescence intensity of the produced fluorescein exhibited an increase also in both samples near 41°C as indicated by the arrows on the top of the figures (A) and (B).

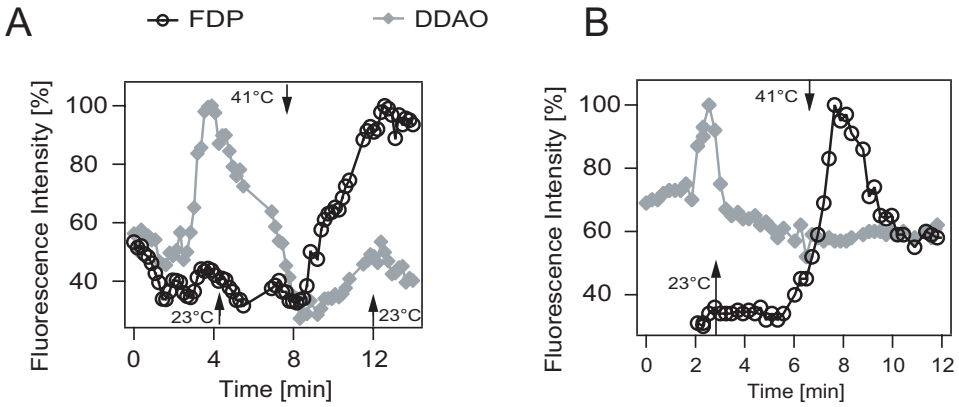

Figure 5.3: Time course of the consecutive enzymatic reactions. *The fluorescence intensity of the two enzymatic products (DDAO in gray and FDP in black) are reported as s function of time upon heating and cooling (identical experimental conditions as described above in figure5.1).*

Both in figures 5.2 and 5.3 a decrease of the fluorescence intensity was observed for both products above Tt after the reaction is completed. This was also observed to a lower extent for single substrate experiment. However, it did not affect significantly the characterization of the reaction at the beginning, which was only taken for analysis in figure4.9. This observation might be due to photo-bleaching which was more pronounced in figure 5.3 due principally to a longer period of excitation time. In addition, the amount of SUVs, and hence the number of reactants, was lower than in the preceding experiments which in turn required a higher laser power for measurements. Another explanation for the decrease in fluorescence intensity would come from a passive leakage of the products out of the LUVs. But, since the reactants with a similar chemical structure and size remain encapsulated in the SUVs for several days, the mentioned effect certainly comes from photo-bleaching.

5.4 Conclusion

Despite high photobleaching, the results presented in this chapter demonstrate that we have developed a system suitable to perform and observe multiple consecutive enzymatic reactions. This could be useful to study in a confined volume, complex bio-chemical reaction systems like competitive reactions, inhibitions or cascade reactions which would be a starting point to simulate complex biochemical cellular reactions, i.e. to construct an artificial cell. Compared to a real complex native cell, the artificial system can reduce the complexity allowing to better control all the participating components.

Chapter 6

Characterization of nanoreactors by FCS

6.1 Introduction

The results presented in the previous chapters demonstrate that mixing reactants to initiate bio-chemical reactions can be performed within ultra-small vesicular reactors. The presented results are based on average fluorescence intensity measurements on single LUVs for two types of experiments: (i) dilution of dyes, and (ii) initiation of enzymatic reactions. However the techniques used up to now cannot quantify in detail the content of each reactor, particularly the number of SUVs per LUVs. This parameter is important to know since the performance of a LUV as reaction container depends on its capability to incorporate a sufficient and measurable amount of SUVs.

Here we use fluorescence correlation spectroscopy (FCS) to characterize reactants and products inside of a LUV. In a typical FCS experiment, a laser beam is focused by confocal optics into a sample; the diffusion of single fluorescent particles / molecules across the confocal volume of (sub)femtoliter size is measured. FCS counts the number of fluorescent particles / molecules and measures their diffusion constant and thus, it is possible to distinguish free diffusing dyes from those encapsulated in SUVs.

FCS was invented by Magde et.al. [93], and Rigler et.al. [94] and reviewed recently by Krichevsky et.al. [95] and Schwille et.al. [96]. FCS has been already used to study the interaction of peptides with small vesicles interaction (Pramanik et.al. [97]).

6.2 Materials and methods

6.2.1 Principle of FCS

The FCS results presented in this chapter are obtained using the commercial LSM 510 confocal microscope from Carl Zeiss. This is the same microscope used for confocal data acquisition and thus enables to combine the two techniques for precise localization of the FCS focus inside the immobilized LUVs. Using pinhole diaphragms the detection volume can be reduced to few hundreds of nano-meters in diameter corresponding typically to $\sim 3 \cdot 10^{-16}$L $\Leftrightarrow$ 0.3 femtoliters of the detection volume. This specific feature is important since the focal volume fits inside the LUVs but is still large enough to measure correctly the diffusion time of the SUVs in the LUVs [98]. The figure 6.1 illustrates the shape of the detection volume and the principles of the FCS technique.

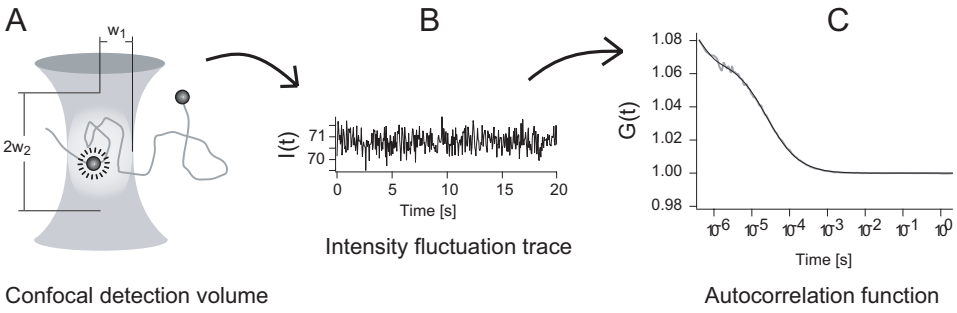

Figure 6.1: Illustration of the principle of FCS. *(A) The fluorescent particle is only excited when present in the confocal detection volume. (B) The fluorescence intensity is recorded versus time and gives the intensity fluctuation trace I(t) due to the diffusion of particles in and out of the detection volume. (C) From this trace, the autocorrelation curve G(τ) is calculated.*

6.2.2 FCS theory

The confocal detection volume is characterized by its radius w_1 and its height $2w_2$ (figure 6.1A. Diffusing fluorescent particles, free dye molecules in the bulk or loaded inside SUV are excited only when they are present in the confocal volume. In order to obtain reasonable data [98, 99], the particles must be considerably smaller than the confocal volume, thus only particles below $w_1 \simeq 200$ nm can be characterized by FCS. To respect this limitation, the SUVs analyzed are produced by extrusion through filters of 100 nm pore size. The fluorescence intensity is recorded over time yielding traces I(t) which show characteristic fluctuations δI(t) around the average fluorescence signal $\langle I \rangle$. The fluctuations might be due to changes in the fluorescence

quantum yield or to the number of fluorescent particles in the detection volume. In order to get experimental parameters, the normalized autocorrelation function (ACF) G(τ) is calculated numerically from I(t) as follow.

$$G(\tau) = 1 + \frac{\langle I(t) \cdot I(t+\tau) \rangle}{\langle I \rangle^2} \tag{6.1}$$

The fluorescence intensity shows characteristic fluctuations around the average fluorescence intensity due to particular molecular processes. The autocorrelation function compares the value of the fluorescence signal at any arbitrary time t with the fluorescence signal at a short time interval τ later. The angular brackets $\langle\rangle$ indicate time average over t and τ. If the decay of Gτ is much shorter than the translational diffusion, the ACF can be fitted according to the following equation.

$$G(\tau) = 1 + \frac{1}{N} \cdot \frac{1}{1 + 4D\tau/w_1^2} \left(\frac{1}{1 + 4D\tau/w_2^2} \right)^{\frac{1}{2}} \tag{6.2}$$

The fitting parameters are:

D: the diffusion coefficient is D = $w_1{}^2/4\tau_D$

w_1: the radius of the detection volume (figure 6.1)

w_2: the half height of the detection volume (figure 6.1)

and the experimental parameters extracted from the fitted ACF are:

▷ N: the number of molecules in the detection volume

▷ τ_D: the translational diffusion time of the detected particle.

In cases where different populations of particles are present in the analyzed solution, the following particular equation describes this condition [100]:

$$G(\tau) = \frac{\sum_{i=1}^{R} \alpha_i^2 Y_i N g_{xi}(\tau)}{\left(\sum_{i=1}^{R} \alpha_i Y_i N \right)^2} + G_\infty \tag{6.3}$$

αi depends on the quantum yield of the ith particle, g_{xi} depends on the appropriate model of fitting for species i, and Y_i is the mole fraction for each species i with N the average number of particles. This latter equation implies an important restriction [101] of the FCS experimental applications. Since the ACF depends on the quantum yield of every species detected, this quantum yield needs to be determined. Unfortunately, the SUVs to be analyzed encapsulate an undetermined amount of fluorophores and thus have different brightness, depending on the number of fluorophores per SUVs.

In conclusion to this introductory remarks, FCS is useful to determine qualitatively whether the detected fluorophore is encapsulated in SUV diffusing slowly, i.e. with high τ_D or if the fluorophore is diffusing fast with low τ_D. However, for the case where no loaded SUVs are detected, the number of fluorophores and hence, after calibration of the detection volume, its absolute concentration can be quantified either in solution or entrapped in LUVs. The following results summarize some thermotropic release processes under different conditions of SUVs' lipids, different fluorescent dyes and SUVs dilution. They characterize also LUVs under similar conditions as used in the previous chapter by exploiting the FCS results in an adapted manner.

All the experimental conditions during FCS measurements are identical. The measurements first begin with an automatic pinhole adjustment to find the maximal detected intensity from a solution of 100 nM A488 and with a pinhole diameter of 70 μm for the 488 excitation line (for A488, CF and Rhodamine 6G) and 90 μm for the excitation line 633 (Cy5 and A647). The laser power transmission is usually 1 % but may be adjusted to obtain a sufficient intensity per particles. When the intensity is high enough (but not higher than 1000 [kHz]), the laser power do not influence the parameter obtained by the ACF. The extruded (100 nm pores diameter filter) vesicle concentration is not quantified before FCS experiments but correspond to about 50 μg/ml of lipids and 3.17μM for the initial dyes concentrations for most of the measurements.

6.3 FCS on SUVs in solution

Before analyzing the more complex system SUVs in LUVs, the SUVs are first characterized in bulk solution by FCS experiments.

6.3.1 Detection of SUVs

First of all, the release process is characterized qualitatively by measuring the diffusion times of the fluorophores both entrapped in SUVs and in bulk solution. As presented in figure 6.2, three conditions can be clearly distinguished. (i) The thin black ACF curve represents the A488 fluorophore in buffer solution. (ii) The thick black curve, represents the ACF of the same fluorophore encapsulated in dispersion of SUVs before heating; the ACF shows a large shift to higher diffusion time. (iii) After heating the SUV dispersion, the ACF shifts back to the same curve as seen for free fluorophores in bulk solution shown in (i) (gray curve).

The results depicted in figure 6.2 demonstrate the ability to clearly distinguish the dye encapsulated in SUVs from the free dye in bulk solution. Due to the large difference in size, the SUVs diffuse much slower than free dye. Therefore, FCS is suited to detect the release of dyes from SUVs determining parameters inaccessible with the other techniques already presented. The results presented in figure 6.2 demonstrate that the majority of fluorophores are efficiently released from SUVs. Details of the parameters affecting the dye release efficiency from SUVs will be presented in the following.

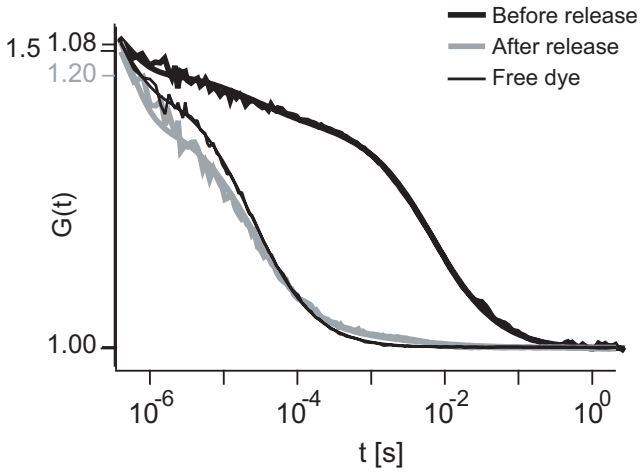

Figure 6.2: FCS autocorrelation curves of DPPG SUVs before and after release of to Alexa488FH (A488). *The thin black autocorrelation curve represents a solution of A488 in absence of SUVs. The thick black autocorrelation curve stems of A488 dyes encapsulated in SUVs (DPPG) before heating. The gray autocorrelation curve is obtained from the same SUV solution after heating.*

6.3.2 Effect of the lipid bilayer composition

The lipid composition of the bilayer of SUVs influence the dye release; figure 6.3, shows FCS experiments for DPPG-SUVs (black ACF curve) and DPPC-SUVs (gray curve) and SUVs composed of DPPC:DPPG (thick black curve) always after heating above Tt. The ACF of DPPG-SUVs have no contribution from slow moving particles, showing a complete release of A488. On the other hand, the ACF curves from less or non charged SUVs reflect an important contribution from slow diffusing particles. Therefore, we conclude that the electrical charge of the polar head groups of the SUV lipids plays an important role during the release of hydrophilic molecules from the inside of SUVs to bulk buffer. The release of A488, seems to be more efficient in the presence of negatively charged lipids such as DPPG. This will

be exploited during the next experiments.

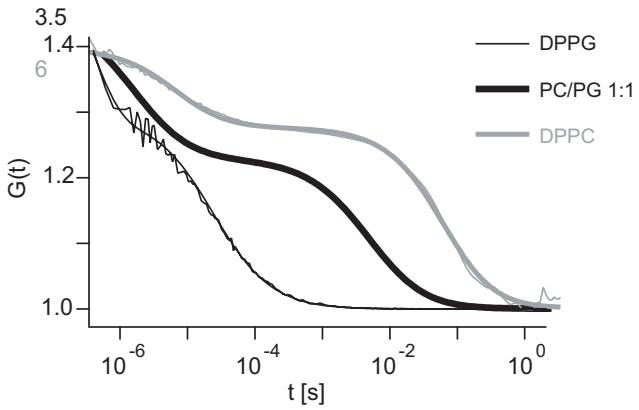

Figure 6.3: FCS autocorrelation curves of SUVs composed of different lipids always after heating above Tt. *The thin black curve represents the autocorrelation curve of a solution of DPPG-SUVs; no vesicles with encapsulated dyes could be detected. The thick black line represents an autocorrelation curve of DPPG:DPPC (1:1) SUVs, the gray line that of DPPC-SUVs.*

6.3.3 Effect of the dye properties on release from vesicles.

Since the charge of the lipids influence the release process, the hydrophobicity of the dyes encapsulated should also play a role during this process. Intuitively, the molecular weight is expected to affect the release efficiency; smaller dyes should diffuses faster and hence should be released out of SUVs more rapidly and efficiently. Here we investigated four different dyes with different chemical properties. Their chemical structures (except for A647 which structure is not accessible) and molecular weights are depicted in figure 6.4.

Figures 6.5 (A) and (B) represent the ACF curves of DPPG SUVs after heating diluted hundred times after purification ($\sim$50 μg/ml of lipids), loaded with the different dyes tested. These curves are calculated by averaging a series of measurements with long acquisition time (20 seconds per single measurement). These autocorrelation curves indicate that in nearly all cases the fluorophores are efficiently released from the SUVs. Thus FCS allows to determine the number of released fluorophores.

6.3.4 Effect of dilution of the vesicle solution

In the case of CF, only a very few SUVs are detected, but it is sufficient to miscalculate the number of free dyes within a mixture of particles of different brightness. However, it is possible to perform a suitable evaluation procedure by considering

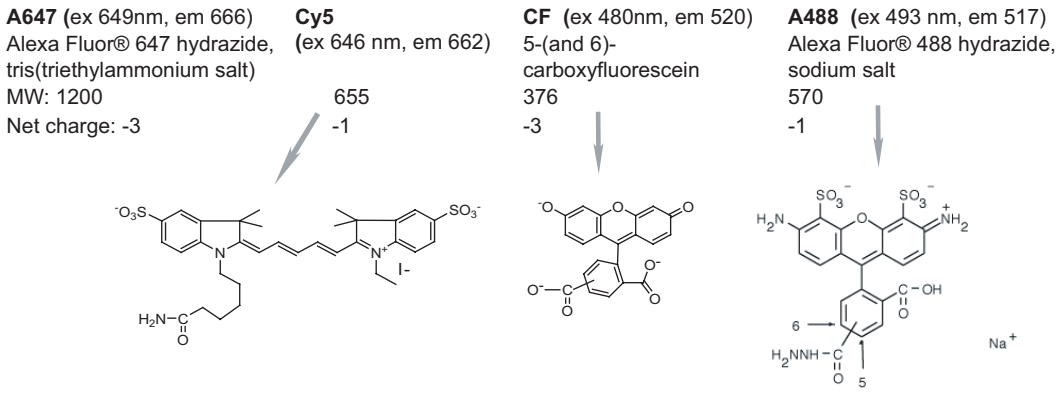

Figure 6.4: Four fluorescent dyes used for the FCS experiments. *The molecular mass, the net electrical charge and excitation and emission wavelengths are indicated in the figure.*

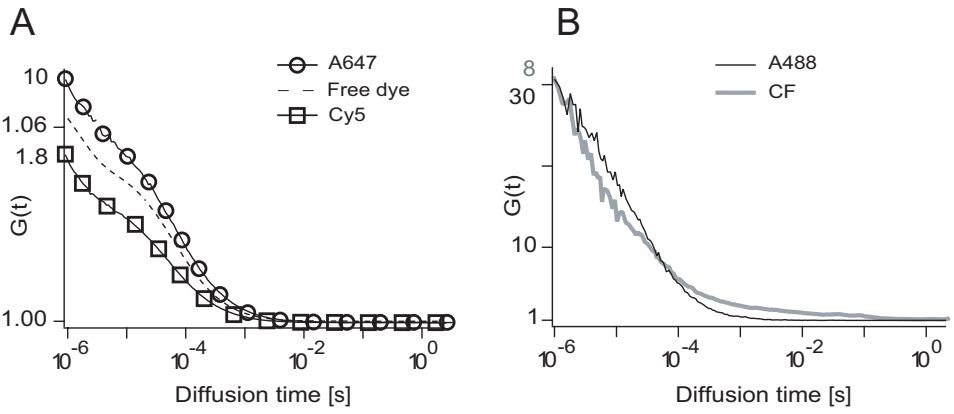

Figure 6.5: FCS autocorrelation curves of 4 different solutions of DPPG-SUVs, diluted 100 times after purification (∼50 μg/ml lipids); in each sample the SUVs are loaded with 4 different fluorescent dyes after the same heating treatment. *(A) circles A647; squares Cy5; dashed curve free Cy5 without SUVs. (B) Black curve A488; gray curve CF. Under the same conditions, almost no SUVs are detected except for the CF represented by the gray curve in (B), i.e. the dyes are not from SUVs. Measurements were performed after the samples were heated above their corresponding Tt.*

only the autocorrelation curves where no SUVs have been detected. This can be achieved by taking a large number of measurements (for example 20) during a small acquisition time (for example 1 second). Finally the number of free dyes is calculated by averaging only the measurements containing no contribution of SUVs. However, for undiluted solutions, in most of the cases the number of free released dyes could not be calculated.

We have used this method to compare the efficiency of release for the four different dyes. Figure 6.6A reports the relative (compared to undiluted sample) number of Cy5 dyes released from SUVs diluted 10 and 100 times before heating. Figure 6.6B depicts the relative (compared to 10 fold dilution = 500 μg/mL of lipids before heating) number of four different dyes released at 100 times dilution (50 μg/mL of lipids) before heating.

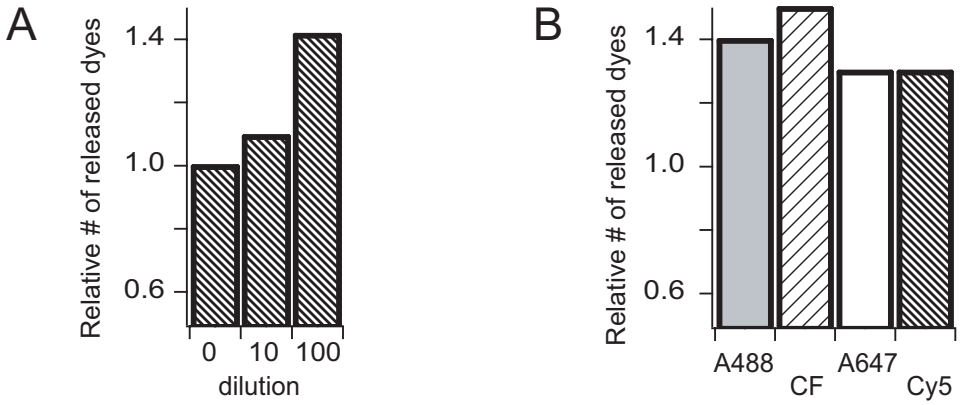

Figure 6.6: Relative number of released dyes at different dilution condition as obtained from FCS. *(A) represents the relative (compared to undiluted sample) number of released Cy5 dyes for different dilutions. (B) reports the number of dyes of A488, CF, A647 and Cy5 at 100 fold dilution relative to 10 fold dilution.*

Figure 6.6A reveals that the number of released dyes increases with the dilution. The difference between the dilution 100 and 10 is higher than between dilution 10 and 0.

Figure 6.6B shows that there are no significant differences between the various dyes at 100 fold dilution. Thus the release efficiency depends not much on the properties of the dyes but more on the extent of dilution. Obviously, the concentration gradient between the interior of the SUVs and the bulk solution influences the efficiency of dye release.

6.3.5 Quantification of the number of SUVs

In order to evaluate the number of SUVs, the evaluation of FCS data needs some adaptations. The intensity trace of a none-heated solution of SUVs diluted 100 times (∼50 μg/ml of lipids) is shown in figure 6.7A. This trace exhibits peaks due to the detection of individual highly fluorescent SUVs. In dilute solutions, high intensity events can be distinguished because each of this events arise from individual SUVs, it is possible to count them by a histogram as shown in figure 6.7B. This way of counting is similar to the photon counting histogram (PCH) where particles are distinguished according to their relative brightness instead according to their diffusion time as is done normally in FCS. In the present case of high dilution the bright particles generate individual intensity peaks and are easily distinguished from background intensity.

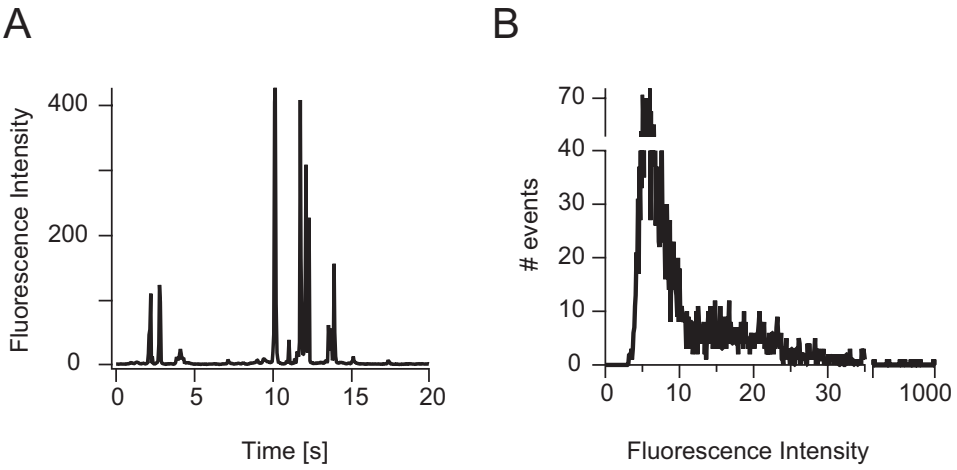

Figure 6.7: Determination of the number of SUVs suspended in buffer and loaded with A488; (before heating). *(A) Fluorescence intensity as function of time; each high fluorescence intensity event corresponds to a single SUV. (B) Intensity histogram of the events observed in (A). From this histogram it is possible to count the number of SUVs above background intensity of 12 [a.u.]. Experimental conditions: Room temperature, 3.17 μM initial concentration of A488 inside SUVs, buffer is 10 mM Tris-HCl pH 7.0.*

Since the time bin of the intensity trace in figure 6.7A (50 μs) is larger than the average diffusion time measured by FCS (2μs) of SUVs, those counts of the histogram 6.7B which are beyong the background threshold (determined at 12 [a.u.] for this example) correspond to SUVs. To obtain the number of SUVs in the detection volume, the number of counts higher than 12 [a.u.] is divided by the total number of counts (background + SUVs).

$$\sharp SUVs = \frac{\sharp counts(I > threshold)}{\sharp counts_{total}(I_{all})} \tag{6.4}$$

This evaluation is used to determine the number of SUVs before the entrapped fluorophores are released. Subsequently, FCS measurements on the same diluted sample after heating determine the absolute number of dye molecule; in turn the average number of dye molecule per SUV can be estimated and hence the encapsulation efficiency can be calculated. This procedure delivers an average number of 8 dyes per SUV. This number can be compared to the value of 10 dyes per SUVs [102], calculated from the initial dye concentration (31.7μM) used to produce the SUVs. Thus the encapsulation efficiency is estimated to be 80%. In the classical FCS evaluation, the brighter particles are dominating the autocorrelation curve, thus underestimating the number of SUVs containing a low number of fluorophores. Actually the "classical" FCS calculation yields a value of ∼50 dyes per SUVs which is unrealistic.

Validation of the technique used to count the SUVs — This subsection reports results supporting the validity of the method used to count the SUVs in solution. First of all, the concentration of free dyes is calculated with the traditional FCS technique. By measuring the diffusion time (τ_D) of a reference dye (Rhodamine 6G) with know diffusion coefficient, the diffusion coefficient of the A488 dye is determined as follow:

$$D_{A488} = D_{Rho6G}\frac{\tau_D(A488)}{\tau_D(Rho6G)} \tag{6.5}$$

The detection volume (V_{det}) can then be calculated using the diffusion time of the dyes (D_{A488}) and (τD_{A488}), and the structure parameter (S) obtained with the ACF fit curve:

$$V_{det} = 2 \cdot \pi \cdot S \cdot (4 \cdot D_{A488} \cdot \tau_{D_{A488}})^{3/2} \tag{6.6}$$

The absolute concentration (c_{A488} [M]) is then calculated using the detection volume (V_{det} [L]), the Avogadro number (N_{AV}) and the number of dyes measured by FCS (N) and corrected using a calibration curve (not shown):

$$c_{A488} = \frac{N}{V_{det} \cdot N_{AV}} \tag{6.7}$$

Figure 6.8A verifies the proportionality between the released concentration of dyes and the initial concentration encapsulated in SUVs. Figure 6.8B verifies from the same sample, the proportionality between the released dyes and the SUVs dilution ratio. Figure 6.8C verifies from the same initial sample the proportionality between the number of calculated SUVs and the SUVs dilution ratio.

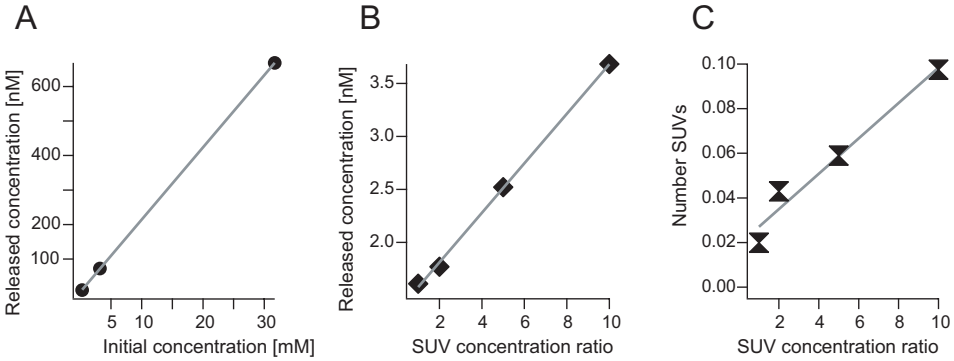

Figure 6.8: Quantitative results from DPPG SUVs in solution. *(A) The concentration of released dyes is proportional to the initial encapsulated dye concentration. (B) The concentration of released dyes is proportional to the dilution of the SUVs solution (same SUV sample). (C) The number of SUVs is also proportional to the dilution of the SUV solution. The concentration ratio represents the inverse of the dilution ratio (number of times more concentrated than the more diluted sample).*

Figure 6.9 analyzes using traditional FCS a mixed solution of SUVs and free dyes in order to evaluate under which conditions each species can be correctly quantified [101]. Figure 6.9A shows the ACF of one SUV solution after addition of different concentrations of free dyes; figure 6.9B summarizes the calculated fraction of free dyes. This figure demonstrates the sensitivity of the FCS technique; concentrations down to 0.08 nM within a mixture can be detected. From this figure, two limiting conditions are distinguishable: (i) Concentrations of less than 0.01 nM of free dye surrounding the SUVs are not detected. (ii) At concentrations higher than 65nM of free dye in the surrounding of SUVs, the SUVs are no more detected.

6.4 Characterization of the content of LUVs by FCS

The utilization of the FCS technique was not only motivated by the possibility to distinguish the free diffusing dyes from the encapsulated ones, but also by the ability to probe the lumen of individual LUVs with a sub-femtoliter detection volume (dimension in the 250 nm rage; figure 6.10A). Figure 6.10B demonstrates that it is

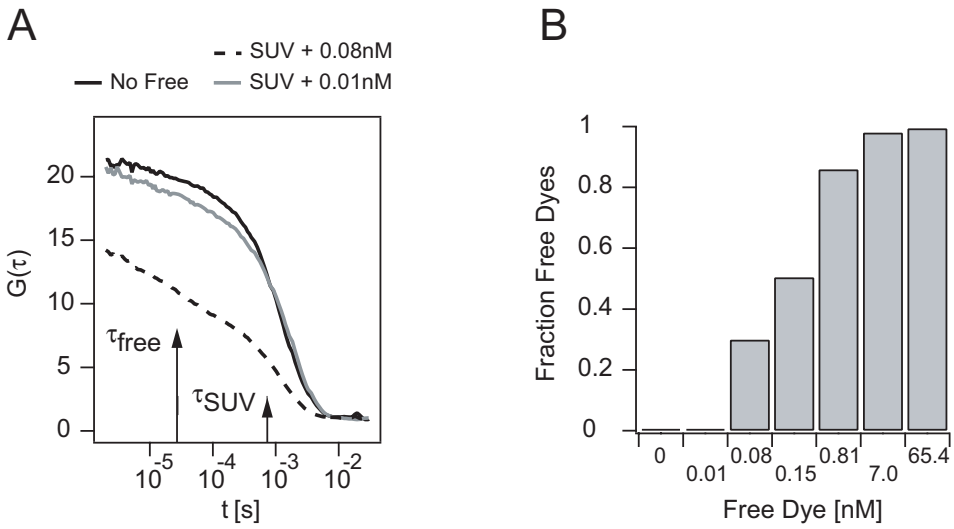

Figure 6.9: Limit of the detection of free dyes in the presence of dye-loaded SUVs. *(A) ACF of a dispersion of SUVs (5 mg DPPG /mL loaded with an initial concentration of 3.17 μM of A488) after adding different concentrations of free dye in the bulk. (B) Fraction of free dyes (relative to the total number of detected particles; SUVs + dyes) calculated with traditional FCS technique. The FCS detection limit is 0.01 nM of dyes in a mixture of SUVs and free dyes.*

possible to distinguish by autocorrelation curves free dyes from encapsulated ones in LUVs. The autocorrelation curve after heating is nearly identical to that of free dyes in solution, demonstrating an efficient release of dyes from SUVs and entrapping them in LUVs. The confocal detection volume is positioned inside the LUV of interest before measurement and checked also after the data acquisition if it is still inside the LUV. An efficient immobilization of the LUV stable in position and over time is prerequisite in order to realize these measurements.

As already explained in the previous sections, only the two most important parameters can be quantified at the particular condition of SUVs in solution or confined in LUVs. The first parameter is the number of incorporated SUVs within each LUV before reaction which determines the amount of reactants incorporated in the reactor. The second parameter is the number of reactants released from these SUVs, which determines the amount of reactant accessible to perform a bio-chemical reaction.

The major results obtained within individual LUV are summarized in figure 6.11. Two different LUV samples, incorporating SUVs loaded with either low (3.17μM; 1 dye/SUV [103]; squares) or high (31.7μM; 10 dyes/SUV; circles) initial concentration are analyzed before and after heating treatment. Due to technical

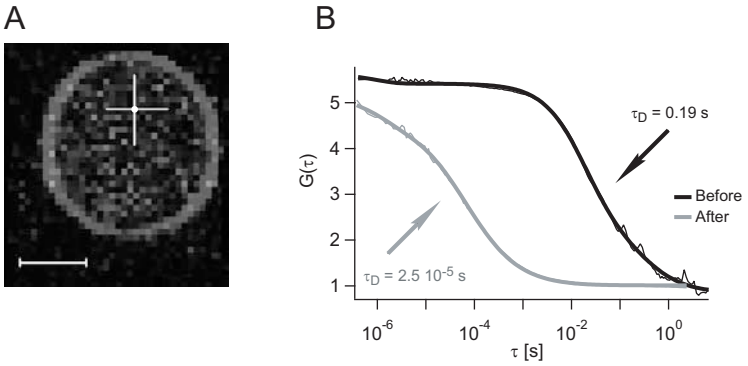

Figure 6.10: FCS measurements performed inside single LUV. *(A) Confocal image of a a cross section of a LUV (TRITC-DHPE) containing SUVs, indicating also the coordinates of the detection volume taken before and after the FCS measurements. The detection volume defined by the confocal pinholes is 0.38 fL with dimension ω_1 = 190 nm and S 8.4 [a.u.]. (B) Autocorrelation traces obtained inside a single LUV. The black curve indicates the presence of slow diffusing dyes encapsulated in SUVs (A488 3.17 μM) before (black trace) and after (gray trace) release induced by a temperature shift from 22 °C to 45 °C. Scale bar is 10 μm. The indicated diffusion times τ_D are calculated by the ACF as described in equation 6.2.*

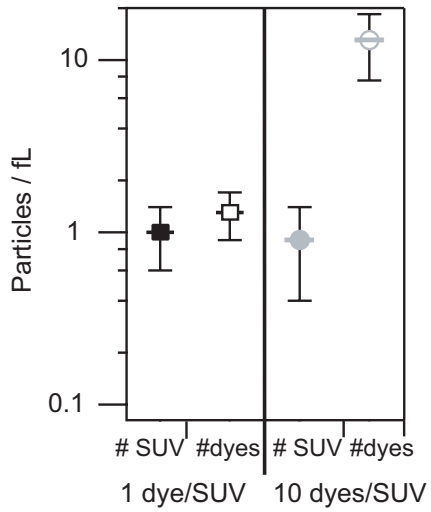

Figure 6.11: FCS measurements inside single LUVs. *Each point represents averaged results obtained from several individual LUVs. The number of SUVs per femtoliter (plain black square) loaded with a low initial concentration of 3.17 μM (1 dye/SUV) and the number of released dyes (open black square) from these SUVs are depicted. The number SUVs (plain gray circle) loaded with 31.7 μM (10 dyes/SUV) and the corresponding released dyes (open gray circle).*

problems, the LUVs analyzed before and after heating comes from exactly the same batch sample, but is not the same individual LUV. For comparison between each case, the calculated number of SUVs or dyes are expressed per femto liter. Despite a certain error on each data point, consistent results were obtained which can be summarized as follows:

1. First the number of dyes released from SUVs loaded with low initial concentration is very close to the number of SUVs before heating. Statistically, a SUV contains on average 1 dye molecule. Therefore, the number of released dyes would be equal to the number of SUVs if all dyes would be released from the SUVs into the corresponding LUV. The number of released dyes is slightly higher than the number of SUVs. From figure 6.9 the number of dyes inside the LUV and non-incorporated in SUVs is evaluated to 0.006 molecules. Thus, the higher number of released dyes can not result from non-detected free dyes before heating. Statistics (over 323 SUVs) obtained by Boukobza et.al. [103] by single molecule spectroscopy reports a Poisson distribution of around 70% of SUVs with one dye, 22% with two dyes and 5% with three dyes. Thus the result obtain is meaningful since FCS take into account only the loaded SUVs but not the empty ones.

2. The number of SUVs loaded with low dye concentration is very close to the number of highly loaded SUVs. Effectively, the SUVs are produced with the same lipid concentrations (5 mg/ml) and should not depend on the encapsulated dye concentration.

3. Finally, as expected, the number of dyes released from highly loaded SUVs - statistically 10 dyes per SUV - is about ten times higher than the number of SUVs before heating, and is also ten times higher than the number of dyes released from SUVs loaded with one dye per SUV.

For control, measurements were also performed outside LUVs but give invaluable results due to low counts per molecules in most of the cases and 0.7 molecules per femtoliter in the case after release with high initial concentration. This might result from the release from SUVs in bulk non incorporated in LUVs.

Up to now some articles have evaluated encapsulation efficiency [104–107] based on bulk analysis and represented the average of a given preparation. But only few groups mention the possibility to characterize either by FCS the number molecules released from single vesicle [108] or by single molecule spectroscopy the number of fluorescent protein within single small vesicle [103, 109, 110]. This demonstrates the utility and power of the FCS technique in this context.

6.5 Characterization by other techniques

6.5.1 Freeze-fracture Electron Microscopy

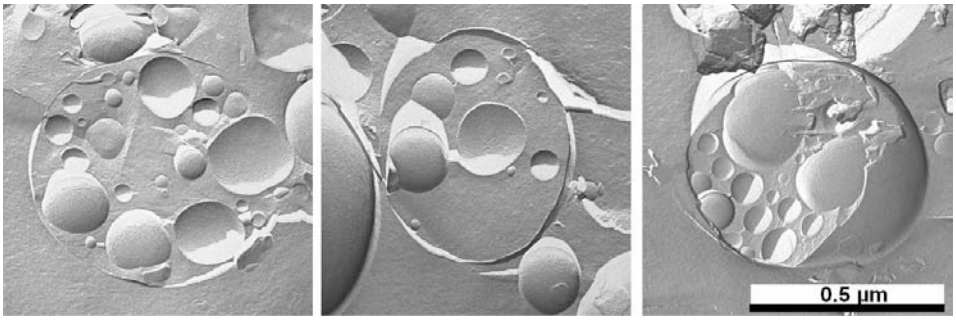

Figure 6.12: Freeze fracture electron microscopy of nested LUV / SUVs. *Same lipid composition and buffer as used in chapter 3. SUVs concentration 15 mg / ml of lipids and LUV concentration 10 mg / ml lipids.*

In order to image the LUVs / SUVs at 10 nm resolution, freeze fracture electron microscopy (EM) was performed. This particular EM technique is able to probe both the external and the internal surfaces and containment of vesicles (LUVs and SUVs). Figure 6.12 shows a series of freeze fracture electron micrographs of LUVs which contain SUVs at three different concentration levels: High packing density on the right hand side, intermediate loading level on the left hand side and low level in the center. The number of SUVs counted in the area of the LUV on the EM micrograph gives an estimation of the total number of SUVs in LUVs. From the picture of the left hand side presented here, two population of SUVs can be observed (also with DLS in the following section). The number of small SUVs with average diameter of 100 nm is 507 SUVs/fL. The number of larger SUVs (average diameter; 210 nm) is 58 SUVs/fL.

In order to compare these values with FCS results (obtained with SUVs of only 100 nm), the number of larger SUVs is converted into number of smaller ones by: $\sharp$ SUVs $\propto \sharp$ lipids / 2 $\cdot$ Surface(SUV) $\Rightarrow \sharp$ SUVs(100nm) $= 4.41 \cdot \sharp$ SUVs(210). So the total number of SUVs(100nm) is evaluated at 760 SUVs(100nm) / fL. The lipid concentration in the samples used for the freeze-fracture EM was four times higher than for FCS experiments. By taking this into account, we obtain a concentration of 190 SUVs/fL, which is similar as the concentration obtained by FCS measurements of 100 SUVs/fL.

6.5.2 Dynamic Light Scattering

The different types of SUVs used in the previous experiments are also characterized by dynamic light scattering (DLS). By proper calibration with latex beads of defined sizes, DLS delivers information of average sizes and size distribution of lipid vesicle preparations. Different vesicles composed of lipids with different acyl chain lengths and charges were analyzed. Figure 6.13A shows the size distribution of DPPG SUVs (black curve) extruded through a filter with 100 nm pore size and in comparison latex beads (gray curve) of 100 nm diameter. It demonstrates that the SUVs have similar average maximal size but a slightly larger size distribution as the calibration beads. Figure 6.13B compares DPPG SUVs extruded either through filters of 100 nm (black curve) or 400 nm diameters (gray curve). As expected, [74] the filters with larger pores produce larger SUVs (average value of 210 nm). The size distribution is also larger with two main populations around 100 and 250 nm. These two main populations are in agreement with the freeze-fracture EM especially with the picture on left hand-side of figure 6.12. On this micrograph, we can see clearly two sorts of SUVs; small ones with diameter around 100 nm and bigger ones with diameter around 200 nm.

These characteristics motivated us to chose the 100 nm extruded SUVs for FCS measurements. The 210 nm extruded SUVs were chosen for the fluorescence de-quenching and enzymatic reactions because they have a higher encapsulation capacity, enhancing the number of dyes released thus increasing the fluorescence response.

Table 6.1: DLS data summary. *Average (5 runs of 3min) of fitted (cumulant fit of correlation function 2nd order) data obtained by DLS (ALV 3.0) measured at 90°. Lipids concentration; 50 µg/ml in Tris-HCl 10 mM pH 7.0.*

Extrusion pores	Lipid used	Hydrodynamic Radius [nm]	Width [nm]
100nm	DPPG	**57**	23
100nm	DPPG:DPPC 5:5	**50**	14
100nm	DPPG:DPPC 1:9	**52**	17
100nm	DMPG:DMPC 2:8	**48**	14
250nm	DPPG	**96**	46
250nm	DPPG:DPPC 5:5	**94**	38
250nm	DPPG:DPPC 1:9	**105**	44
250nm	DMPG:DMPC 2:8	**90**	32
100nm	Latex Beads	**57**	1

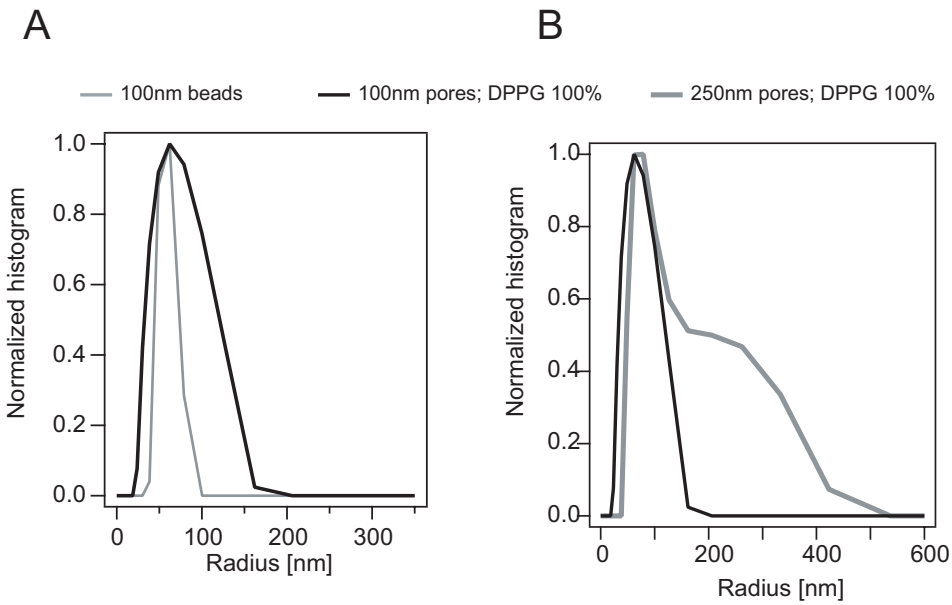

Figure 6.13: Size distribution of SUVs determined by dynamic light scattering (DLS). *(A) Comparison between latex beads of 100 nm in diameter (gray line) and DPPG vesicles extruded through a filter of 100 nm pores-size (black line). (B) Comparison between DPPG vesicles extruded through filter with 100 nm (black line) and 250 nm (thick gray line) pore-size.*

Table 6.1 summarizes the hydrodynamic radii and the widths of all SUVs analyzed with DLS. Several remarks can be made from these data. The major parameter influencing the size and size distribution is the pore-size of the extrusion filter used for the production of SUVs. The acyl chain length of the lipids have little effect on the size; shorter chains give smaller SUVs. The charge density of the lipid bilayer have no significant effect on the size. For comparison, the hydrodynamic radius of DPPG SUVs extruded through a filter with 100 nm pores is 58 nm, calculated by FCS and using the Stokes-Einstein relation, $D = k_b T/6\pi\eta R_h$, where D is the diffusion coefficient which is related to k_b the Boltzmann constant, T the temperature in Kelvin, η the viscosity and R_h the hydrodynamic radius.

6.6 Conclusion

It was demonstrated that FCS is able to follow and quantify the fluorescent SUVs and the dyes released into an individual LUV. With this technique, it was possible to quantify in dilute solutions the absolute concentration of reactants available for confined (bio-)chemical reactions which were investigated in the chapter 4. Different experiments showed that the presence of charged lipids in the SUVs bilayer and high

dilution of SUVs increased the release efficiency.

DLS was applied to characterize the size distribution of the SUVs in solution. Freeze-fracture EM showed a high SUVs encapsulation inside individual LUVs. The results obtained by these two techniques are in good agreement and revealed that SUVs extruded through a filter of 400 nm pores-size have two main populations around 100 nm and 250 nm.

Chapter 7

Conclusion and Outlook

7.1 Contribution of this research project

The results presented in the thesis demonstrate an innovative method that allows the parallel self-assembled production of nanoreactor systems whose function is controlled by a remote stimulus.

A nested system comprised large micrometer-sized vesicles (LUVs) encapsulating smaller nanometer-sized vesicles (SUVs). The larger ones are immobilized on a glass substrate. By using different lipids for each type of vesicles, we can increase the temperature and drive only the SUVs through a phase transition that makes them permeable while the LUVs remain impermeable. At the temperature of the SUVs' lipid phase transition the initially loaded hydrophilic molecules are released. The controlled release of reactants inside the large vesicles was demonstrated first by the release of CF fluorophores. The dilution in the LUVs resulted in dequenching and an increase of the CF fluorescence, proven unambiguously that the dye is release from the loaded SUVs at Tt but remained confined in the interior of the larger vesicle. The applied progressive temperature scan revealed a transition width of 3°C and a half time of release of 1min.

Triggered enzymatic reactions were also demonstrated by incorporating in LUVs an enzyme together with SUVs loaded with a substrate. The resulting enzymatic transformation of the substrates produced fluorescent signals which permitted to localize by confocal microscopy the products at single vesicle level. The developed system allowed monitoring many vesicular reactors at the same time and demonstrated that the confined biochemical reactions were triggered synchronically. By comparing different reactors we see that the initial reaction rate shows a dependency to the substrate concentration.

In a further step we performed two sequential enzymatic reactions within one single vesicular reactor. In order to achieve this two populations of SUVs made of different lipids were introduced together with an enzyme in the lumen of the LUV. One kind of SUV released its substrate around 23°C and the other kind around 41°C. Triggering was realized by applying a temperature ramp to the whole sample.

FCS was adapted and successfully applied to characterize the system in an unprecedented manner. The small detection volume enabled to probe the lumen of different LUVs before and after the release of substrates from incorporated SUVs. Under diluted conditions, the concentration of encapsulated SUVs and also the resulting released concentration of dyes were determined down to the single vesicle level. The averaged number of SUVs in LUV was evaluated at 1 SUV per femtoliter, a bit more than 1 fluorophore released from the SUV with initial dye concentration of 3.2 μM (1 dye / SUV) and around 10 fluorophores released from SUVs loaded 10 times more (32 μM (10 dyes / SUV).

7.2 Applications

This work is not at its end but demonstrates a novel approach which may be applied to trigger single enzyme reactions in confined volumes in a parallel manner. This could also be applied in a high-throughput screening system as mentioned in chapter 4 with the figure4.10 using different sorts of LUVs fluorescently marked.

The possibility to trigger successive reactions within one container could contribute to analyze inhibition or activation effects from different reactants in a confined volume. As the lipid vesicles mimic cell membranes, transmembrane proteins like g-protein coupled receptors (GPCRs) or ion channels could be incorporated and assayed [12]. This system may thus offers the possibility to investigate these protein interacting with molecules released from the inner part of the container as it would happen in a biological cell.

7.3 Improvements

The results obtained demonstrate the proof of principle for the proposed approach, but during this thesis project, some important parameters were still not quantified especially the number of enzymes per reactor. Also, due to mentioned technical problems, the kinetics of reactions were not quantified in details and thus the confinement effect was not determined.

Possible optimizations or improvements should be considered towards a valu-

able single molecule system. For an efficient immobilization the SUVs non incorporated in LUVs need to be removed by filtration which certainly disrupts (qualitative observations) part of the LUVs. In order to preserve the integrity of the LUVs, a UV polymerizable network (as [111]) in the lipid bilayer will increase their mechanical stability. If the immobilization is more efficient, this could permit some washing cycles. A more clean sample will enable to apply more sensitive single-molecule spectroscopy techniques such as wide-field microscopy coupled to a sensitive CCD camera.

Developing another strategy to release the substrates from SUVs that would prevent a temperature difference between the sample and the microscope objective could increase the data quality. The release could be induced for example by a pH change (membrane of LUVs being permeable to protons) with SUVs composed of pH sensitive lipids [112–114], or by photo-irradiation either on incorporated gold nanoparticles [50] or on photosensitive lipids [115, 116].

Using emulsion systems instead of LUVs would be an attractive approach as these systems offer certain advantages. The encapsulation efficiency of enzymes and SUVs (maybe modified) could be more reproducible, controllable and would not need a separation process to remove the non incorporated SUVs. Particularly, by applying microfluidic systems [43–45] the generated emulsion droplets would have a uniform and well defined internal concentration of reactants. The size of the droplets would also be controlled so as to define the absolute number of enzymes. In addition, the droplets can also be used as templates for lipid bilayers or more rigid polymerized structures.

Abbreviations

LUV	large unilamellar vesicle
SUV	small unilamellar vesicle
Tt	lipid phase transition temperature
Tc	temperature of consigne
Tris-HCl	2-Amino-2-(hydroxymethyl)-1,3-propanediol, hydrochloride
DDAO	7-hydroxy-9H(I,3-dichloro-9,9-dimethylacridin-2-one)
FDP	fluorescein di-phosphate
CF	carboxy fluorescein
DOPG	1,2-Dioleoyl-sn-Glycero-3-[Phospho-rac-(1-glycerol)]
DMPC	1,2-Dimyristoyl-sn-Glycero-3-Phosphocholine
DMPG	1,2-Dimyristoyl-sn-Glycero-3-[Phospho-rac-(1-glycerol)]
DPPC	1,2-Dipalmitoyl-sn-Glycero-3-Phosphocholine
MPPC	1-Palmitoyl-2-Hydroxy-sn-Glycero-3-Phosphocholine
DPPG	1,2-Dipalmitoyl-sn-Glycero-3-[Phospho-rac-(1-glycerol)]
TRITC-DHPE	N-(6-tetramethylrhodaminethiocarbamoyl)- 1,2-dihexadecanoyl-sn-glycero-3-phosphoethanolamine
PEG	Polyethylene glycol
BSA	bovine serum albumin
FCS	fluorescence correlation spectroscopy
ACF	autocorrelation function
DSC	differential scanning calorimetry
DLS	dynamic light scattering
EM	electron microscopy
MM	Michaelis-Menten

Bibliography

[1] D.M. Vriezema, M. ComellasAragones, J.A.A.W. Elemans, J.J.L.M. Cornelissen, A.E. Rowan, and R.J.M. Nolte. Self-assembled nanoreactors. *Chem. Rev.*, 105(4):1445–1490, 2005.

[2] P. Walde and S. Ichikawa. Enzymes inside lipid vesicles: Preparation, reactivity and applications. *Biomolecular Engineering*, 18(4):143–177, 2001.

[3] M. Karlsson, M. Davidson, R. Karlsson, A. Karlsson, J. Bergenholtz, Z. Konkoli, A. Jesorka, T. Lobovkina, J. Hurtig, M. Voinova, and O. Orwar. Biomimetic nanoscale reactors and networks. *Annual Review of Physical Chemistry*, 55:613–649, 2004.

[4] A. V. Barzykin and M. Tachiya. Reaction kinetics in monodisperse systems. *Heterogenous Chemistry Reviews*, 3:105–167, 1996.

[5] A. P. Minton. The influence of macromolecular crowding and macromolecular confinement on biochemical reactions in physiological media. *The Journal of Biological Chemistry*, 276(14):10577–10580, 2001.

[6] A. Ishijima and T. Yanagida. Single molecule nanobioscience. *Trends in Biochemical Sciences*, 26(7):438–444, 2001.

[7] Gilad Haran. Single-molecule fluorescence spectroscopy of biomolecular folding. *Journal of Physics: Condensed Matter*, 15(32):R1291–R1317, 2003. TY - JOUR.

[8] X. S. Xie and H. P. Lu. Single-molecule enzymology. *Journal of Biological Chemistry*, 274(23):15967–15970, 1999.

[9] H. Pick, E. L. Schmid, A. P. Tairi, E. Ilegems, R. Hovius, and H. Vogel. Investigating cellular signaling reactions in single attoliter vesicles. *Journal of the American Chemical Society*, 127(9):2908–2912, 2005.

[10] E. Rhoades, E. Gussakovsky, and G. Haran. Watching proteins fold one molecule at a time. *Proceedings of the National Academy of Sciences of the United States of America*, 100(6):3197–3202, 2003.

[11] J. J. Benkoski and F. Hook. Lateral mobility of tethered vesicle - dna assemblies. *Journal of Physical Chemistry B*, 109(19):9773–9779, 2005.

[12] Georg Kaim, Michael Prummer, Beate Sick, Gert Zumofen, Alois Renn, Urs P Wild, and Peter Dimroth. Coupled rotation within single f0f1 enzyme complexes during atp synthesis or hydrolysis. *FEBS Letters*, 525(1-3):156–163, 2002. TY - JOUR.

[13] C. Yoshina-Ishii and S. G. Boxer. Arrays of mobile tethered vesicles on supported lipid bilayers. *Journal of the American Chemical Society*, 125(13):3696–3697, 2003.

[14] B. Stadler, D. Falconnet, I. Pfeiffer, F. Hook, and J. Voros. Micropatterning of dna-tagged vesicles. *Langmuir*, 20(26):11348–11354, 2004.

[15] M. R. Dusseiller, B. Niederberger, B. Stadler, D. Falconnet, M. Textor, and J. Voros. A novel crossed microfluidic device for the precise positioning of proteins and vesicles. *Lab on a Chip*, 5(12):1387–1392, 2005.

[16] H. Schonherr, D. I. Rozkiewicz, and G. J. Vancso. Atomic force microscopy assisted immobilization of lipid vesicles. *Langmuir*, 20(17):7308–7312, 2004.

[17] K. Dimitrievski, A. Zach, V. P. Zhdanov, and B. Kasemo. Imaging and manipulation of adsorbed lipid vesicles by an afm tip: Experiment and monte carlo simulations. *Colloids and Surfaces B-Biointerfaces*, 47(2):115–125, 2006.

[18] R. Michel, I. Reviakine, D. Sutherland, C. Fokas, G. Csucs, G. Danuser, N. D. Spencer, and M. Textor. A novel approach to produce biologically relevant chemical patterns at the nanometer scale: Selective molecular assembly patterning combined with colloidal lithography. *Langmuir*, 18(22):8580–8586, 2002.

[19] D. Stamou, C. Duschl, E. Delamarche, and H. Vogel. Self-assembled microarrays of attoliter molecular vessels. *Angewandte Chemie-International Edition*, 42(45):5580–5583, 2003.

[20] N.D. Kalyankar, M.K. Sharma, S.V. Vaidya, D. Calhoun, C. Maldarelli, A. Couzis, and L. Gilchrist. Arraying of intact liposomes into chemically functionalized microwells. *Langmuir*, 2006.

[21] J. Korlach, C. Reichle, T. Muller, T. Schnelle, and W. W. Webb. Trapping, deformation, and rotation of giant unilamellar vesicles in octode dielectrophoretic field cages. *Biophysical Journal*, 89(1):554–562, 2005.

[22] D. Stamou, C. Duschl, E. Delamarche, and H. Vogel. Self-assembled microarrays of attoliter molecular vessels. *Angewandte Chemie-International Edition*, 42(45):5580–5583, 2003.

[23] B. Y. Sun, D. S. W. Lim, J. S. Kuo, C. L. Kuyper, and D. T. Chiu. Fast initiation of chemical reactions with laser-induced breakdown of a nanoscale partition. *Langmuir*, 20(22):9437–9440, 2004.

[24] B. Y. Sun and D. T. Chiu. Determination of the encapsulation efficiency of individual vesicles using single-vesicle photolysis and confocal single-molecule detection. *Analytical Chemistry*, 77(9):2770–2776, 2005.

[25] V. Noireaux and A. Libchaber. A vesicle bioreactor as a step toward an artificial cell assembly. *Proceedings of the National Academy of Sciences of the United States of America*, 101(51):17669–17674, 2004.

[26] Y. Yamashita, M. Oka, T. Tanaka, and M. Yamazaki. A new method for the preparation of giant liposomes in high salt concentrations and growth of protein microcrystals in them. *Biochimica Et Biophysica Acta-Biomembranes*, 1561(2):129–134, 2002.

[27] L. Limozin and E. Sackmann. Polymorphism of cross-linked actin networks in giant vesicles. *Physical Review Letters*, 89(16), 2002.

[28] R. Grimm, M. Barmann, W. Hackl, D. Typke, E. Sackmann, and W. Baumeister. Energy filtered electron tomography of ice-embedded actin and vesicles. *Biophysical Journal*, 72(1):482–489, 1997.

[29] J. Bohm, O. Lambert, A. S. Frangakis, L. Letellier, W. Baumeister, and J. L. Rigaud. Fhua-mediated phage genome transfer into liposomes: A cryo-electron tomography study. *Current Biology*, 11(15):1168–1175, 2001.

[30] M. S. Long, C. D. Jones, M. R. Helfrich, L. K. Mangeney-Slavin, and C. D. Keating. Dynamic microcompartmentation in synthetic cells. *Proceedings of the National Academy of Sciences of the United States of America*, 102(17):5920–5925, 2005.

[31] D. T. Chiu, C. F. Wilson, F. Ryttsen, A. Stromberg, C. Farre, A. Karlsson, S. Nordholm, A. Gaggar, B. P. Modi, A. Moscho, R. A. Garza-Lopez, O. Orwar, and R. N. Zare. Chemical transformations in individual ultrasmall biomimetic containers. *Science*, 283(5409):1892–1895, 1999.

[32] S. Kulin, R. Kishore, K. Helmerson, and L. Locascio. Optical manipulation and fusion of liposomes as microreactors. *Langmuir*, 19(20):8206–8210, 2003.

[33] G. H. Lei and R. C. MacDonald. Lipid bilayer vesicle fusion: Intermediates captured by high-speed microfluorescence spectroscopy. *Biophysical Journal*, 85(3):1585–1599, 2003.

[34] G. Tresset and S. Takeuchi. Utilization of cell-sized lipid containers for nanostructure and macromolecule handling in microfabricated devices. *Analytical Chemistry*, 77(9):2795–2801, 2005.

[35] D. Needham and E. Evans. Structure and mechanical-properties of giant lipid (dmpc) vesicle bilayers from 20-degrees-c below to 10-degrees-c above the liquid-crystal crystalline phase-transition at 24-degrees-c. *Biochemistry*, 27(21):8261–8269, 1988.

[36] P. Ratanabanangkoon, M. Gropper, R. Merkel, E. Sackmann, and A. P. Gast. Mechanics of streptavidin-coated giant lipid bilayer vesicles: A micropipet study. *Langmuir*, 19(4):1054–1062, 2003.

[37] E. Evans, H. Bowman, A. Leung, D. Needham, and D. Tirrell. Biomembrane templates for nanoscale conduits and networks. *Science*, 273(5277):933–935, 1996.

[38] A. Karlsson, R. Karlsson, M. Karlsson, A. S. Cans, A. Stromberg, F. Ryttsen, and O. Orwar. Molecular engineering - networks of nanotubes and containers. *Nature*, 409(6817):150–152, 2001.

[39] K. Sott, T. Lobovkina, L. Lizana, M. Tokarz, B. Bauer, Z. Konkoli, and O. Orwar. Controlling enzymatic reactions by geometry in a biomimetic nanoscale network. *Nano Lett.*, 6(2):209–214, 2006.

[40] Alan I. Lee and James P. Brody. Single-molecule enzymology of chymotrypsin using water-in-oil emulsion. *Biophys. J.*, 88(6):4303–4311, 2005.

[41] A. V. Pietrini and P. L. Luisi. Cell-free protein synthesis through solubilisate exchange in water/oil emulsion compartments. *Chembiochem*, 5(8):1055–1062, 2004.

[42] K. Bernath, M. T. Hai, E. Mastrobattista, A. D. Griffiths, S. Magdassi, and D. S. Tawfik. In vitro compartmentalization by double emulsions: sorting and gene enrichment by fluorescence activated cell sorting. *Analytical Biochemistry*, 325(1):151–157, 2004.

[43] T. Thorsen, R. W. Roberts, F. H. Arnold, and S. R. Quake. Dynamic pattern formation in a vesicle-generating microfluidic device. *Physical Review Letters*, 86(18):4163–4166, 2001.

[44] Y.-C. Tan, K. Hettiarachchi, M. Siu, Y.-R. Pan, and A.P. Lee. Controlled microfluidic encapsulation of cells, proteins, and microbeads in lipid vesicles. *J. Am. Chem. Soc.*, 128(17):5656–5658, 2006.

[45] A. S. Utada, E. Lorenceau, D. R. Link, P. D. Kaplan, H. A. Stone, and D. A. Weitz. Monodisperse double emulsions generated from a microcapillary device. *Science*, 308(5721):537–541, 2005.

[46] K.T. Rodolfa, A. Bruckbauer, D. Zhou, A.I. Schevchuk, Y.E. Korchev, and D. Klenerman. Nanoscale pipetting for controlled chemistry in small arrayed water droplets using a double-barrel pipet. *Nano Lett.*, 6(2):252–257, 2006.

[47] M. Gratzl, H. W. Lu, T. Matsumoto, C. Yi, and G. R. Bright. Fine chemical manipulations of microscopic liquid samples. 1. droplet loading with chemicals. *Analytical Chemistry*, 71(14):2751–2756, 1999.

[48] S. Katsura, A. Yamaguchi, H. Inami, S. Matsuura, K. Hirano, and A. Mizuno. Indirect micromanipulation of single molecules in water-in-oil emulsion. *Electrophoresis*, 22(2):289–293, 2001.

[49] F. Caruso, R. A. Caruso, and H. Mohwald. Nanoengineering of inorganic and hybrid hollow spheres by colloidal templating. *Science*, 282(5391):1111–1114, 1998.

[50] B. Radt, T. A. Smith, and F. Caruso. Optically addressable nanostructured capsules. *Advanced Materials*, 16(23-24):2184–+, 2004.

[51] A. A. Antipov, G. B. Sukhorukov, Y. A. Fedutik, J. Hartmann, M. Giersig, and H. Mohwald. Fabrication of a novel type of metallized colloids and hollow capsules. *Langmuir*, 18(17):6687–6693, 2002.

[52] A. D. Dinsmore, M. F. Hsu, M. G. Nikolaides, M. Marquez, A. R. Bausch, and D. A. Weitz. Colloidosomes: Selectively permeable capsules composed of colloidal particles. *Science*, 298(5595):1006–1009, 2002.

[53] A. Graff, M. Sauer, P. Van Gelder, and W. Meier. Virus-assisted loading of polymer nanocontainer. *Proceedings of the National Academy of Sciences of the United States of America*, 99(8):5064–5068, 2002.

[54] D. M. Vriezema, J. Hoogboom, K. Velonia, K. Takazawa, P. C. M. Christianen, J. C. Maan, A. E. Rowan, and R. J. M. Nolte. Vesicles and polymerized vesicles from thiophene-containing rod-coil block copolymers. *Angewandte Chemie-International Edition*, 42(7):772–776, 2003.

[55] Y. Rondelez, G. Tresset, K. V. Tabata, H. Arata, H. Fujita, S. Takeuchi, and H. Noji. Microfabricated arrays of femtoliter chambers allow single molecule enzymology. *Nature Biotechnology*, 23(3):361–365, 2005.

[56] D. M. Rissin and D. R. Walt. Digital concentration readout of single enzyme molecules using femtoliter arrays and poisson statistics. *Nano Letters*, 6(3):520–523, 2006.

[57] T. Rindzevicius, Y. Alaverdyan, A. Dahlin, F. Hook, D. S. Sutherland, and M. Kall. Plasmonic sensing characteristics of single nanometric holes. *Nano Letters*, 5(11):2335–2339, 2005.

[58] M. Margulies, M. Egholm, W. E. Altman, S. Attiya, J. S. Bader, L. A. Bemben, J. Berka, M. S. Braverman, Y. J. Chen, Z. T. Chen, S. B. Dewell, L. Du, J. M. Fierro, X. V. Gomes, B. C. Godwin, W. He, S. Helgesen, C. H. Ho, G. P. Irzyk, S. C. Jando, M. L. I. Alenquer, T. P. Jarvie, K. B. Jirage, J. B. Kim, J. R. Knight, J. R. Lanza, J. H. Leamon, S. M. Lefkowitz, M. Lei, J. Li, K. L. Lohman, H. Lu, V. B. Makhijani, K. E. McDade, M. P. McKenna, E. W. Myers, E. Nickerson, J. R. Nobile, R. Plant, B. P. Puc, M. T. Ronan, G. T. Roth, G. J. Sarkis, J. F. Simons, J. W. Simpson, M. Srinivasan, K. R. Tartaro, A. Tomasz, K. A. Vogt, G. A. Volkmer, S. H. Wang, Y. Wang, M. P. Weiner, P. G. Yu, R. F. Begley, and J. M. Rothberg. Genome sequencing in microfabricated high-density picolitre reactors. *Nature*, 437(7057):376–380, 2005.

[59] Papahadj.D, K. Jacobson, S. Nir, and T. Isac. Phase-transitions in phospholipid vesicles - fluorescence polarization and permeability measurements concerning effect of temperature and cholesterol. *Biochimica Et Biophysica Acta*, 311(3):330–348, 1973. Times Cited: 612 Article English Cited References Count: 43 Q1231.

[60] O.G. Mouritsen. *Permeability of lipid bilayers near the phase transition.* Permeability and Stability of Lipid Bilayers. CRC Press, Boca Raton, 1995.

[61] J. F. Nagle and H. L. Scott, Jr. Lateral compressibility of lipid mono- and bilayers. theory of membrane permeability. *Biochimica et Biophysica Acta (BBA) - Biomembranes*, 513(2):236–243, 1978. TY - JOUR.

[62] S. Doniach. Thermodynamic fluctuations in phospholipid bilayers. *Journal of Chemical Physics*, 68(11):4912–4916, 1978. TY - JOUR.

[63] E. Evans and R. Kwok. Mechanical calorimetry of large dimyristoylphosphatidylcholine vesicles in the phase transition region. *Biochemistry*, 21(20):4874–4879, 1982. TY - JOUR Cited By: 0; Export Date: 2 May 2006; Source: Scopus.

[64] D. Marsh, A. Watts, and P.F. Knowles. Evidence for phase boundary lipid. permeability of tempo choline into dimyristoylphosphatidylcholine vesicles at the phase transition. *Biochemistry*, 15(16):3570–3578, 1976. TY - JOUR Cited By: 0; Export Date: 2 May 2006; Source: Scopus.

[65] E. Corvera, O.G. Mouritsen, M.A. Singer, and M.J. Zuckerman. The permeability and the effect of acyl-chain length for phospholipid bilayers containing cholesterol: Theory and experiment. *Biochim. Biophys. Acta*, 1107:261–270, 1991. TY - JOUR Cited By: 0; Export Date: 2 May 2006; Source: Scopus.

[66] O.G. Mouritsen and M.J. Zuckermann. Model of interfacial melting. *Physical Review Letters*, 58(4):389–392, 1987. TY - JOUR.

[67] J. K. Mills and D. Needham. Lysolipid incorporation in dipalmitoylphosphatidylcholine bilayer membranes enhances the ion permeability and drug release rates at the membrane phase transition. *Biochimica Et Biophysica Acta-Biomembranes*, 1716(2):77–96, 2005.

[68] Schel R. Bramhall J., Montestruque S. Temperature dependence of membrane ion conductance anlayzed by using the amphiphilic anion 5/6-carboxyfluorescein. *biochemistry*, 26:6330–6340, 1987.

[69] M. C. Blok, E. C. M. Vanderneutkok, L. L. M. Vandeenen, and J. Degier. Effect of chain-length and lipid phase-transitions on selective permeability properties of liposomes. *Biochimica Et Biophysica Acta*, 406(2):187–196, 1975.

[70] D. Stamou. *Organic monolayers : characterization by AFM and their use for the patterned immobilization of vesicles*. PhD thesis, EPFL, 2000.

[71] D. Needham and D. H. Kim. Peg-covered lipid surfaces: bilayers and monolayers. *Colloids and Surfaces B-Biointerfaces*, 18(3-4):183–195, 2000.

[72] F. Szoka and D. Papahadjopoulos. Comparative properties and methods of preparation of lipid vesicles (liposomes). *Annual Review of Biophysics and Bioengineering*, 9:467–508, 1980. Times Cited: 760 Review English Cited References Count: 229 Jt951.

[73] M. J. Hope, M. B. Bally, G. Webb, and P. R. Cullis. Production of large unilamellar vesicles by a rapid extrusion procedure - characterization of size distribution, trapped volume and ability to maintain a membrane-potential. *Biochimica Et Biophysica Acta*, 812(1):55–65, 1985.

[74] L. D. Mayer, M. J. Hope, and P. R. Cullis. Vesicles of variable sizes produced by a rapid extrusion procedure. *Biochimica Et Biophysica Acta*, 858(1):161–168, 1986.

[75] L. D. Mayer, M. J. Hope, P. R. Cullis, and A. S. Janoff. Solute distributions and trapping efficiencies observed in freeze-thawed multilamellar vesicles. *Biochimica Et Biophysica Acta*, 817(1):193–196, 1985.

[76] B. L. S. Mui, P. R. Cullis, E. A. Evans, and T. D. Madden. Osmotic properties of large unilamellar vesicles prepared by extrusion. *Biophysical Journal*, 64(2):443–453, 1993.

[77] Kinosita K. Akashi, K. Preparation of giant liposomes in physiological conditions and their characterization under an optical microscope. *Biophys. J.*, 71(6),:3242–3250, 1996.

[78] K. Akashi, H. Miyata, H. Itoh, and K. Kinosita. Formation of giant liposomes promoted by divalent cations: Critical role of electrostatic repulsion. *Biophysical Journal*, 74(6):2973–2982, 1998. English Article JUN BIOPHYS J.

[79] Miglena I. Angelova. Liposome electroformation. *Perspect. Supramol. Chem.*, 6(Giant Vesicles):27–36, 2000.

[80] D. S. Dimitrov and M. I. Angelova. Lipid swelling and liposome formation mediated by electric fields. *Bioelectrochemistry and Bioenergetics*, 19(2):323–336, 1988. TY - JOUR.

[81] Raymond F. Chen and Jay R. Knutson. Mechanism of fluorescence concentration quenching of carboxyfluorescein in liposomes: Energy transfer to nonfluorescent dimers. *Analytical Biochemistry*, 172(1):61–77, 1988. TY - JOUR.

[82] M. M. Martin and L. Lindqvist. Ph-dependence of fluorescein fluorescence. *Journal of Luminescence*, 10(6):381–390, 1975.

[83] Joseph R. Lakowicz. *Principles of fluorescence spectroscopy.* London, 1983.

[84] R. B. Gennis. *Biomembranes; Molecular Structure and Function.* Springer-Verlag, 1989.

[85] P. Y. Bolinger, D. Stamou, and H. Vogel. Integrated nanoreactor systems: Triggering the release and mixing of compounds inside single vesicles. *Journal of the American Chemical Society*, 126(28):8594–8595, 2004.

[86] Y. Rondelez, G. Tresset, K. V. Tabata, H. Arata, H. Fujita, S. Takeuchi, and H. Noji. Microfabricated arrays of femtoliter chambers allow single molecule enzymology. *Nature Biotechnology*, 23(3):361–365, 2005.

[87] A. Karlsson, K. Sott, M. Markstrom, M. Davidson, Z. Konkoli, and O. Orwar. Controlled initiation of enzymatic reactions in micrometer-sized biomimetic compartments. *Journal of Physical Chemistry B*, 109(4):1609–1617, 2005.

[88] D. T. Chiu, C. F. Wilson, F. Ryttsen, A. Stromberg, C. Farre, A. Karlsson, S. Nordholm, A. Gaggar, B. P. Modi, A. Moscho, R. A. Garza-Lopez, O. Orwar, and R. N. Zare. Chemical transformations in individual ultrasmall biomimetic containers. *Science*, 283(5409):1892–1895, 1999. English Article MAR 19 SCIENCE.

[89] A. Fischer, A. Franco, and T. Oberholzer. Giant vesicles as microreactors for enzymatic mrna synthesis. *Chembiochem*, 3(5):409–417, 2002.

[90] L. Michaelis and M. L. Menten. Die kinetic der invertinwikung [the kinetics of invertin activity]. *Biochemische Weitschrift*, 49:333–369, 1913.

[91] L. Stryer. *biochemistry.* Freeman, New York, 1996.

[92] H. Gutfreund. *Kinetics for the Life Sciences; receptors, transmitters and catalysts.* Cambridge University Press, 1995.

[93] D. Magde, W. W. Webb, and E. Elson. Thermodynamic fluctuations in a reacting system - measurement by fluorescence correlation spectroscopy. *Physical Review Letters*, 29(11):705–708, 1972.

[94] R. Rigler, ÃIJ. Mets, J. Widengren, and P. Kask. Fluorescence correlation spectroscopy with high count rate and low background: analysis of translational diffusion. *European Biophysics Journal*, 22(3):169–175, 1993. TY - JOUR.

[95] Oleg Krichevsky and Gregoire Bonnet. Fluorescence correlation spectroscopy: the technique and its applications. *Reports on Progress in Physics*, 65(2):251–297, 2002. TY - JOUR.

[96] P. Schwille. Fluorescence correlation spectroscopy and its potential for intracellular applications. *Cell Biochemistry and Biophysics*, 34(3):383–408, 2001.

[97] Aladdin Pramanik, Per Thyberg, and Rudolf Rigler. Molecular interactions of peptides with phospholipid vesicle membranes as studied by fluorescence correlation spectroscopy. *Chemistry and Physics of Lipids*, 104(1):35–47, 2000. TY - JOUR.

[98] Konstantin Starchev, Jingwu Zhang, and Jacques Buffle. Applications of fluorescence correlation spectroscopy– particle size effect. *Journal of Colloid and Interface Science*, 203(1):189–196, 1998. TY - JOUR.

[99] P. Rigler and W. Meier. Encapsulation of fluorescent molecules by functionalized polymeric nanocontainers: Investigation by confocal fluorescence imaging and fluorescence correlation spectroscopy. *J. Am. Chem. Soc.*, 128(1):367–373, 2006.

[100] Thorsten Wohland. *Fluorescence correlation spectroscopy simulations and biological applications*. PhD thesis, EPFL, 2000.

[101] Ulrich Meseth, Thorsten Wohland, Rudolf Rigler, and Horst Vogel. Resolution of fluorescence correlation measurements. *Biophys. J.*, 76(3):1619–1631, 1999.

[102] E. Boukobza, A. Sonnenfeld, and G. Haran. Immobilization in surface-tethered lipid vesicles as a new tool for single biomolecule spectroscopy. *Journal of Physical Chemistry B*, 105(48):12165–12170, 2001.

[103] E. Boukobza, A. Sonnenfeld, and G. Haran. Immobilization in surface-tethered lipid vesicles as a new tool for single biomolecule spectroscopy. *Journal of Physical Chemistry B*, 105(48):12165–12170, 2001.

[104] G. V. Betageri and D. L. Parsons. Drug encapsulation and release from multilamellar and unilamellar liposomes. *International Journal of Pharmaceutics*, 81(2-3):235–241, 1992.

[105] B. Elorza, M. A. Elorza, M. C. Sainz, and J. R. Chantres. Comparison of particle-size and encapsulation parameters of 3 liposomal preparations. *Journal of Microencapsulation*, 10(2):237–248, 1993.

[106] M. Fresta, A. Villari, G. Puglisi, and G. Cavallaro. 5-fluorouracil - various kinds of loaded liposomes - encapsulation efficiency, storage stability and fusogenic properties. *International Journal of Pharmaceutics*, 99(2-3):145–156, 1993.

[107] S. B. Kulkarni, G. V. Betageri, and M. Singh. Factors affecting microencapsulation of drugs in liposomes. *Journal of Microencapsulation*, 12(3):229–246, 1995.

[108] B. Y. Sun and D. T. Chiu. Determination of the encapsulation efficiency of individual vesicles using single-vesicle photolysis and confocal single-molecule detection. *Analytical Chemistry*, 77(9):2770–2776, 2005.

[109] E. Rhoades, E. Gussakovsky, and G. Haran. Watching proteins fold one molecule at a time. *Proceedings of the National Academy of Sciences of the United States of America*, 100(6):3197–3202, 2003.

[110] Burak Okumus, Timothy J. Wilson, David M. J. Lilley, and Taekjip Ha. Vesicle encapsulation studies reveal that single molecule ribozyme heterogeneities are intrinsic. *Biophys. J.*, 87(4):2798–2806, 2004.

[111] C. Nardin, T. Hirt, J. Leukel, and W. Meier. Polymerized aba triblock copolymer vesicles. *Langmuir*, 16(3):1035–1041, 2000. English Article FEB 8 LANGMUIR.

[112] D. Collins, D. C. Litzinger, and L. Huang. Structural and functional comparisons of ph-sensitive liposomes composed of phosphatidylethanolamine and 3 different diacylsuccinylglycerols. *Biochimica Et Biophysica Acta*, 1025(2):234–242, 1990. Times Cited: 44 Cited Reference Count: 35 Cited References: English Article DN879 BIOCHIM BIOPHYS ACTA.

[113] M. Sauer, D. Streich, and W. Meier. ph-sensitive nanocontainers. *Advanced Materials*, 13(21):1649–1651, 2001. English Article NOV 2 ADVAN MATER.

[114] Y. Sumida, A. Masuyama, M. Takasu, T. Kida, Y. Nakatsuji, I. Ikeda, and M. Nojima. New ph-sensitive vesicles. release control of trapped materials from the inner aqueous phase of vesicles made from triple-chain amphiphiles

bearing two carboxylate groups. *Langmuir*, 17(3):609–612, 2001. Times Cited: 2 Cited Reference Count: 28 English Article 398PT LANGMUIR.

[115] H. You and D. A. Tirrell. Photoinduced, polyelectrolyte-driven release of contents of phosphatidylcholine bilayer vesicles. *Journal of the American Chemical Society*, 113(10):4022–4023, 1991. Times Cited: 18 Cited Reference Count: 14 English Note FL177 J AMER CHEM SOC.

[116] D. A. Frankel, H. Lamparski, U. Liman, and D. F. Obrien. Photoinduced destabilization of bilayer vesicles. *Journal of the American Chemical Society*, 111(26):9262–9263, 1989.

Acknowledgements

It would never have been possible to achieve all the work presented here without the help of many persons to whom I want to address all my gratitude.

In particular, I wish to thank my supervisor, Professor Horst Vogel, for giving me the opportunity to discover such fascinating interdisciplinary domain, and for his perceptiveness, advices and the way he trust me during all this project.

In addition, I am especially grateful to following people whose expert knowledge was of great value;
Ruud Hovius in lipid physical-chemistry and general biochemistry,
Dimitri Stamou in surface physics and innovative vision,
Jean-Manuel Segura imaging technology and
Hanna Jankevics in FCS technique.

I would like to thank Dimitri Stamou for careful reading of parts of the manuscript, as well as Christophe Danelon, Ruud Hovius and Michael Prummer. My thanks also to Verena Tabet for all the administrative procedures. Of course, I thank all the members of the Vogel lab, for the nice atmosphere and for all the parties, who made working in this institute a pleasure. Moreover, I would like to thank all my friends who were of great support.

And last but not least, I would like to thank my family; my wife, my children, my parents, my sister and brother for their love, encouragement and support throughout these years.

Curriculum Vitæ

Pierre-Yves Bolinger
Born on January, 1974 in Lausanne, Switzerland
Citizen of Kaiseraugst, AG, Switzerland

since 2001	PhD thesis under supervision of Prof. Horst Vogel at the Institute of Chemical Sciences and Engineering of ETH Lausanne, Switzerland.
1995 – 2001	Chemical engineering at ETH Lausanne, Switzerland.
1993 – 1995	Maturité fédérale C, Gymnase Bugnon in Lausanne, Switzerland. Prize of class.
1984 – 1993	CFC cabinetmaker, ETML Lausane, Switzerland. Prizes for best theoretical final exam + best second year exam.